



A.D. MDLXII

University of Sassari

Department of Biomedical sciences

PhD School in Life Sciences and Biotechnologies

XXXI cycle

Coordinator: Prof. Leonardo Sechi

***In vitro* and *in silico* studies of Syk inhibitors as
new antimalarial drugs**

Tutor: Prof. Antonella Pantaleo

Co Tutor: Alessandro Dessì
Roberto Dallochio

PhD candidate

Giuseppe Marchetti

A. A 2017 - 2018

Contents

ABBREVIATIONS	5
SUMMARY	6
1. INTRODUCTION	8
1.1. Background and epidemiology of Malaria	9
1.2. Malaria parasite life cycle and <i>P. falciparum</i>	11
1.3. Protection from malaria infection	14
1.3.1. Genetic factors	14
1.3.2. Acquired immunity	14
1.4. Diagnosis of Malaria	16
1.4.1. Uncomplicated Malaria	16
1.4.1.1. Incubation Period	17
1.4.2 Severe malaria	18
1.4.3 Cerebral malaria	18
1.5. Erythrocytes plasmatic membrane	20
1.5.1. Red blood cells plasmatic membrane structure	20
1.6. The spleen tyrosine kinase (Syk)	23
1.7. Treatments for Malaria	27
1.7.1. Artemisinin and Artemisinin derivatives	27
1.7.1.1. The artemisinin mechanism of action	28
1.7.1.2. Artemisinin derivatives	28
1.8. Artemisinin-based combination therapies (ACTs)	29
1.9. Drugs resistance development	30
1.9.1. State of partial artemisinin resistance around the world	31
1.9.2. Current state of ACTs failures	31
1.10. Computational studies to explain the biological phenomenon	33
1.11. Syk inhibitors as treatment for malaria	38
1.11.1 Kinase inhibitors mainly used in therapy	39
2. AIM OF THE PROJECT	42
3. MATERIALS & METHODS	44
3.1. Experimental <i>In vitro</i> studies	45
3.1.1. ICEstimator 1.2 software	46
3.1.2. Treatment of red blood cells (RBCs)	46

3.1.3. RBCs membrane preparation	47
3.1.4. SDS-PAGE preparation	47
3.1.5. Western blot analyses	47
3.2. Computational studies	48
3.2.1. Molecular Mechanics (MM) and Quantum Mechanics (QM)	48
3.2.2. Molecular docking	48
3.2.2.1. Docking validation protocol (close conformation of Syk)	49
3.2.3. Quantum Mechanics molecular descriptors	51
3.2.3.1. Homo-Lumo	51
3.2.3.2. Molecular Electrostatic Potential (MEP)	51
3.2.4. Molecular dynamics (MD)	52
3.2.4.1. RMSD maps in Molecular dynamics	53
3.2.5. Identification of receptor for the Virtual Screening	54
3.2.5.1. 3D alignment superposition of Syk	54
3.2.5.2. UCSF Chimera software	55
3.2.6. Docking validation protocol with 43 crystal structures of Syk	55
3.2.6.1. PyMOL software	55
3.2.7. Residues assessment providing Syk specificity in the human kinome	56
3.2.7.1. Alignment method: ClustalX software	56
3.2.8. Virtual screening (VS)	57
4. RESULTS & DISCUSSION	58
4.1. <i>In vitro</i> results	59
4.1.1. IC ₅₀ evaluation of Syk inhibitors in parasitized erythrocytes	59
4.1.2. Proteomic profile of Tyr phosphorylation in treated RBCs	60
4.2. Computational results	63
4.2.1. Results of docking validation protocol (close conformation of Syk)	64
4.2.2. Docking results	65
4.2.3. Assessment of Syk inhibitors efficacy	70
4.2.4. Identification of residues as new sites for Syk specificity	70
4.2.5. Docking validation to select the target for VS (open conformation of Syk)	71
4.2.6. Molecular dynamic results	75
4.2.7. RMSD maps results in Molecular Dynamics	78
4.2.8. Virtual Screening results	79

4.2.9. Compounds to test <i>in vitro</i> selected from Virtual screening	81
5. CONCLUSION & PERSPECTIVES	86
6. REFERENCES	89
Publications & communications	99

ABBREVIATIONS

WHO : World Health Organization

RBCs : Red Blood Cells

SYK : Spleen Tyrosine Kinase

Hb : Haemoglobin

PKs : Protein Kinases

ACTs : Artemisinin Combination Therapies

ART : Artemisinin

DHA : Dihydroartemisinin

AS : Artesunate

ATH : Artemether

LMF : Lumefantrine

PPQ : Piperaquine

Hz : Hemozoin

MDR : Multidrug resistance

IC₅₀ : Inhibitory Concentration of 50%

Fe-PPIX : Ferriprotoporphyrin IX

SDS-PAGE : Sodium Dodecyl Sulphate - PolyAcrylamide Gel Electrophoresis

MM : Molecular Mechanics

QM : Quantum Mechanics

HOMO : highest occupied molecular orbital

LUMO : lowest unoccupied molecular orbital

MEP : Molecular Electrostatic Potential

VS : Virtual Screening

LBVS : Ligand-Based Virtual Screening

SBVS : Structure-Based Virtual Screening

MD : Molecular Dynamics

RMSD: Root mean square deviation

Fig. : Figure

Tab : Table

Summary

Malaria remains one of the most devastating infectious diseases and despite the current therapies are efficient, the WHO recommends Artemisinin Combination Therapies (ACTs) as the frontline treatments against *P. falciparum* malaria to limit the artemisinin resistance. Unfortunately, in the Greater Mekong subregion, the efficacy of artemisinin-based combined therapies (ACTs) has recently been questioned by resistance to both artemisinin derivatives and to the partner drugs. Recently, a new mechanism of action based on the release of denatured haemoglobin products (haemichromes), bound to erythrocyte membrane through the cytoplasmic domain of the AE1 (Band 3 protein) has been characterized. More specifically phosphorylated band 3 becomes uncoupled from the cytoskeleton, leading to the formation of membrane clusters containing haemichromes – band 3 aggregates that can either be released from red blood cells as microvesicles or picked by spleen macrophages by a mechanism known as erythrocyte pitting. This process is mediated by erythrocytic Syk kinase that carries out the Tyr phosphorylation of band 3.

The consequent destabilization of the membrane is thought to be essential for parasite egress from the red cell at the end of the parasite's life cycle, since inhibitors of the Syk tyrosine kinase block band 3 tyrosine phosphorylation, membrane weakening and parasite reinfection.

In vitro and *in silico* studies have been performed in order to investigate the inhibitory activity of these compounds and acquire as much as possible information about the ligands and protein structure, in order to add more evidence to the process occurring in infected erythrocytes.

The aim of this study was to examine the effects of the Syk inhibitors on critical events during parasite growth and maturation within the human erythrocyte through *in vitro* experiments and explore current molecular docking strategies used in drug discovery and medicinal chemistry, considering the advances in the field and the role played by the integration of structure- and ligand-based methods.

In vitro studies have involved the treatment of parasitized erythrocytes cultures with different concentrations of Syk inhibitors and we evaluated the Tyr phosphorylation levels in Band 3 residues by proteomic approach.

In silico studies were based on different approaches of molecular modelling (docking, molecular dynamics and virtual screening). In presence of Syk inhibitors we observed a marked decrease of band 3 phosphorylation, proportional to the increase of drug dosage. The proteomic data about the IC₅₀ values follow the same trend in relation to the computational analyses results. These studies enabled us to better analyse the structure of different Syk inhibitors and to possibly discover new molecules through virtual screening analysis. In the long term, we aim to further investigate the efficacy of these compounds by evaluating their inhibitory activity through proteomic and *in vitro* studies.

1. INTRODUCTION

1.1 Background and epidemiology of Malaria

Malaria is a parasitic disease caused by a protozoa emosporidae belonging at genus of plasmodium. This infective disease is transmitted by the female Anopheles mosquito bite, which lives mainly in the region with a temperate and hot climate. Among all studied mosquitoes species, only few of them are responsible of malaria disease, whereas the others are harmless, as they prefer animal blood compared to human blood.

The main vector responsible of malaria in the Afrotropical region is *Anopheles Gambiae* specie (Fig.1).

In the past few years, the disease has spread through the western continents even though it has been eradicated in these regions few years ago. The migrants fluxes have been claimed as a possible cause of this unexpected event.

Malaria is an infective disease that causes a high level of deaths in the world. The 2017 Malaria report of registered 216 million new cases and 455 thousands dead. Over 77 % of children die with severe cerebral damages and convulsions under 5



Fig. 1. Female *Anopheles* mosquito

years old (around 300 thousands), for this reason malaria is also known as “disease of childhood” [1]. The sub-Saharan region is the most malaria endemic area in the world registering around 90% of cases in the world.

The number of *Plasmodium falciparum* malaria cases has rapidly decreased in the last five years [2].

In the period 2011-2016 have been registered 3600 cases in Italy mainly due to the migratory fluxes.

Malaria remains one of the most devastating infectious diseases in the world, thereby the main effort consists in eradicate it.

This disease is endemic in 103 nation therefore many people are exposed to this kind of pathology. Malaria affects also pregnant women and infants, who

contract the pathology directly from the mother, through the blood exchange [3,4].

Annually around 100 thousand of infants die for malaria infected from their mother [5] and 25 million of pregnant women are at risk of infection around the world [6].

Exist five protozoa species able to cause Malaria in humans. They belong to *Plasmodium* genus:

- *P. falciparum*
- *P. vivax*
- *P. ovale*
- *P. malariae*
- *P. knowlesi* (humans and macaques)

These species of *Plasmodium* cause different kinds of malaria and is important to differentiate them, because the mortality, incidence and distribution are completely different between them.

Among the *Plasmodium* species, two are the most severe, *P. vivax* (endemic region) and *P. falciparum* (Africa, Asia, latin America).

The most common cause of death is due to *Plasmodium falciparum*. The immune system plays an important role in the attack of the illness. The first time that our organism makes contact with the infective agent is crucial, dangerous and potentially, because the appropriate immune response is not yet present to prevent the infection. For this reason, people who are physiologically immunosuppressed such as kids and breastfeeding women are more prone to die.

1.2 Malaria parasite life cycle and *P. falciparum*

The malaria parasite life cycle involves two hosts. As shown in figure 3, during a blood meal, a malaria-infected female *Anopheles* mosquito inoculates sporozoites into the human host **1**. The sporozoites infect liver cells **2** and mature into schizonts **3**, with consequent rupture of membrane and release of merozoites **4**. In *P. vivax* and *P. ovale* a dormant stage [hypnozoites] can persist in the liver and cause relapses by invading the bloodstream weeks, or even years later.

After this initial replication in the liver (exo-erythrocytic schizogony **A**), the parasites undergo asexual multiplication in the erythrocytes (erythrocytic schizogony **B**). Merozoites infect red blood cells **5**. The ring stage (1-24 hours) and trophozoites (24-36 hours) mature into schizonts (36-48 hours), with lysis of red blood cells (RBCs) membrane (Fig.2) and release of merozoites **6**. Some parasites differentiate into sexual erythrocytic stages (gametocytes) **7**.

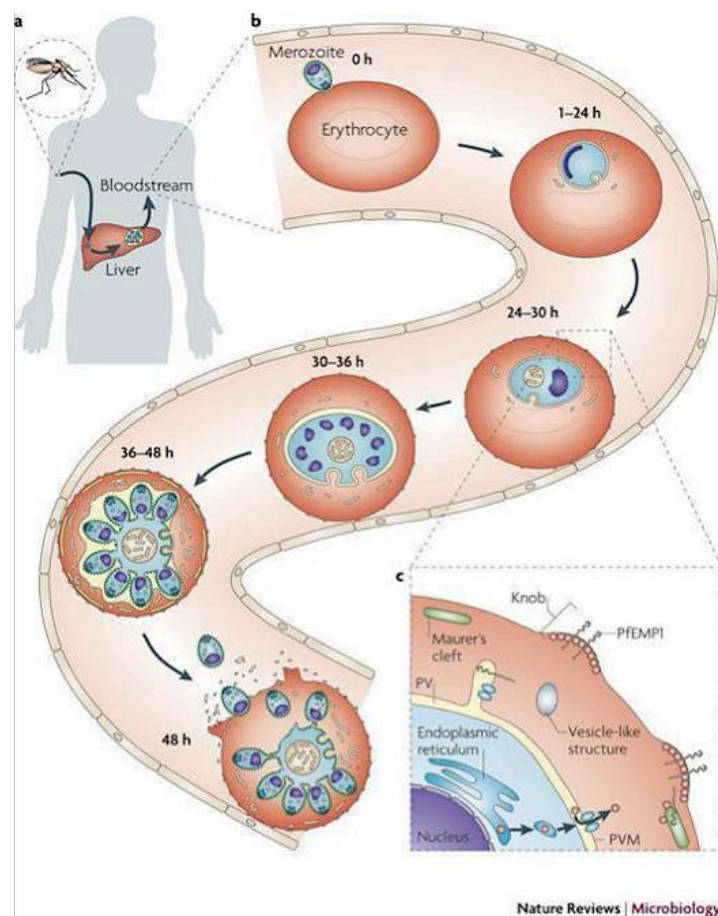


Fig. 2. Intraerythrocytic cycle of parasite

Blood stage parasites are accountable for the clinical manifestations of the disease. The gametocytes, male (microgametocytes) and female (macrogametocytes), are ingested by an *Anopheles* mosquito during a blood meal **8**. The parasites proliferation in the mosquito is known as the sporogonic cycle **C**. At the same time, in the mosquito's stomach, the microgametes penetrate the macrogametes generating the zygotes **9**. The zygotes in turn become motile and elongated (ookinetes) **10** which invade the midgut wall of the mosquito where they develop into oocysts **11**. The oocysts grow, rupture, and release sporozoites **12**, which make their way to the mosquito's salivary glands. Inoculation of the sporozoites **1** into a new human host perpetuates the malaria life cycle (Fig.3) [7].

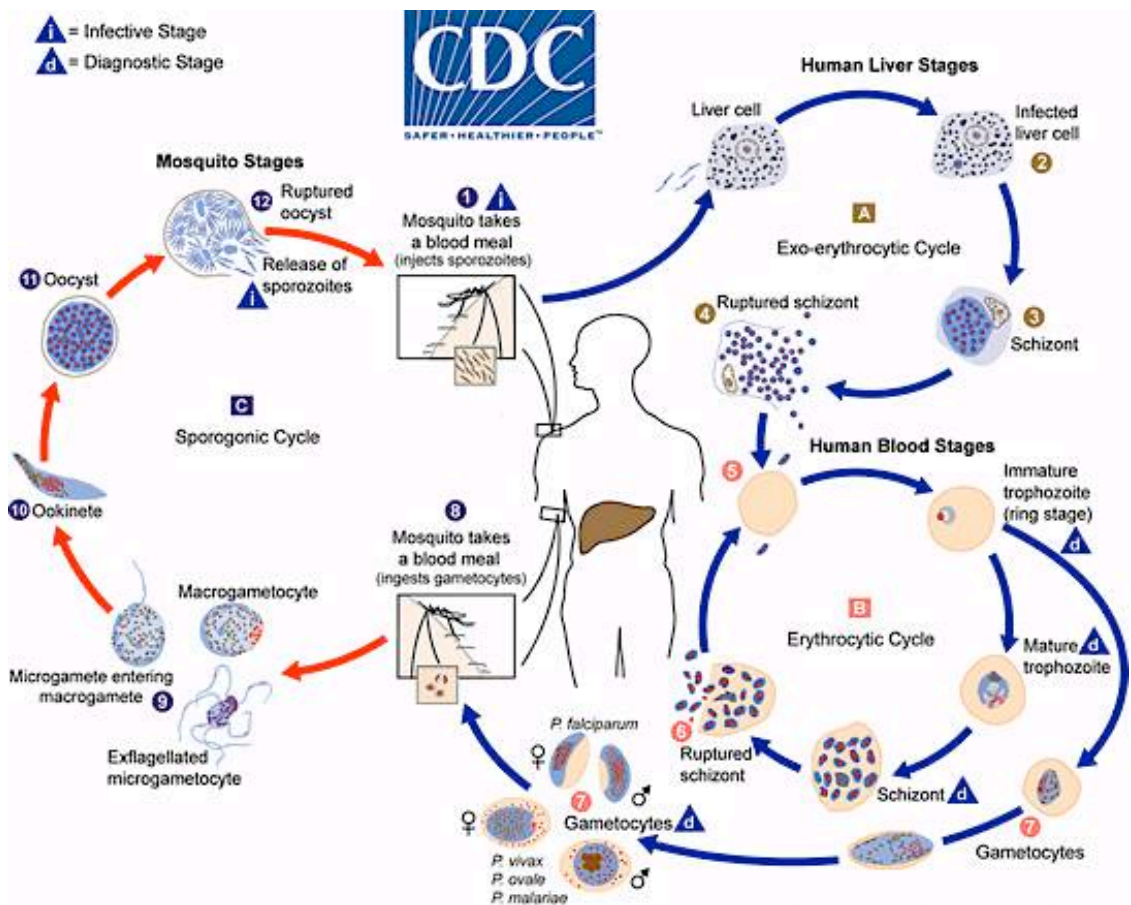


Fig. 3. Sexual and asexual life cycle of plasmodium

The activation of parasite metabolic processes inside the RBCs, triggers alterations of host cell energetic metabolism, deep proteins and membrane structural changes. An example in *P. falciparum* consists of molecules

expression on the erythrocytes external surface that mediates the infected RBCs process of adhesion to the endothelial cells in capillary of some organs. This phenomenon, known as “abduction”, represents an essential pathogenic mechanism in *P. falciparum* severe malaria. Malaria parasites use haemoglobin (hereafter referred to as Hb) as a major nutrient source in the intraerythrocytic stage, during which the heme group is converted to hemozoin (hereafter referred to as Hz), which is essential for parasite survival [8]. Mature trophozoites digest the haemoglobin and metabolize the glucose, through the anaerobic glycolysis. An infected RBC increases of 50-100% the consumption of glucose with the production of lactic acid. The degradation of Hb occurs in a specialized parasite organelle called the food vacuole. A number of studies have suggested that Hb degradation is a cooperative process that involves proteases of multiple catalytic classes, including cysteine, aspartic, and metallo proteases [9]. These proteases produce short peptides that are further degraded to amino acids, probably by aminopeptidases [10]. During the process of Hb degradation, heme group released in the food vacuole is toxic to *Plasmodium*, as it induces oxygen-derived free radical formation, lipid peroxidation and protein and DNA oxidation. Organisms such as *Plasmodium*, *Schistosoma*, and *Rhodnius*, which use Hb as a nutrient source, have evolved different strategies to detoxify this free heme group. *Plasmodium* spp. converts the heme group to β -hematin, which is a dark brown pigment also known as Hz, through a process that is essential for the life cycle of these organisms [14,15]. Hz is a cyclic dimer of ferriprotoporphyrin IX [Fe(III)PPIX] in which the propionate group of each Fe(III)PPIX molecule coordinates the Fe(III) centre of its partner [15].

The formation of mature schizonts containing a variable number of merozoites (24-32), entails their release and the lysis of erythrocytes. This process occurs every 48h corresponding with the parasite life cycle. During this event, the first clinic symptoms of the disease are shown: the characteristic fever ‘malignant tertian’ in *P. falciparum*, ‘benign tertian’ in *P. vivax* and *P. ovale* and ‘quartan’ in *P. malariae* (Fig 4.).

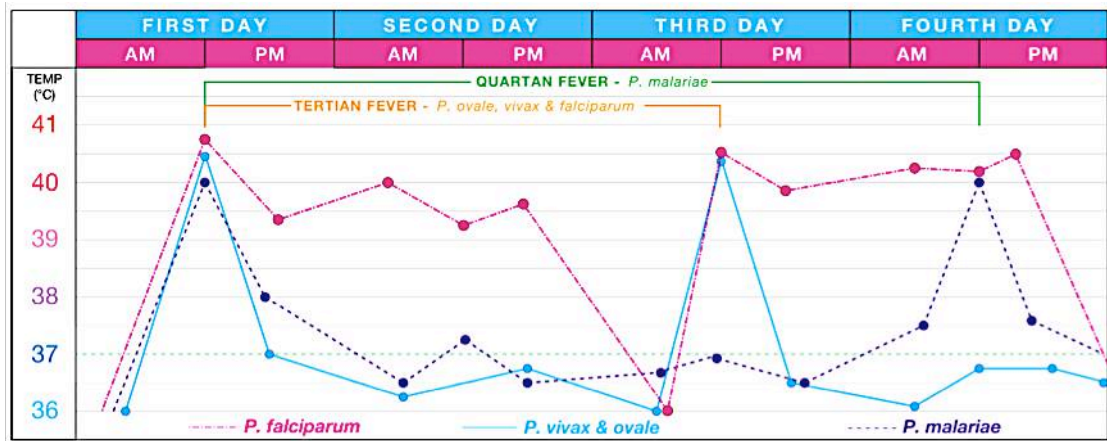


Fig. 4. Fever cycle in in different kind of plasmodium

1.3. Protection from Malaria infection

1.3.1. Genetic Factors

Biologic characteristics present from birth can protect against certain types of malaria. Two genetic factors, both associated with human red blood cells, have been shown to be epidemiologically important [13]. People who have the sickle cell trait (heterozygotes for the abnormal haemoglobin gene HbS) are relatively protected against *P. falciparum* malaria and therefore, hold a biologic advantage. As *P. falciparum* malaria has been a leading cause of death in Africa since remote times, the sickle cell trait is now more frequently found in this region and in people of African ancestry than in other population groups. In general, the prevalence of haemoglobin-related disorders and other blood cell dyscrasias, such as Hemoglobin C, the thalassemia and G6PD deficiency, are more prevalent in malaria endemic areas and are thought to provide protection from malarial disease.

Other genetic factors related to red blood cells also influence malaria but with a minor impact. Various genetic determinants (such as the “HLA complex,” which plays a role in control of immune responses) may equally influence an individual’s risk of developing severe malaria.

1.3.2. Acquired Immunity

Acquired immunity greatly influences how malaria, affects an individual and a community [13]. After repeated malaria infections a person may develop a partially protective immunity (Fig.5). Such “semi-immune” persons often can

still be infected by malaria parasites but may not develop a severe form of this disease, lacking any typical malaria symptoms indeed.

In areas with high *P. falciparum* transmission (most of Africa south of the Sahara), newborns will be protected during the first few months of life presumably by maternal antibodies transferred to them through the placenta. As these antibodies decrease with time, these young children become vulnerable to disease and death by malaria. In high transmission areas, young children are at major risk group and are targeted preferentially by malaria control interventions.

In areas with lower transmission (such as Asia and Latin America), infections are less frequent and a larger proportion of the older children (2-5 years old) and adults have no protective immunity. In such areas, malaria disease can be found in all age groups, and epidemics can occur.

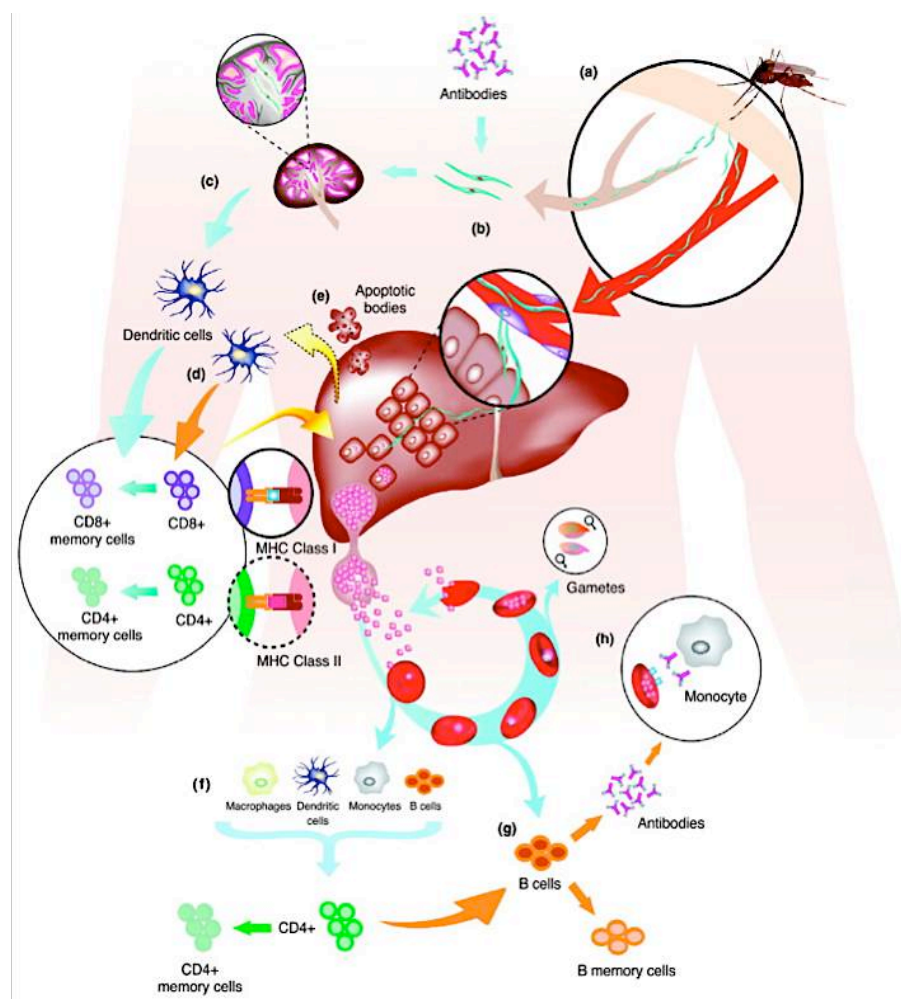


Fig. 5. Immune response with *P. falciparum* infection

1.4. Diagnosis of Malaria

Diagnosis of malaria depends on the demonstration of parasites in the blood, usually by microscopy. Additional laboratory findings may include mild anaemia, mild decrease in blood platelets (thrombocytopenia), higher bilirubin and aminotransferases. Depending on the malaria parasites, it may present a variety of symptoms [14], ranging from absent or very mild symptoms to severe disease and even death. For this reason, malaria disease can be classified as uncomplicated or complicated (severe) [15].

1.4.1. Uncomplicated Malaria

The classical (rarely observed) malaria attack lasts 6-10 hours. It consists of

- a cold stage (sensation of cold, shivering)
- a hot stage (fever, headaches, vomiting; seizures in young children)
- and finally a sweating stage (sweats, return to normal temperature, tiredness).

Usually attacks occur every second day with the “tertian” parasites (*P. falciparum*, *P. vivax*, and *P. ovale*) and every third day with the “quartan” parasite (*P. malariae*).

More commonly, the patient presents a combination of the following symptoms (Fig. 6):

- Fever
- Chills
- Sweats
- Headaches
- Nausea and vomiting
- Body aches
- General malaise

In countries where cases of malaria are infrequent, these symptoms may be attributed to influenza, cold, or other common infections, especially if malaria is

not suspected. On the other hand, in countries where malaria is frequent,

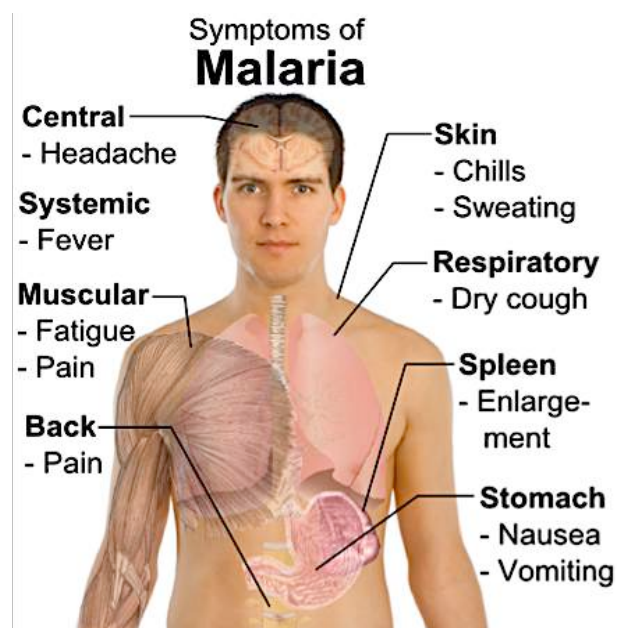


Fig. 6. Main symptoms of malaria

residents often recognize the symptoms as malaria and treat themselves without seeking diagnostic confirmation (“presumptive treatment”).

Physical signs may include:

- Elevated temperatures
- Perspiration
- Weakness
- Enlarged spleen
- Mild jaundice
- Enlargement of the liver
- Increased respiratory rate

1.4.1.1. Incubation Period

Following the infective bite by the Anopheles Mosquitos a period of time (the “incubation period”) elapses before the first symptoms appear (Tab.1). The incubation period in most cases varies from 7 to 30 days. The shortest periods are observed most frequently with *P. falciparum* and the longest ones with *P. malariae*.

Antimalarial drugs used for prophylaxis purposes by travellers can delay the appearance of malaria symptoms by weeks or months, long after the traveller has left the malaria-endemic area. (This can happen particularly with *P. vivax* and *P. ovale*, both of which can produce dormant liver stage parasites; the liver stages may reactivate and cause disease months after the infective mosquito bite.)

	Plasmodium species			
	<i>P. vivax</i>	<i>P. ovale</i>	<i>P. malariae</i>	<i>P. falciparum</i>
Pro-erythrocytic phase (days)	6-8	9	14-16	5-7
Erythrocytic cycle (hours)	48	50	72	48
Incubation period (days)	12-17 or even 6-12 months	16-18 or more	18-40 or more	9-14
Sporogony (days)	8-10	12-14	14-16	9-10

Tab. 1. Period of incubation in different species of plasmodium

Such long delays between exposure and development of symptoms can result in misdiagnosis or delayed diagnosis due to reduced clinical suspicion by the health-care provider. Returned travellers should always remind their health-care providers of any travel in areas where malaria occurs during the past 12 months.

1.4.2. Severe Malaria

Severe malaria occurs when infections are complicated by serious organ failures or abnormalities in the patient's blood or metabolism [16]. The manifestations of severe malaria include:

- Cerebral malaria, with abnormal behaviour, impairment of consciousness, seizures, coma, or other neurologic abnormalities
- Severe anaemia due to haemolysis (destruction of the red blood cells)
- Haemoglobinuria (haemoglobin in the urine) due to haemolysis
- Acute respiratory distress syndrome (ARDS), an inflammatory reaction in the lungs that inhibits oxygen exchange, which may occur even after the parasite counts have decreased in response to treatment
- Abnormalities in blood coagulation
- Low blood pressure caused by cardiovascular collapse
- Acute kidney failure
- Hyperparasitemia, where more than 5% of the red blood cells are infected by malaria parasites
- Metabolic acidosis (excessive acidity in the blood and tissue fluids), often in association with hypoglycaemia
- Hypoglycaemia (low blood glucose). Hypoglycaemia may also occur in pregnant women with uncomplicated malaria, or after treatment with quinine.
-

1.4.3. Cerebral malaria

Despite decades of research, cerebral malaria remains one of the most serious complications of *Plasmodium* infection [17]. The erythrocytes infected by parasite in the microcirculation, especially cerebral circulation have a tendency to accumulate, forming "rosette" (on the surface are present

plasmodium antigens that bond to the endothelial receptors) causing the formation of clots, blocking the bloodstream (Fig. 7).

This process is not a classic thrombosis, because is caused by infected RBCs. Since the brain and the hematic microcirculation cannot be infected, immediately the immune system induces an acute inflammatory response leading to a degeneration of cerebral tissue.

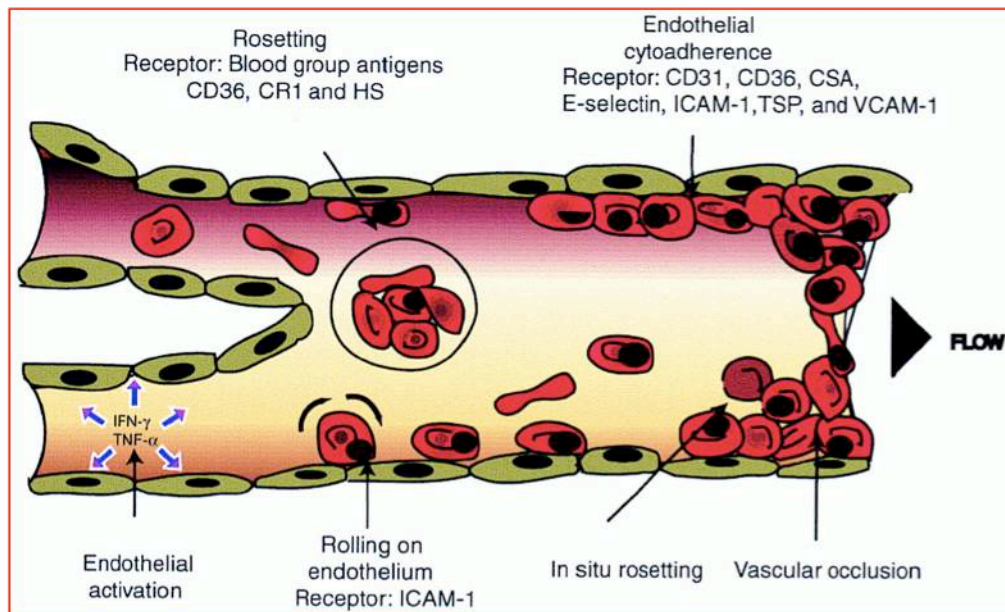


Fig. 7. Erythrocytes endothelial vessel adhesion with formation of clots

The process involves the release of the cerebral TNF and $\text{INF-}\gamma$, causing the increase of fever and definitely the death. During the lysis process, there is the release of a substance, known as hemozoin (the heme group is an amphipathic and toxic molecule, able to enter the membranes).

In order to detoxify from the heme, the parasite forms the crystals through the specific enzymes. The macrophages recognize the accumulation of heme and phagocyte it. Once phagocytize the heme, they cannot play their role and the consequence is an immunosuppression due to the complete blocking of phagocytosis functions of macrophages. Instead, the erythrocytes are seized in the microcirculation of some organs, as lung, heart, spleen and brain. Once seized, they release more heme causing a big inflammatory state that lead to the patient death.

1.5. Erythrocytes plasmatic membrane

The RBCs plasmatic membrane is constituted for 50% of protein (mainly intrinsic), 40% of lipids and 10% of carbohydrate. The erythrocyte is different from the other cells since the cytoskeleton forms a shell to support the plasmatic membrane.

1.5.1. Red blood cells plasmatic membrane structure

Protein Band 3 (Anion Exchange 1) is the main protein (25%) in the red blood cells membrane, involved in different cell process. Its molecular weight is 95 KDa and it can exist in monomeric, dimeric, tetrameric form or aggregates [18]. In the red blood cells, the Band 3 mediates the anionic exchange between the bicarbonate ion (HCO_3^-) presents in cytoplasm and ion chloride (Cl^-) presents in the plasma (Fig. 8).

The bicarbonate ion is involved in the following reaction catalysed from the carbonic anhydrase.



The presence of bicarbonate ion activates the Band 3 that through an anion exchange allows the diffusion of chloride ion. The reaction among a proton and anion chloride leads to the formation of hydrochloric acid that modify the pH to lower values (acidic). The presence of acidic cytoplasm, decrease the affinity between the haemoglobin and the oxygen in order to regulate the transfer of it to the tissues.

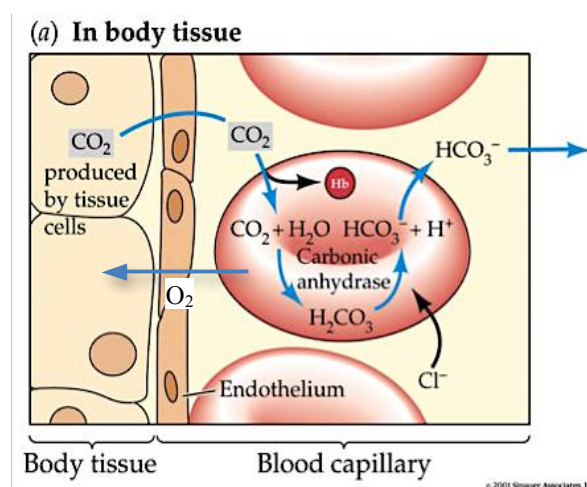


Fig. 8. Role of Band 3 in RBCs anion exchange

The protein Band 3 (Fig. 9) is composed of a transmembrane domain and two cytoplasmic domains [19]. Each protein domain has precise and different cellular functions:

- **The transmembrane hydrophobic domain** is a region of 52KDa, includes the aminoacidic residues 360-911, dipped in the bilayer phospholipidic forming a series of 12-14 folding. This domain lead to the formation of an anionic channel that allows the Exchange of Cl^- and HCO_3^- among the external and internal of cell.
- **The N-terminal hydrophilic domain (cytoplasmic domain)**, of 43KDa, includes the aminoacidic residues 1-359, known as cytosolic domain of Band 3 (cdb3). It penetrates in the cytosol playing a role of anchorage to the cytoskeleton and for some protein as haemoglobin and aldolase.
- **The C-terminal hydrophilic domain** includes the last 33 aminoacidic residues directed towards the cytoplasm.

At the **N-terminal domain** can bind different kind of proteins including the ankyrin and Band 4.1 and 4.2 that characterize the erythrocyte shape.

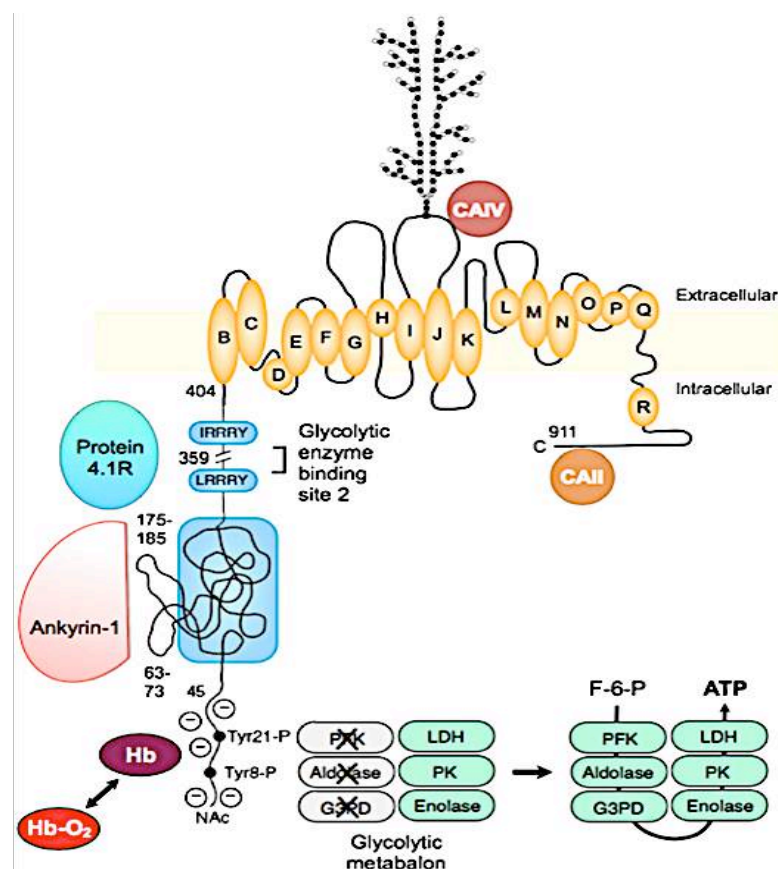


Fig. 9. Model of human erythrocyte band 3. The protein contains 2 structurally and functionally distinct domains: a cytoplasmic binding domain (amino acids 1-359) and a transmembrane domain (amino acids 360-911) that forms the anion-exchange channel

The cytoskeleton is constituted from the Ankyrin complex and Actin junctional complex (Fig.10). The cytoskeletal proteins are situated in the internal surface of erythrocyte membrane and it forms a fibrillar skeleton with the function of holding the red blood cell structure (Fig.11).

The Ankyrin protein has the role to bind the Band 3 with high molecular weight protein as the α and β spectrins, belonging to the erythrocytes membrane [20].

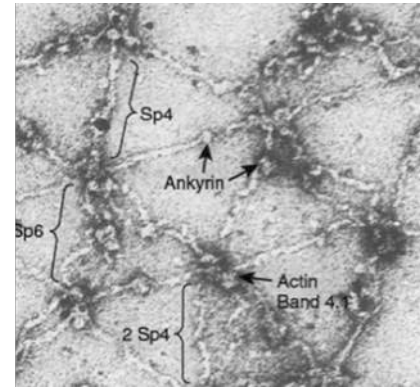


Fig. 11. Organization of the skeleton and the location of RBCs proteins in microscopy.

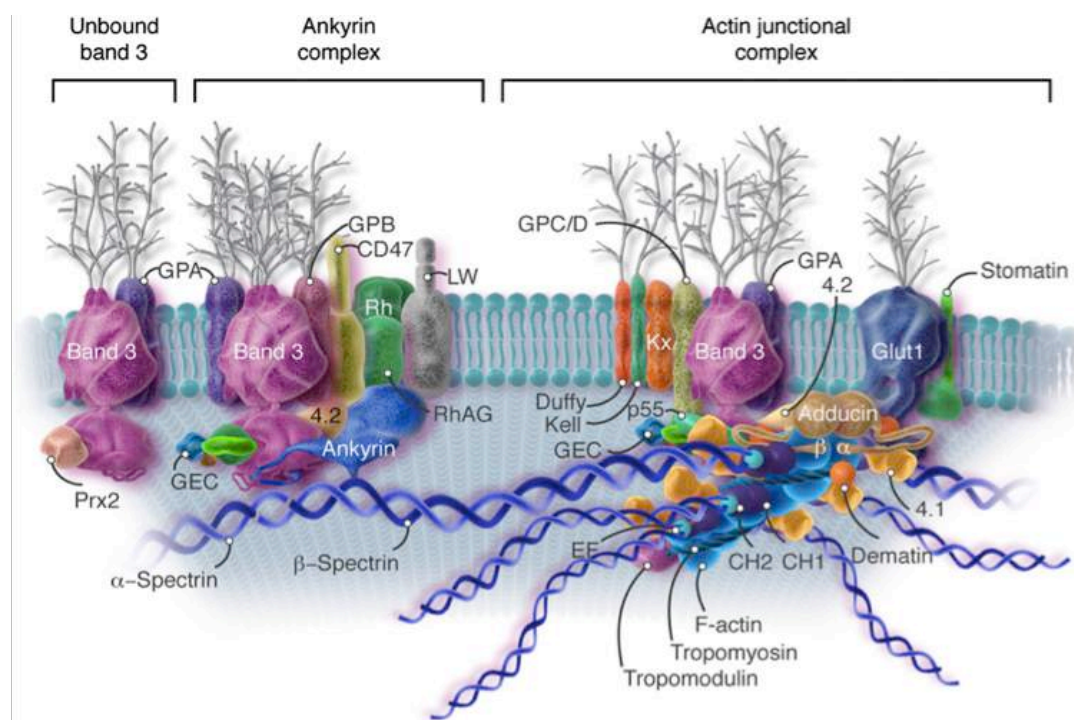


Fig. 10. Ankyrin and Actin junctional complex representation

These proteins create few anchorage points between the β subunit of spectrin and the integral proteins of membrane as Band 3 and glycoporin.

The spectrin dimers associate in tetramers, forming with other proteins as actin, adducin, 4.9 and 4.1 protein and tropomyosin, a fibrillar net (Fig.12) that contribute to stabilize the erythrocytes structure. Furthermore in the junctional complex are present three more proteins as adducin, P55 and dematin [21,22].

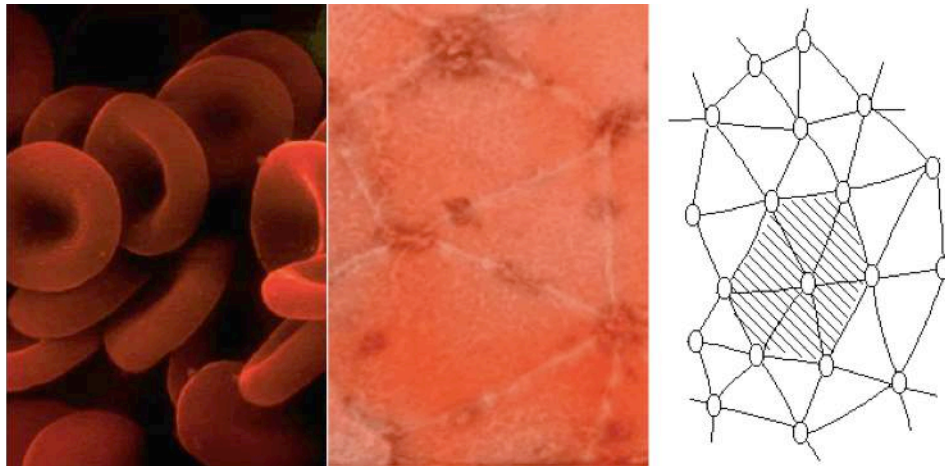


Fig. 12. Characteristic network structure of spectrin in RBCs

1.6. The spleen tyrosine Kinase (Syk)

Spleen tyrosine kinase (Syk, EC 2.7.10.2) is a cytosolic non-receptor tyrosine kinase (Fig.13) that performs its function downstream of antigen receptors in immune cells such as mast cells, B-lymphocytes, or macrophages. Syk is a crucial signal transducer of activated immunoreceptors to multiple events depending on the cell types including proliferation, differentiation, and phagocytosis [23-26]. Inhibiting this protein is possible to avoid all cascade of events causing the onset of many disorders. Furthermore Syk is one of the principal proteins involved in oxidative stresses processes. The therapeutic intervention on mechanisms in which Syk is involved might provide an attractive target for autoimmune or inflammation diseases [27].

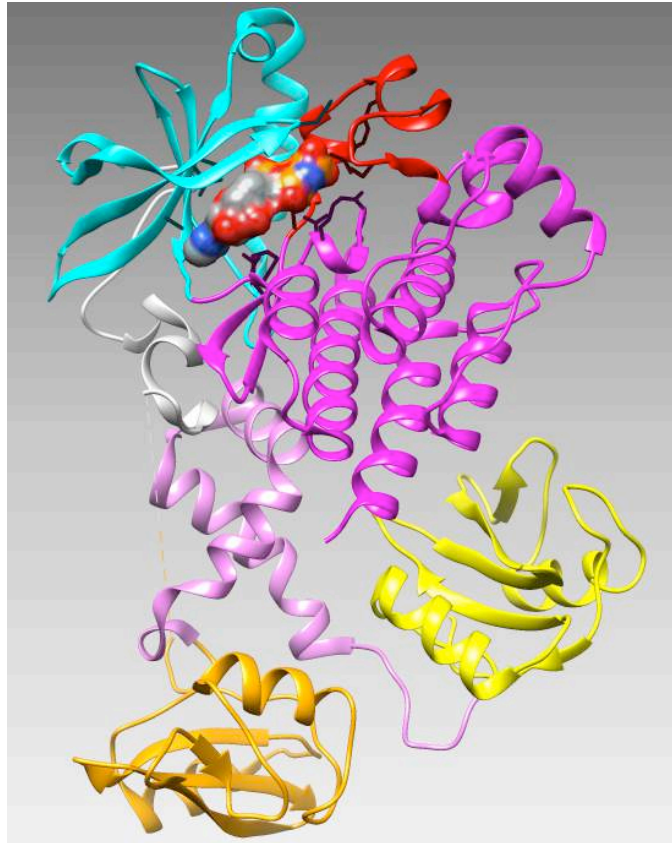


Fig. 13. 3D beta-sheet structure of Spleen tyrosine kinase (Syk) (PDB ID: 4FL2). Represented with yellow is the **N-SH2 domain**; cyan the **interdomain linker SH2**; orange the **C-SH2 domain**; grey the **interdomain linker**; magenta and water green **the catalytic domain or SH1** and with red **the activation loop**.

Syk belongs to the same subfamily as the closely related Zeta-chain-associated protein kinase 70 (ZAP-70). The Spleen tyrosine kinase (72KDa) is composed of two Src homology tandem domains defined N-SH2 and C-SH2; these are important for the activity regulation and to localize this kinase in cell membrane (Fig.14).

The protein consisting of:

- **a tandem SH2 module (N-SH2 and C-SH2)**, that presents an α -helix which has an important role in the interaction protein-protein and serves as a docking platform for immune receptor tyrosine-based activating motifs (ITAMs) which are displayed on the cytosolic side of the plasma membrane

- **an interdomain linker SH2**, between N-SH2 and C-SH2 constituted of 50 amino acids; it represents the most conserved region in family kinase with 65% of homology sequence.
- **an interdomain linker** of 80-100 amino acids located between C-SH2 and catalytic domain and it is important to regulate the kinase activity and for the presence of phosphotyrosine residues.
- **a catalytic domain or SH1** constituted of 300 amino acids follows the interdomain linker. It contains the binding sites for ATP and two autophosphorylation sites (Tyr525 and Tyr526).

Syk protein ends with a **C-terminal tail** with unidentified function yet.

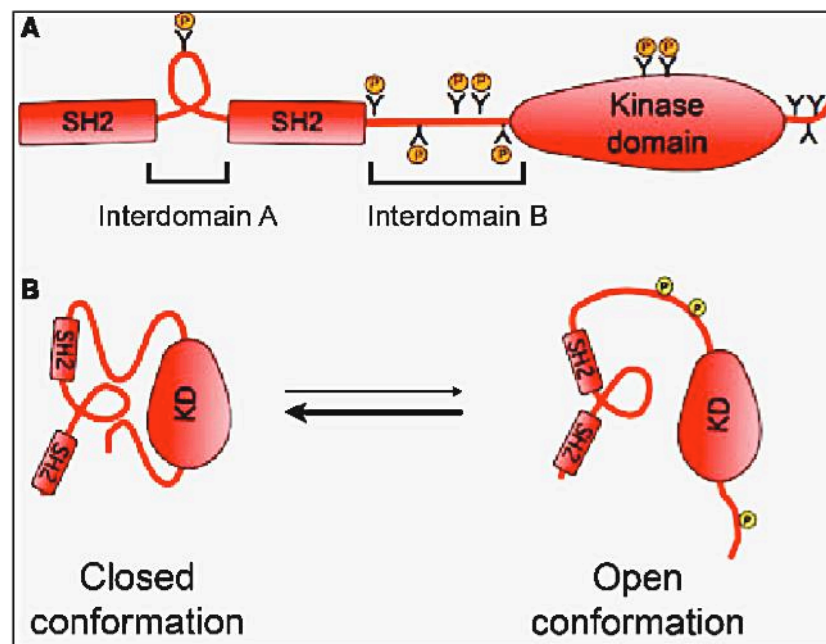


Fig. 14. Graphical abstract showing Syk protein (A) and its closed and open conformation (B), [28].

The comparison of inactive and phosphorylated Syk structures reveals significant movement of the tandem SH2 domains region that could disrupt the interaction with the kinase domain characteristic of the inactive state. These data with that reported by different authors permitted the proposal of a model for the regulation of Syk kinase.

Syk is maintained in auto-inhibited conformation by the interaction involving the tandem and kinase domains.

Recent studies have previously observed that the erythrocytes possess a mechanism finalized to the expulsion of denatured haemoglobin requiring the activation of Syk kinase [29]. Syk kinase could play a role in the process of asexual *P. falciparum* growth [30,31] as malaria parasite exerts oxidative stress in erythrocytes causing the denaturation of haemoglobin, with formation of aggregates known as haemichromes in which the Fe^{2+} has been oxidized to Fe^{3+} . The haemichromes binding to band 3 cause its oxidation and its subsequent phosphorylation by Syk kinase especially in two aminoacidic residues of Band 3 (Tyr 8 and 21). The Anion exchange 1 (AE1) is the more abundant protein of the red cell membrane constituting the major linkage between the lipid bilayer and the cytoskeleton. Under steady conditions, this linkage confers to the membrane the required elasticity and mechanical stability. The oxidation of band 3 and its phosphorylation by Syk protein, cause its detachment from the cytoskeleton and the destabilization of the membrane with the release of microvesicles containing band 3 (Fig.15), membrane and haemichromes. [32-36].

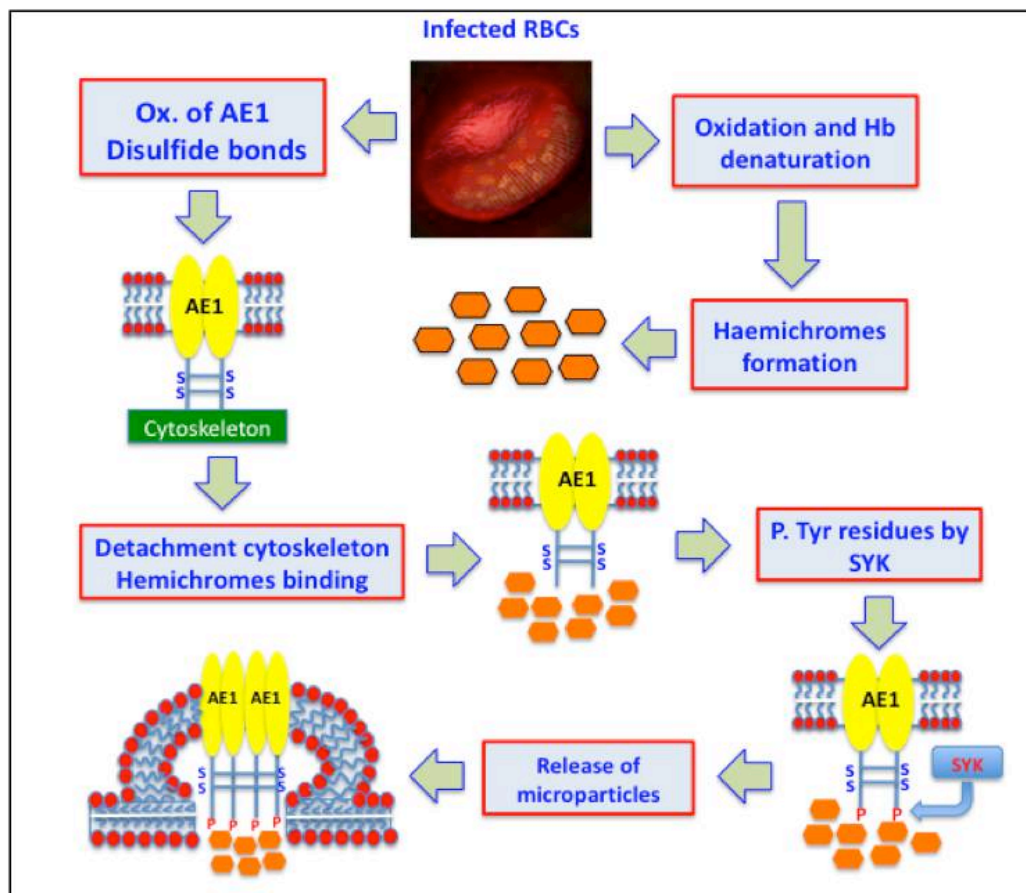


Fig. 15. Graphical abstract of the mechanism, which leads to the release of microparticles

1.7 Treatments for Malaria

1.7.1. Artemisinin and Artemisinin derivatives

Artemisinin (ART) and its semi-synthetic derivatives are a group of drugs used against *Plasmodium falciparum* malaria [37]. Treatments containing an artemisinin derivative actually represent the standard therapies worldwide for *P. falciparum*. Artemisinin is isolated from the plant *Artemisia annua*, (Fig.16) sweet wormwood, an herb employed in Chinese traditional medicine.



Fig. 16. *Artemisia Annua*

Chemically, artemisinin is a sesquiterpene lactone containing an unusual peroxide bridge (Fig.17). This peroxide is believed to be responsible for the drug's mechanism of action. Few other natural compounds with such a peroxide bridge are known [38].

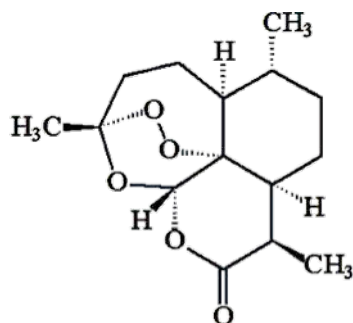


Fig. 17. Structure of Artemisinin

Artemisinin and its endoperoxide derivatives have been used for the treatment of *P. falciparum* related infections but low bioavailability, poor pharmacokinetic properties and high cost of the drugs are a major drawback of their use.

Use of the drug by itself as a monotherapy is explicitly discouraged by the World Health Organization, which declared that malarial parasites are developing resistance to the drug [39].

Therapies that combine artemisinin or its derivatives with some other antimalarial drug are the preferred treatment for malaria and are both effective and well tolerated in patients.

1.7.1.1. The artemisinin mechanism of action

The mechanism of action of artemisinin is not known, but the most widely accepted theory is that they are first activated through cleavage after reacting with heme and iron (II) oxide, which results in the generation of free radicals that in turn damage susceptible proteins, resulting in the death of the parasite [40,41]. In 2016 artemisinin was shown to bind to a large number of targets suggesting that it acts in a promiscuous manner [42].

1.7.1.2. Artemisinin derivatives

Because the physical properties of artemisinin itself, such as poor bioavailability, limit its effectiveness, semisynthetic derivatives of artemisinin have been developed. These include:

- Artesunate (AS), (water-soluble: for oral, rectal, intramuscular, or intravenous use)
- Artemether (ATH), (lipid-soluble: for oral, rectal or intramuscular use)
- Dihydroartemisinin (DHA).
- Artelinic acid
- Artemotil

Dihydroartemisinin (Fig.18) in particular (also known as dihydroqinghaosu, artemimol or **DHA**) is the active metabolite of all artemisinin compounds (artemisinin, artesunate, artemether, etc.) and is also available as a drug in itself. It is a semi-synthetic derivative of artemisinin and is widely used as an intermediate in the preparation of other artemisinin-derived antimalarial drugs [43]. It is sold

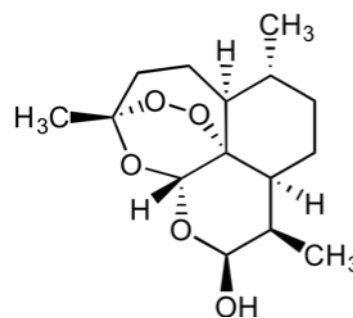


Fig. 18. Structure of Dihydroartemisinin

commercially in combination with piperazine (PPQ) and has been shown to be equivalent to artemether/lumefantrine (LMF) [44].

The proposed mechanism of action of artemisinin involves cleavage of endoperoxide bridges by iron, producing free radicals (hypervalent iron-oxo species, epoxides, aldehydes, and dicarbonyl compounds), which damage

biological macromolecules causing oxidative stress in the cells of the parasite [45]. Malaria is caused by apicomplexans, primarily *Plasmodium falciparum*, which largely reside in red blood cells and itself contains iron-rich heme-groups (in the form of hemozoin) [46]. In 2015 artemisinin was shown to bind to a large number targets suggesting that it acts in a promiscuous manner. Recent studies discovered that artemisinin targets a broad spectrum of proteins in the human cancer cell proteome through heme-activated radical alkylation [47].

1.8. Artemisinin-based combination therapies (ACTs)

The artemisinin-combination therapies (ACTs) have been integrated to the recent success of global malaria control, and protecting their efficacy for the treatment of malaria is a global health priority. The World Health Organization (WHO) recommends ACTs for the treatment of uncomplicated malaria caused by *P. falciparum*.

The main advantage of ACTs is that the artemisinin quickly reduces most of the malaria parasites and the partner drug clears the remaining ones. However, the efficacy of ACTs is threatened by the emergence of both artemisinin and partner drug resistance. Partial resistance to artemisinin causes delayed parasite clearance following treatment with an ACT. Such resistance does not usually lead to treatment failure; however, if the artemisinin component is less effective, the partner drug has to clear a greater parasite mass, jeopardizing the future efficacy of the partner drug.

In addition, partner drug resistance can arise independently of artemisinin resistance. Given that an effective partner drug is essential for clearing all remaining parasites, partner drug resistance carries a high risk of treatment failure. Because of their different roles, the efficacy of the artemisinin and the partner drug must be monitored concomitantly but separately.

1.9. Drug resistance development

Resistance and treatment failures to antimalarial medicines can be defined as follows:

- **Antimalarial resistance** is defined as the ability of a parasite strain to survive and/or multiply despite the administration and absorption of a drug given in doses equal to or higher than those usually recommended but within tolerance of the subject;
- **Artemisinin partial resistance** is defined as delayed parasite clearance following treatment with an artesunate monotherapy or with an ACT – this represents partial resistance;
- **Multidrug resistance (MDR)** is resistance to more than 2 antimalarial compounds of different chemical classes. This term usually refers to *P. falciparum* resistance to chloroquine, sulfadoxine-pyrimethamine, and a third antimalarial compound;
- **Treatment failure** is the inability to clear parasites from a patient's blood or to prevent their recrudescence after the administration of an antimalarial. Many factors can contribute to treatment failure, including incorrect dosage, poor patient compliance, poor drug quality, and drug interactions and resistance. Most of these factors are addressed by therapeutic efficacy studies.

In reporting the findings of therapeutic efficacy studies, the term "ACT resistance" is imprecise. ACT treatment failure (defined as treatment failure following treatment with an ACT, regardless of the presence of artemisinin partial resistance) is a more appropriate term that notes the specific ACT and the nature of the resistance if confirmed (i.e. artemisinin partial resistance or partner drug resistance, or both). The problem of antimalarial drug resistance is compounded by cross resistance, in which resistance to one drug confers resistance to other drugs that belong to the same chemical family or which have similar modes of action.

1.9.1. State of partial artemisinin resistance around the world

Artemisinin partial resistance likely emerged prior to 2001, and prior to the widespread deployment of ACTs in the GMS. To date, it has been confirmed in 5 countries of the GMS: Cambodia, the Lao People's Democratic Republic, Myanmar, Thailand and Viet Nam.

In late 2013, researchers identified a new molecular marker: mutations in the Kelch 13 (K13) propeller domain were shown to be associated with delayed parasite clearance *in vitro* and *in vivo* [48]. The molecular marker allows for a more precise mapping and monitoring of the geographical distribution of resistance. It could also be a mechanism for retrospective mapping of resistance in a large number of settings.

Parasites carrying mutations in the K13 propeller domain have been reported in all 5 GMS countries listed above as well as in Guyana, where studies are ongoing to evaluate impact of this mutation on delayed clearance and ACT efficacy and its potential spread within and outside South America.

Molecular studies have shown that partial artemisinin resistance has emerged independently in several locations in the GMS and spread within the subregion. The K13 mutation identified in South America has also emerged independently. Artemisinin partial resistance has not been confirmed in Africa. Partial artemisinin resistance has occurred as a consequence of several factors: poor treatment practices, inadequate patient adherence to prescribed antimalarial regimens, and the widespread availability of oral artemisinin-based monotherapies and substandard forms of the drug.

1.9.2. Current state of ACT failures

Artemisinin resistance alone rarely leads to treatment failure. However, resistance of malaria parasites to ACT partner drugs can lead to treatment failure (regardless of the presence of artemisinin partial resistance). As a consequence, WHO in the 2017 Malaria report showed the maps of several ACTs that are failing (Artesunate-Amodiaquine) in the African regions (Fig.19) and Greater Mekong area (Artemether-Lumefantrine), (Fig.20).

The geographic scope of the problem could widen quickly and have important public health consequences: the spread or independent emergence of partner

drug resistance or multidrug resistance globally could pose a public health threat, as no alternative antimalarial medicine is available at present with the same level of efficacy and tolerability as ACTs [49].

The efficacy of WHO-recommended ACTs is assessed through therapeutic efficacy studies (TES). Such studies at regular intervals at the same sites allow for the early detection of declines in drug efficacy, providing evidence for guiding national malaria treatment policies.



Fig. 19. Map indicating the % of patients with ACT treatment failure (Artesunate-Amodiaquine)

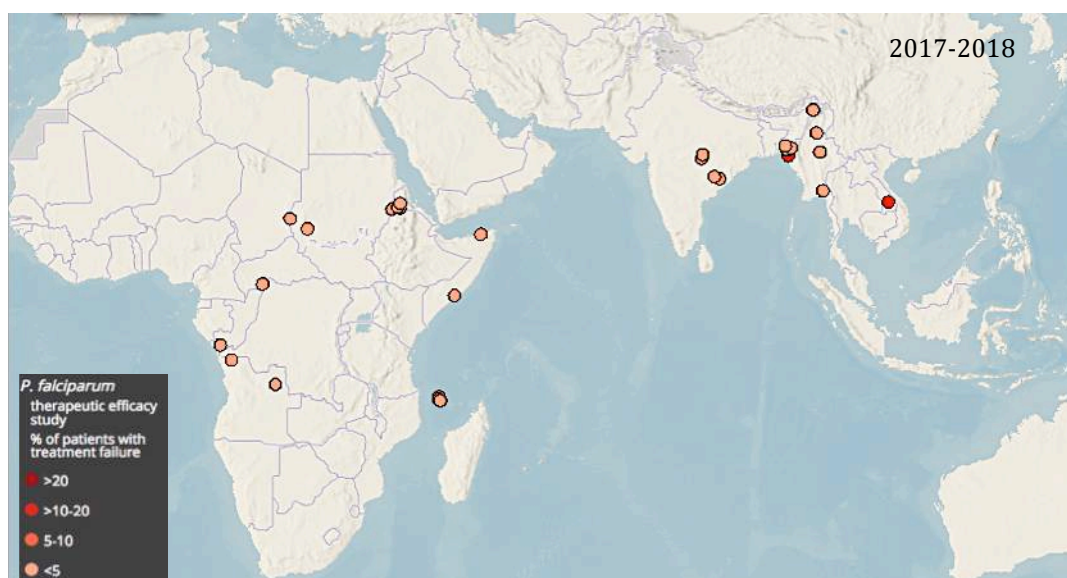


Fig. 20. Map indicating the % of patients with ACT treatment failure (Artemether-Lumefantrine)

Taking in consideration the resistance increasing, the monotherapy with artemisinin and ART derivatives is strongly not recommended and for this

reason, the ACT is substituted from the standard therapy. The development and research of new antimalarial drugs is necessary to avoid the increasing of parasite resistance. A promising approach in the antimalarial therapy consists in utilization of Syk kinase inhibitors with the purpose to block the expulsion of denatured haemoglobin and its accumulation inside the parasitized erythrocytes [50] and not allow the growth and proliferation of plasmodium. Moreover, an innovative method as molecular modelling appears an interesting way to better understand and explain the biological mechanism and discover some molecules able to inhibit the protein target.

1.10. Computational studies to explain the biological phenomenon

In the last years, several researches about the *in vitro* experiments on biological mechanism supplemented of computational sciences have led to the development of different molecular modelling approaches. Actually is possible to determine several molecules conformation, to evaluate the free energy and compounds energy of binding and calculate the molecular descriptors (lipophilicity, molecular electrostatic potential, molecule volume, accessible surface to the solvent and molecular orbitals). Moreover, different software has been developed in order to simulate the ligand-protein interaction, protein-protein with or without solvent aimed to a rational drugs design. These techniques, in a multidisciplinary approach, represent the interface among chemistry, biology and computational science with the purpose to study and deepen the interaction between the proteins and the ligand with low molecular weight and the different mechanism of action.

Many studies demonstrated that the molecular modelling can be a powerful methodology for biomedical research, useful for analysing the three dimensional structure of biological macromolecules with the aim to better understand and explain the cell processes as well as for drug discovery in pharmaceutical science and research in bionanotechnology [51-53].

The main approaches used in molecular modelling for studying the biological systems and the molecule interacting with the human protein, regard:

- **Conformational analysis** is necessary to determine the protein and ligands conformations with the lowest energy and protein flexibility, namely the more stable and with a better interaction in the biological environment. For this reason, have been used techniques of Molecular Mechanics (MM) that are involved in most of Computational Structure-Based Drug Discovery (CSBDD) projects [54].

The conformational research has been carried out using the compound of interest seeking the minimum conformational (the different disposition of that structure in the space) depending from the number of different simple bond that are present in the molecule. This phase is even known as “minimization”. The following step consist on the computation of the best energy (the lowest value) using the Quantum Mechanics (QM), which is the science that explains the behaviour of matter and its interactions with energy on the scale of atoms and subatomic particles. This method allows the computation of bond length, binding angles and charge density with short time for small molecules and longer time with more atoms in compounds [55].

- **Virtual screening (VS)** is a computational technique used in drug discovery to search libraries of small molecules in order to identify those structures, which are most likely to bind to a drug target, typically a protein receptor or enzyme [56-58]. Virtual screening has been defined as the "automatically evaluating very large libraries of compounds" using computer programs. As this definition suggests, VS has largely been a numbers game focusing on how the enormous chemical space of over 10^{60} conceivable compounds can be filtered to a manageable number that can be synthesized, purchased, and tested [59]. Although searching the entire chemical universe may be a theoretically interesting problem, more practical VS scenarios focus on designing and optimizing targeted combinatorial libraries and enriching libraries of available compounds from in-house compound repositories or vendor offerings. As the accuracy of the method has increased, virtual screening has become an integral part of the drug discovery process [60].

Virtual Screening can be used to select in house database compounds for screening, choose compounds that can be purchased externally, and to choose which compound should be synthesized next.

Ligand-Based Virtual Screening (LBVS)

Given a set of structurally diverse ligands that binds to a receptor, a model of the receptor can be built by exploiting the collective information contained in such set of ligands. These are known as pharmacophore models. A candidate ligand can then be compared to the pharmacophore model to determine whether it is compatible with it and therefore likely to bind [61].

A popular approach to ligand-based virtual screening is based on searching molecules with shape similar to that of known actives, as such molecules will fit the target's binding site and hence will be likely to bind the target.

Structure-Based Virtual Screening (SBVS)

Structure-based virtual screening involves docking of candidate ligands into a protein target followed by applying a scoring function to estimate the likelihood that the ligand will bind to the protein with high affinity [62-64]. Web servers oriented to prospective virtual screening are available to everyone [65,66].

Structure-based VS for drug discovery (SBDD) is becoming an essential tool in assisting fast and cost-efficient lead discovery and optimization. The application of rational, structure-based drug design is proven to be more efficient than the traditional way of drug discovery since it aims to understand the molecular basis of a disease and utilizes the knowledge of the three-dimensional structure of the biological target in the process.

- **Docking** is a detailed study of protein-ligand or protein-protein interaction aimed to explain their chemical behaviour and biological activity or give more information about unknown mechanism of action. The disadvantage of this method consists in the fact it cannot take in consideration the concentration of compounds such as in the *in vitro* studies. For this reason, the *in silico* obtained results may not be related to *in vitro* data. The protein is blocked in a position derivate from the X-ray crystal structure while the

ligand is examined to see how it interacts with the protein once is established the binding site. The obtained results are analysed in basis on how many times a single conformation of compound interacts with the macromolecule in a precise site with a lowest value of Energy. In this phase, the molecule can freely move in the protein changing its conformation to better adapt to binding site of protein but is not possible changing the bonds length. For this reason is important to carry out the quantum mechanics calculation in order to give more information about the specific bonds length [67].

- **Molecular dynamics (MD)** is a computational method for studying the physical movements of atoms and molecules over time in which the simulation is implemented from nanoseconds (ns) up to a maximum of seconds (s) depending from the facilities used for the computation. The interaction of atoms and molecules is allowed for a fixed period of time, giving a view of the dynamic evolution of the system. In the most common version, the trajectories of atoms and molecules are determined by numerically solving Newton's equations of motion for a system of interacting particles, where forces between the particles and their potential energies are often calculated using interatomic potentials with molecular mechanics force fields. Using the molecular dynamic we observe as the molecules move into the protein site of interaction surrounded by thousands of water molecules in order to simulate the biological environment [68].

Actually, the molecular modelling represents one of the fastest growing fields in science. It may vary from building and visualizing simple molecules in three dimensions (3D) to performing complex computer simulations on large proteins and nanostructures. Molecular modelling is a collection of computer-based techniques for driving, representing and manipulating the structures and reactions of molecules, and those properties that are dependent on these 3D structures. The techniques *in silico* cover several issues among them computational chemistry, drug design, computational biology, nanostructures, and material science [69].

The so far carried out studies for the development of new *in silico* drugs and the laboratory tests have been focused on different molecules that can be used as possible drugs for the protein complex inhibition needed for the growth and proliferation of malaria parasite [70-72].

Computational studies conducted on protein kinases (Pks) of *Plasmodium falciparum* are of particular interest since they catalyse a reaction of phosphorylation to control the parasite growth and differentiation throughout its life cycle.

In 2011 started a new project known as GO (Global Online) Fight Against Malaria belonging at the IBM (International Business Machines) World Community Grid. At this project participated the Art Olson Lab of TSRI (The Scripps Research Institute) in San Diego, CA, USA. This laboratory is one of the leaders in this sector and its effort consists to discover promising drug candidates that could be developed into new drugs that cure drug resistant forms of malaria. The computing power of World Community Grid has been used to perform computer simulations of the interactions between millions of chemical compounds and certain target proteins, to predict their ability to eliminate malaria. The best compounds were tested and further developed into possible treatments for the disease.

Following these ideas, we developed and took in consideration some chemical compound. The host target Drug resistance arguably constitutes the biggest problem faced in the field of infectious diseases today and is a major obstacle to the development of effective strategies to combat infection. Pathogens, particularly those with an intracellular habitat, exploit and subvert various host factors for survival and growth in an otherwise hostile environment. As such, one possible way to circumvent the emergence of a pathogen's resistance is to develop drugs that target non-essential host factors hijacked by the pathogen rather than the pathogens own molecules. Indeed, host proteins are generally well conserved, when compared with the genetic variability of many pathogens [74].

1.11. Syk inhibitors as treatment for malaria

The human genome contains more than 500 PKs that are implicated in nearly all the signalling pathways. The attractiveness of PKs as possible drugs targets is enhanced by the fact that they are enzymes whose biological activity can be turned off by drugs that block their catalytic site. Indeed, although PKs are encoded by less than 2% of the human genome, they represent more than 20% of the druggable genome.

In a number of diseases, specific inhibitors of individual PKs have proved beneficial to cure tumours or other pathologies, and have entered clinical practice or advanced clinical trials [75].

In recent years, a great number of ATP-competitive kinase inhibitors have been isolated from the natural source or synthesized. These compounds are small molecules that interact with the ATP-binding site with high affinity blocking the phosphorylation process of the protein (Fig.21).

A characteristic and drawback of the more active compounds is the lack of selectivity towards the ATP-binding site present in different proteins and especially in kinase enzymes: this reduces or makes pointless the possibility of their clinical application. Despite exists a high sequence similarity in the kinases aminoacidic sequence, several research groups have been able to develop highly potent and selective Syk ATP-competitive inhibitors.

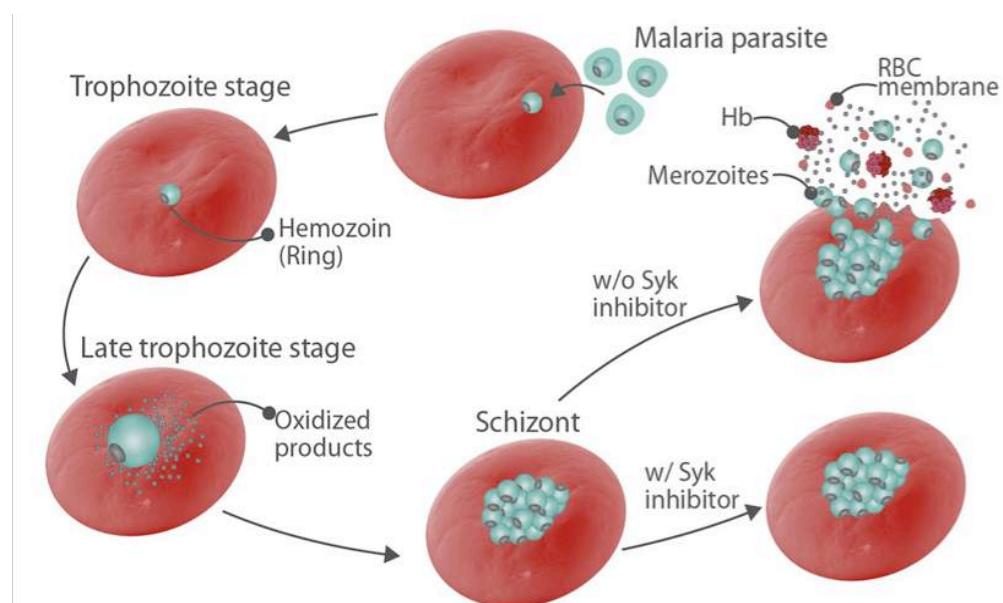


Fig. 21. The biological activity of Syk inhibitors in infected erythrocytes.

1.11.1. Kinase inhibitors mainly used in therapy

Imatinib: (4-[(4-Methyl-1-piperazinyl)methyl]-N-[4-methyl-3-[[4-(3-pyridinyl)-2-pyrimidinyl]amino]-phenyl]benzamide (Fig.22). It is known as Gleevec in United States and Glivec in Europe, in commerce from pharmaceutical company Novartis. It is drug non-specific for Syk protein (IC_{50} of $5\mu M$); it is a well-tolerated tyrosine kinase inhibitor that is FDA-approved for use in children, prevents parasite-induced tyrosine phosphorylation of band 3 and terminates *P. falciparum* parasitemia in vitro by blocking parasite egress at clinically relevant concentrations [76]. This Drug is also already used for different cancer as Chronic Myeloid Leukaemia (CML), Acute Lymphoblastic Leukaemia (ALL) and gastrointestinal stromal tumour (GIST).

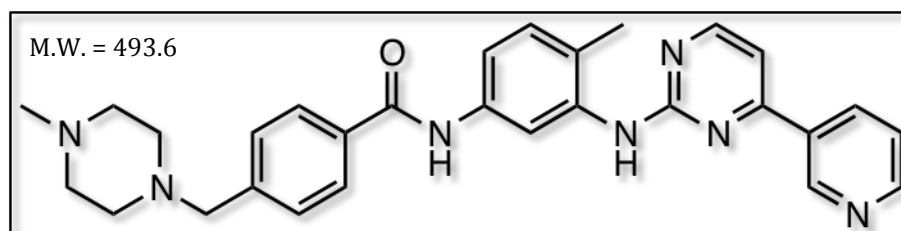


Fig. 22. Structure of Imatinib (Gleevec)

R406(tamatinib):6-(5-fluoro-2-(3,4,5-trimethoxyphenylamino) pyrimidin-4-ylamino)-2,2-dimethyl-2H-pyrido[3,2-b][1,4]oxazin-3(4H)-one (Fig.23). It is an active metabolite of prodrug R788 (fostamatinib) specific, ATP-competitive inhibitor of spleen tyrosine kinase (Syk), which plays a key role in the signalling of activating Fc receptors and the B-cell receptor. It presents an IC_{50} of 41 nM [77] and it is already used in clinical trial for rheumatoid arthritis [78], autoimmune thrombocytopenia [79], autoimmune haemolytic anaemia, IgA nephropathy [80] and Lymphoma [81].

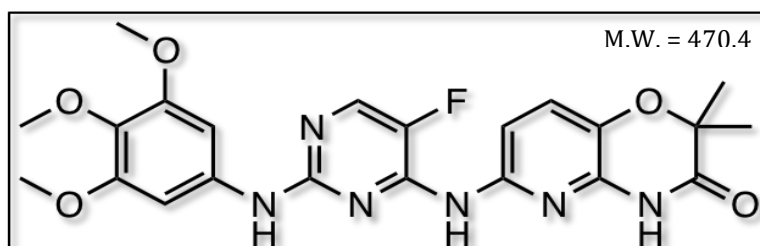


Fig. 23. Structure of R406 (tamatinib)

P505-15:4-((3-(2H-1,2,3-triazol-2-yl)phenyl)amino)-2-(((1R,2S)-2-amino-cyclohexyl)amino)pyrimidine-5-carboxamide-hydrochloride (Fig.24). It is a novel, highly selective Syk inhibitor with IC_{50} of 1 nM in cell-free assays, >80-fold selective for Syk than Fgr, Lyn, FAK, Pyk2 and Zap70. Candidate drug already used in vivo studies in mice for rheumatoid arthritis and used for the treatment of non-Hodgkin lymphoma (NHL) and chronic Lymphocytic Leukaemia (CLL) [82,83].

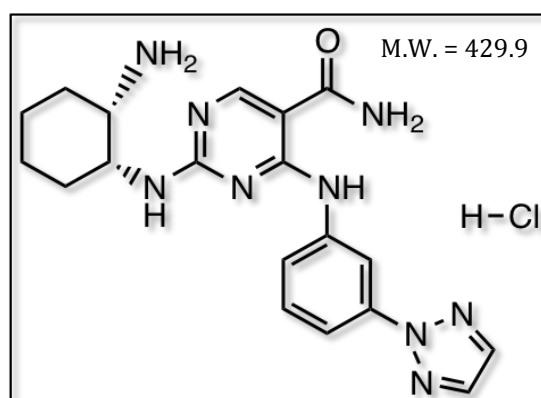


Fig. 24. Structure of P505-15

Syk-inhibitor-II:2-(2-Aminoethylamino)-4-(3-trifluoromethylanilino)-pyrimidine-5-carboxamide (Fig.25). It is a cell-permeable compound that acts as a potent, selective, reversible, and ATP-competitive inhibitor of Syk with IC_{50} 41 nM already used for inhibition of serotonin (5-HT) release in rat basophilic leukaemia (RBL) cells and to treat allergic diseases [84,85].

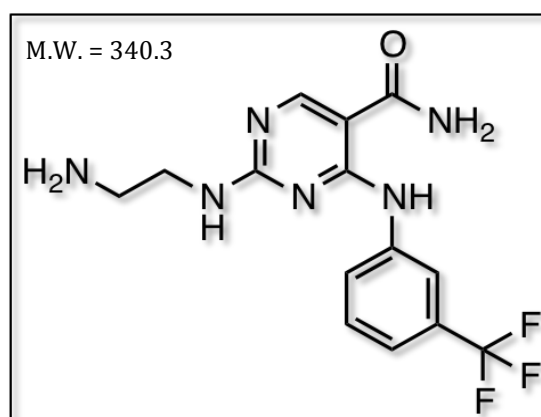


Fig. 25. Structure of Syk inhibitor II

Another Syk inhibitor has been taken in consideration but with less importance considering the low inhibition efficacy *in vitro* tests, although the IC₅₀ concentration of enzymatic assay reported in literature shows a highly potent compound.

Syk-inhibitor-IV:2-(7-(3,4-Dimethoxyphenyl)-imidazo[1,2-c]pyrimidin-5-ylamino)-nicotinamide (Fig.26). Cell permeable imidazopyrimidine compound that acts a potent, ATP-competitive, reversible, and highly selective inhibitor of Syk tyrosine kinase activity (IC₅₀ = 10 nM) with no inhibitory effect against Btk, Fyn, Itk, Lyn, and Src even at concentrations as high as 4.7 μM. This compound showed to inhibit Syk-mediated cellular functions *in vitro* [86] and exhibit good oral bioavailability and *in vivo* efficacy in the treatment of various allergy and asthma conditions in rat models [87].

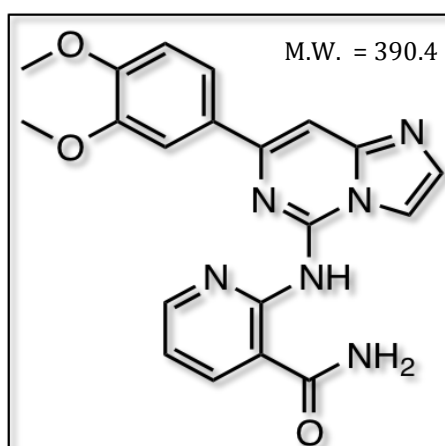


Fig. 26. Structure of *Syk inhibitor IV*

2. Aim of the project

Recently, a new phosphorylative pathway involved in the release of denatured haemoglobin products (haemichromes), bound to erythrocyte membranes through the cytoplasmic domain of the AE1 (band 3 protein), has been characterized. Tyr phosphorylation of the band 3 protein carried out mainly by the erythrocytic Syk kinase mediates this process. Phosphorylated band 3 becomes uncoupled from the cytoskeleton, leading to the formation of membrane clusters containing haemichromes – band 3 aggregates that can either be released from red blood cells as microvesicles or picked by spleen macrophages by a mechanism known as erythrocyte pitting. These mechanisms may be responsible for the elimination of noxious aggregates of denatured haemoglobin; indeed, during their 120-day lifespan, erythrocytes undergo dramatic changes, eliminating approximately 30% of the initial haemoglobin content of the membrane surface. Moreover, it has been observed that those modifications are an essential prerequisite for parasite egression from the host cell constituting the theoretical background of the observed anti-plasmodial activity of Syk inhibitors. Due to the mechanism describe above, in the present thesis the main purpose consists in studying and understanding the effects of different Syk inhibitors on critical events during parasite growth and maturation within the human erythrocyte.

In particular, the central concept was to leverage *in vitro* and computational tools to allow efficient therapy using Syk inhibitors and targeting the host red blood cell instead of parasite, in order to interfere with the growth and reinfection capability of parasite. Taking in consideration that Syk inhibitors block the phosphorylation events, is necessary to have more knowledge on the mechanisms responsible of the protein-ligand recognition and binding, in order to facilitate the design, development and discovery of new promising class of antimalarial drugs. A detailed analysis of Syk /ligand interactions is, therefore the central focus in order to understanding the biological process at the molecular level, also obtaining useful information on the pharmacophore structure of Syk inhibitors. Finally, this research has the purpose to prevent as much as possible the drug resistance by Plasmodium, improving and modifying the compounds structure or screen new molecules with a specific

diversity set selected from database to obtain the highest efficacy in infected RBCs. *In vitro* experimental methods are mainly focused on the evaluation of proteomic profile of Tyr phosphorylation related to biological tests on *Plasmodium falciparum* cultures, whereas *in silico* methods were based on different molecular modelling approaches as the molecular descriptors study, docking, virtual screening (VS) and molecular dynamics (MD).

The inhibition of Syk kinase by small molecules, competing with ATP-binding site, represents a certain approach already approved in the last years for the successful treatment of allergic and antibody-mediated autoimmune diseases, depending on Syk kinase activity, as well as for the treatment of lymphoma and leukaemia. A very interesting way to develop new drugs consists in the use of Quantum Mechanics (QM) method and molecular descriptors as electronic density, molecular electrostatic potential (MEP) and the charge distribution in order to characterize the ligands.

3. MATERIALS & METHODS

In this work, we performed a series of *in vitro* experiments using infected RBCs in order to investigate the biological activity of different Syk inhibitors on *P. falciparum* cultures and evaluate their IC₅₀ concentrations. We measured their activity at different drug concentrations and on different parasite stages. Moreover, *in proteomic* studies have been quantified the levels of Tyr phosphorylation in oxidized RBCs using Diamide (sulfhydryl reagent which oxidizes sulfhydryl groups to the disulphide form). These analyses have been followed by the molecular modelling approach based on the identification of amino acidic interaction and the energy of binding in catalytic site of Syk protein through the molecular docking and molecular dynamic studies. The chemical characteristics of compounds have been analysed using the molecular descriptors. Furthermore, accurate studies on the human kinases crystal structures available on public database RCSB PDB allowed us to gain more information about the ligands and the protein target. Virtual screening was carried out in order to find new compounds having the same pattern of interaction in the catalytic site of Syk, useful to be tested *in vitro*.

3.1. Experimental *in vitro* studies

Experiments were performed using *P. falciparum* (Palo Alto strain) cultures (37°C and CO₂ 5%) in Growth Medium (RPMI, 10% H. plasma, 20mM HEPES pH 7.4, 2% SAGM (Sodium Chloride, Adenine, Glucose, Mannitol) pH 7.4, 10mM Glucose, 40mg/ml Gentamicin). Both haematocrit and parasitemia were at 2%. Before each experiment, cultures have been synchronized at rings stage with 5% Sorbitol. Parasitized red blood cells with 500 µl of Growth Medium contained in each well (24 multiwell plate) were treated with Syk inhibitor II, R406 (Tamatnib), Gleevec (Imatinib) and P505-15 (PRT062607) at concentration (0.2, 0.8, 1, 2, 4, 8, 10 µM) for 24h and 48h. The parasitemia was evaluated by optic microscopy after smears preparation. The smears have been stained using a specific protocol containing, methanol to fix the erythrocytes samples, eosin for the cytoplasm and thiazine in phosphate to stain the parasites. The IC₅₀ of each compound has been calculated using ICEstimator 1.2 software [88].

3.1.1. ICEstimator 1.2 software

ICEstimator carries out a nonlinear regression on the relative effect - concentration points. The relative effects in % are used; they are derived from the raw effects entered by the user. The raw effect(s) for null concentration are used to derive the 100% relative parasite effect. The raw effect(s) for the maximal concentrations are used to derive the 0% relative parasite effect. The resulting curve depicts an inhibitory sigmoid that shows a decrease in the relative effect of the parasite from 100% at the null concentration towards zero when the drug concentration increases to infinity.

ICEstimator applies the following model:

$$RE(\%) = 100 - \frac{100 \times C^\gamma}{C^2 + IC_{50}^\gamma}$$

RE: relative effect of the parasite in %. It defines the Y-axis.

C: concentration of the tested drug. It defines the X-axis.

IC₅₀: drug concentration inhibiting 50% of parasite's activity.

IC₉₀: drug concentration inhibiting 90% of parasite's activity.

IC₉₉: drug concentration inhibiting 99% of parasite's activity.

γ: sigmoidicity factor, which expresses the steepness of the curve.

3.1.2. Treatment of Red Blood Cells.

Venous blood was drawn from healthy volunteers following informed consent and pelleted at 1000 g for 10 minutes at room temperature. After removal of the buffy coat, RBCs were again pelleted and washed 3 times with Phosphate Buffered Saline (127 mM NaCl, 2.7 mM KCl, 8.1 mM Na₂HPO₄, 1.5 mM KH₂PO₄, 20 mM HEPES, 1 mM MgCl₂, and pH 7.4) in 5 mM glucose (PBS glucose) to obtain packed cells. RBCs were suspended at 30% haematocrit in PBS glucose and it were pre-treated in different experiments with Syk inhibitor II, R406, Gleevec and P505-15 at concentration (0.2, 0.8, 1, 2, 4, 8, 10 μM) for 1 hour at 37°C in the dark, and then treated with oxidant diamide at 2 mM concentration for 45 minutes. For all protocols described, untreated controls and treated controls with only diamide 2 mM were processed identically. To prevent

further phosphorylation of band 3, after incubation we washed the cells with cold buffer and membranes were immediately prepared.

3.1.3. RBCs Membrane Preparation.

Membrane proteins were prepared at 4°C on ice and for each sample, 150 µL of packed RBCs was diluted into 1.5 mL of cold haemolysis buffer (HB) (5 mM disodium phosphate, 1 mM EDTA, pH 8) containing a protease and a phosphatase inhibitor cocktail. Thereafter they have been washed up to 4 more times in the same buffer (until membranes became white) in a refrigerated eppendorf microfuge at 25000 g. The samples were stored frozen at -20°C until use. Membrane protein content was quantified using the CD Protein Assay (Bio-Rad).

3.1.4. SDS-PAGE Preparation

To perform one-dimensional electrophoresis (Sodium Dodecyl Sulphate - PolyAcrylamide Gel Electrophoresis), membrane proteins were solubilised in Laemmli Buffer [89] in a volume ratio of 1:1. 30 µg of proteins for anti-phosphotyrosine; then samples were placed in thermomixer at 1400 rpm, 28°C for 30 minutes. After that, the samples were put at 95°C for 5 minutes and then were separated on 8% polyacrylamide gel under reducing and no-reducing conditions. The electrophoretic run was performed using the Bio-Rad mini-protean 3 setup.

3.1.5. Western blot analyses.

Proteins separated by SDS-PAGE were transferred to nitrocellulose membranes as previously described using Trans-blot turbo Bio-Rad and then probed with antibody anti-phosphotyrosine (sc7020, Santa Cruz, CA). This is produced in mouse from Santa Cruz, CA, and it is diluted to 1 : 2000. Secondary antibodies conjugated to infrared fluorescent dyes excitable at 680 nm or 800 nm (IRDye: anti-mouse 800 CW 926-32210, Li-COR, USA) were then used to visualize the desired antigens with an high performance laser scanner (Odyssey, Licor, USA). The quantitative analyses of tyrosine phosphorylation levels were carried out and were measured analysing western blot images by

Image J software, and the values were expressed as arbitrary units. The IC₅₀ of different drugs was calculated through the software ICEstimator 1.2.

3.2 Computational Studies

3.2.1. Molecular Mechanics (MM) and Quantum Mechanics(QM)

Computational modelling was performed on multiprocessor machines, IBM Blade Center HS22 type 7870, with OS Ubuntu 16.04 or Windows 10. The small molecules were constructed with standard bond lengths and angles from the fragment database with MacroModel 5.5 [90]. Minimization of structures by conformational search was performed with the MacroModel/BachMin 6.0 program using the AMBER force field.

An extensive conformational search was further carried out using the Monte Carlo/energy minimization [91] (Ei-E min <5 Kcal/mole, energy difference between the generated conformation and the current minimum).

The atomic charges were assigned using the Gasteiger-Marsili method [92]. Representative minimum energy conformations of each compound were optimised using the quantum chemistry program Gaussian 09W with method DFT B3LYP/6-311G basis set. Visual quantum chemical calculation analysis was performed with GaussView version 5.0, [93,94].

3.2.2. Molecular docking

All docking tests were performed considering a grid 60 x 60 x 60 and the default grid spacing (0.375 Å) was adopted, treating the docking active site as a rigid and the ligands as flexible, i.e., all non rings torsions were considered free to rotate.

Binding of compounds was analysed using MGLTools 1.5.7rc1 [95] and AutoDock 4.2 docking programs [96,97].

From the estimated free energy of ligand binding (E.F.E.B., ΔG), the inhibition constant (K_i) for each ligand was evaluated. K_i is calculated by the equation: $K_i = \exp [(\Delta G * 1000) / (R * T)]$. Where ΔG is docking energy, R (gas constant) is 1.98719 cal K⁻¹ mol⁻¹ and T (Temperature) is 298.15 K. The protein target Syk in complex with AMP-PNP ligand (PDB ID: 4FL2 with resolution of 2,19 Å)

deposited in RCSB Protein Data Bank [98] was chosen. The structure was the most defined and complete except for the first part of N-terminus (a.a. 1-8) and for interdomain linker region (a.a. 265-336). The crystallographic water molecules were stripped, hydrogen atoms were added using ADT module.

3.2.2.1. Docking validation protocol (close conformation of Syk)

The reliability of the docking approach was further verified with two methods, one test performed by extracting the phosphoaminophosphonic acid adenylate ester (ANP, characterised to have a substitution of an oxygen with a nitrogen atom), from the catalytic site of 4FL2, 2.19 Å resolution crystal structure, and then performing the lead compound re-docking.

The second test was conducted by the extraction of N-{6-[3-(piperazin-1-yl)phenyl]pyridin-2-yl}-4-(trifluoromethyl)pyridin-2-amine (OSB) from X-ray of 4F4P.pdb, 2.37 Å resolution and docked with the same macromolecule derived from 4FL2.pdb. The ligand-protein multiple interactions were analysed through a 2D Diagram, LigPlot+ [99] and consequently have been evaluated the RMSD values. (Fig.27).

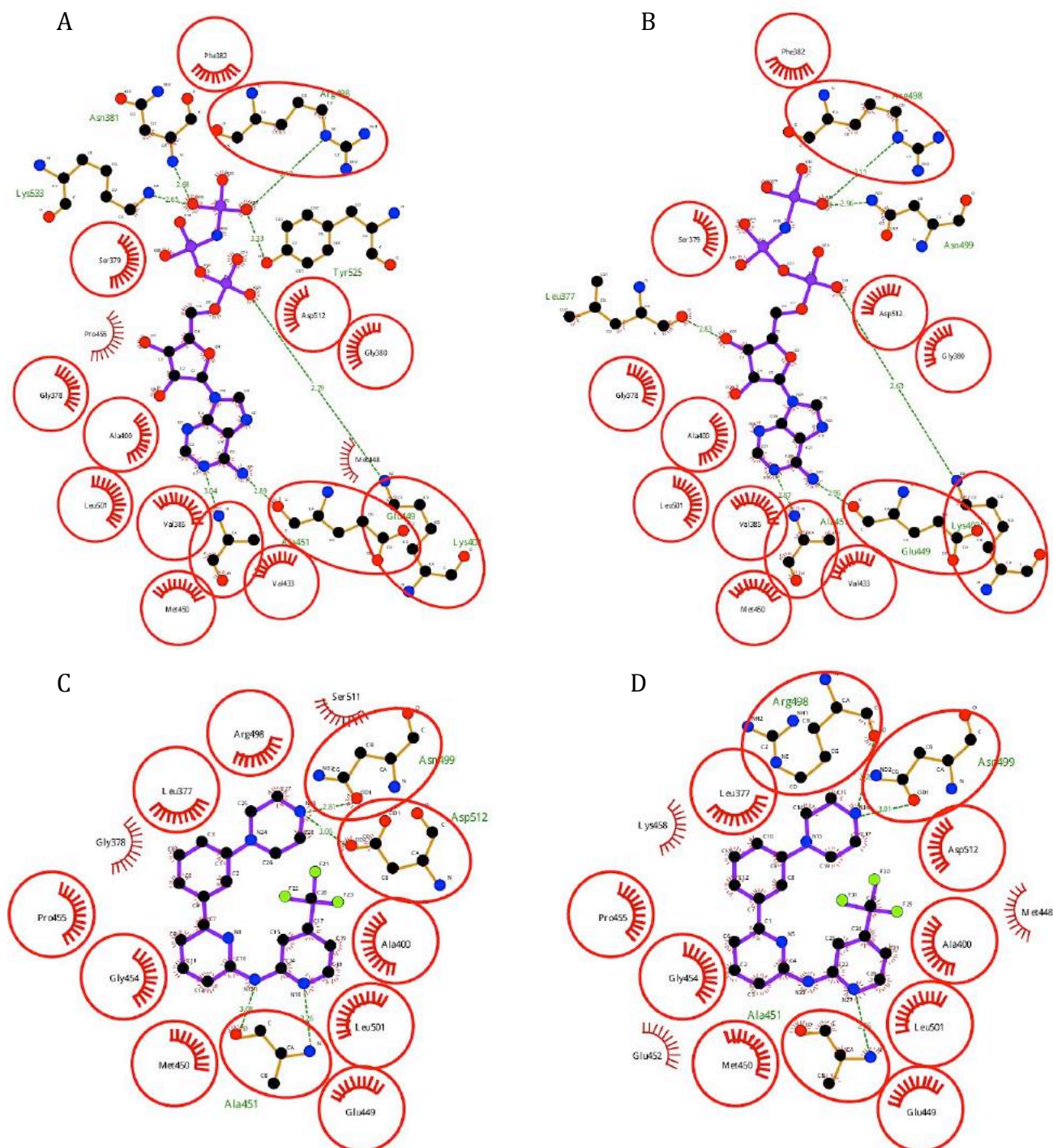


Fig. 27. Two different approaches to validate the protocol of docking analysis related to X-ray crystal 4FL2 (A) and 4F4P (C). The first test consisted in re-docking among 4FL2 and its ligand ANP (B), while the second test involved the docking of 4FL2 with the ligand OSB (D). The 2D diagrams were achieved through LigPlot+ tool.

3.2.3. Quantum Mechanics molecular descriptors

3.2.3.1. Homo - Lumo

Homo-Lumo distribution, respectively "highest occupied molecular orbital" and "lowest unoccupied molecular orbital", was computed evaluating the energies and energy gaps for each compound.

The energy difference between the Homo and Lumo is termed the **HOMO-LUMO gap**. HOMO and LUMO are sometimes called **frontier orbitals** in frontier molecular orbital theory. This was based on three main observations of molecular orbital theory as two molecules interact:

1. The occupied orbitals of different molecules repel each other.
2. Positive charges of one molecule attract the negative charges of the other.
3. The occupied orbitals of one molecule and the unoccupied orbitals of the other interact with each other causing attraction.

The difference in energy between these two frontier orbitals can be used to predict the strength and chemical stability of molecules or transition metal complexes, as well as the colours they produce in solution.

The ligand band gap investigated can be tuned from 3.10 to 6.12 eV. Similar and relatively high ΔE values, highlight a good stability of the inhibitors, Frontier orbital energies including HOMO and LUMO are used to characterize the electronic properties of the compounds. LUMO is directly associated with the electron affinity and system's tendency to accept electron density, whereas HOMO is directly associated with the ionization potential [100,101]

3.2.3.2. Map Electrostatic Potential (MEP)

Electrostatic potential maps, also known as electrostatic potential energy maps, shows the sites with abundant electrons by analysing charges distribution within a molecule in three dimensions; it is related with dipole moment, electronegativity and partial charges; and shows the reactivity of a molecule.

Positive potential values reflect nucleus predominance, while negative values represent rearrangements of electronic charges and lone pairs of electrons.

The MEP allowed us to visualize variably charged regions of a molecule. Knowledge of the charge distributions has been used to determine how molecules interact one with other. The creation of electrostatic potential map consists of the use of electrostatic potential energy, through setting the distance from the nuclei of the molecules. Electrostatic potential energy is fundamentally a measure of the strength of the nearby charges and electrons, in a particular position. One of the purposes of finding the electrostatic potential is to investigate the reactive site of a molecule. The reactive site is a particularly charged region of a molecule that has an affinity for interacting with charged particles.

To accurately analyse the charge distribution of a molecule, a very large quantity of electrostatic potential energy values has been calculated. The best way to convey this data was to visually represent it, as in an electrostatic potential map. To make the electrostatic potential energy data easy to interpret, a colour spectrum, with red as the lowest electrostatic potential energy value and blue as the highest, is employed to convey the varying intensities of the electrostatic potential energy values.

3.2.4. Molecular dynamics (MD)

Molecular dynamics (MD) calculations were performed to simulate the interaction, of the best score conformations predicted by Autodock of the all ligands, with active site of Syk protein. The MD protocol (see Supplementary data for details) for the production simulations were carried out using the parallel version of particle mesh ewald molecular dynamics (PMEMD) version included in the AMBER14 suite program [102], after careful relaxation of the only system using minimization and equilibration protocols.

1000 time step from 10 nanoseconds of molecular dynamics trajectory of production is saved. The ionisable residues were set to their normal ionization states at pH7, the protein atoms, as well as all the water molecules of the crystal structure, were surrounded by periodic box of TIP3P water molecules that extended 10 Å from the protein. Counterions (Cl⁻ or Na⁺) were placed by xleap to neutralize the system with force field for Ewald charges and TIP3P water [103].

The ff10 version of the AMBER force field was used to model the protein, and the GAFF force field was used for the organic ligand. Using the AMBER antechamber program derived AM-BCC partial charges. In the MD simulation protocol, the time step was chosen to be 2 fs (10^{-15} seconds), and the SHAKE algorithm was used to constrain all bonds involving hydrogen atoms. A non-bonded cutoff of 8.0 Å was used. Langevin dynamics was used to control the temperature (300 K) using a collision frequency of 1.0 ps⁻¹, with isotropic position scaling to maintain the pressure (1 atm). Periodic boundary conditions were applied to simulate a continuous system. To include the contributions of long-range interactions, the particle mesh Ewald (PME) method was used with a grid spacing of 1 Å combined with a fourth-order B-spline interpolation to compute the potential and the forces in between grid points. The trajectories were analysed using the PTRAJ module of AMBER.

Molecular Mechanics / Poisson Boltzmann (or Generalized Born) Surface Area (MM/PB(GB)SA) calculations and analysis were made with the program MM-PBSA of Amber14 suite.

Graphical representation of the hypothetical positions derivative from the docking calculation and analysing trajectory of molecular dynamics calculations was performed using the software Chimera [104] and Visual Molecular Dynamics (VMD) [105].

Calculation and comparison energy have been conducted using the method of Ross Walker [106].

3.2.4.1. RMSD maps in Molecular Dynamic

The RMSD maps represented in 2D graphical form show the computation of all pairwise RMSDs between frames and collect the result in greyscale. The axes are the frame numbers; lighter squares reflect pairs of frames with lower RMSDs (more similar structures) and darker squares reflect pairs of frames with higher RMSDs (less similar structures). Precisely the lighter squares show the conformational families of ligands or protein. The RMSDs are directly related to the conformational changing or variation within the family, therefore lower RMSD (lighter square) reflect a minor variation while higher RMSD (darker square) corresponds to a major variation of conformation. The

conformational changing of protein domains or different ligands and atoms poses over time, establish the stability both chemical and energetic of that compounds or protein. Furthermore, the conformation changing implies the modification of atoms distance and the angles width.

3.2.5. Identification of receptor for the virtual screening

3.2.5.1. 3D alignment superposition of Syk

The structures superposition has been conducted picking the available X-ray crystal of Syk protein from public database (RCSB PDB). Forty-three Syk structures were selected (forty-two with open conformation, namely with opened activation loop and only catalytic site, and one (4FL2.pdb) with closed conformation considered as the most complete crystal), (Tab.2).

The alignment has been performed using the UCSF Chimera software and it was based on three criteria in order to assess the flexibility and domain variation.

The first criterion consisted in the use of close (active) structure as reference aligned with the forty-two remaining open (inactive) structures.

The second criterion was based on the alignment among an open conformation as reference compared to the forty-two remaining (one closed and forty-one open). In the last criterion have been considered as reference only the aminoacids that

interact with the ligands into the Syk active pocket aligned to the forty-two structures. Each alignment was examined through the RMSD (Root mean

X-ray crystal structure		Conformation	Resolution
Protein (Syk)	Ligand	Syk	Angstrom (Å)
1XBB	STI	open	1.57
1XBC	STU	open	2
3EMG	685	open	2.6
3FQE	P5C	open	2.5
3FQH	057	open	2.26
3FQS	585	open	2.1
3SRV	S19	open	1.95
3TUB	FPU	open	2.23
3TUC	FPW	open	2.1
3TUD	FPX	open	2.33
3VF8	OJE	open	2.08
3VF9	477	open	2.3
4DFL	OK0	open	1.98
4DFN	OK1	open	2.48
4FL2	ANP	close	2.19
4F4P	05B	open	2.37
4FYN	0VE	open	2.31
4FYO	0VF	open	1.4
4FZ6	0VG	open	1.85
4FZ7	0VH	open	1.75
4GFG	0XF	open	2.35
4I0R	1B4	open	2.1
4I0T	1B6	open	1.7
4PUZ	CG9	open	2.08
4PV0	CG4	open	2
4PX6	2X6	open	1.6
4RSS	4MG	open	1.83
4RX7	3YV	open	1.8
4RX8	3YX	open	1.59
4RX9	3YT	open	1.75
4YJO	4DF	open	1.6
4YJP	4DL	open	1.83
4YJQ	4DK	open	1.34
4YJR	4DJ	open	1.32
4YJS	4DN	open	2.22
4YJT	4DQ	open	1.52
4YJU	4DO	open	1.67
4YJV	4DT	open	1.65
5C26	50H	open	1.95
5C27	50J	open	2.15
5CXH	55M	open	1.9
5CXZ	55U	open	1.7
5CY3	55Y	open	1.76

Tab.2 .The forty-three crystal structures analysed (open and close conformation) with the respective x-ray resolution.

square deviation) value obtained comparing the reference to the rest structures.

3.2.5.2. UCSF Chimera software

UCSF Chimera or Chimera is an extensible program that allows creating High-quality images and movies. It is helpful for interactive visualization and analysis of molecular structures and related data, including density maps, supramolecular assemblies, sequence alignments, docking results, trajectories, and conformational ensembles [107].

3.2.6. Cross-docking validation protocol with 43 crystal structures of Syk

The validation was carried out with the purpose to identify the best pose and interaction of ligand with the protein target considering the RMSD values obtained after the docking analysis. Both forty-three crystal structures of Syk and the respectively ligands have been 3D aligned using the PyMOL software. The cross docking tests have been carried out through Autodock 4.2.6. crossing forty-three crystal structures with forty-three ligands. All tests were performed considering a grid 80 x 60 x 60 and the default grid spacing (0.375 Å) was adopted, treating the docking active site as rigid and the ligands as flexible, i.e., all non rings torsions were considered active (free to rotate). Each RMSD value was been extracted from the docking results and the ligands disposition has been reviewed. An accurate evaluation of the success ligands interaction was determined in order to select the best and suitable structure of Syk protein to use for the virtual screening.

3.2.6.1. PyMOL software

PyMOL is one of a few open-source model visualization tools available for use in structural biology. The *Py* part of the software's name refers to that it extends, and is extensible by, the programming language Python. This tool can produce high-quality 3D images of small molecules and biological macromolecules, such as proteins. It is widely used as a means to raise information about the protein and ligand structure and their interactions [108,109].

3.2.7. Residues assessment providing Syk specificity in the h. kinome

3.2.7.1. Alignment method: ClustalX software

A thorough research of available co-crystallized kinases as been leded to increase the selectivity, comparing the Syk catalytic site with that of other kinases in the kinome. The identification of unique structural features of Syk binding pocket have been assessed in order to provide Syk specificity against other kinases enhancing the compounds binding to these regions. Almost three hundred crystal structures have been found of which 65 Tyr Kinases (different UniProt ID) were chosen. The alignment of selected structures was performed using ClustalX software after the sequence inclusion. Subsequently, in order to demonstrate the specificity of Syk in compare to the other kinases was carried out evaluating the individual residues frequency using Sequence Logo tool.

Clustal is a series of widely used computer programs useful for multiple sequence alignment. ClustalX software align sequences using a heuristic that progressively builds a multiple sequence alignment from a series of pairwise alignments. This method works by analysing the sequences as a whole, then utilizing the UPGMA/Neighbor-joining method to generate a distance matrix. A guide tree is then calculated from the scores of the sequences in the matrix, and then subsequently used to build the multiple sequence alignment by progressively aligning the sequences in order of similarity [110]. Essentially, Clustal creates multiple sequence alignments through three main steps:

1. Make a pairwise alignment using the progressive alignment method
2. Create a guide tree (or use a user-defined tree)
3. Use the guide tree to carry out a multiple alignment

These steps are carried out automatically when the Complete Alignment is selected.

3.2.8. Virtual Screening (VS)

Virtual screening analysis has been performed using Autodock 4.2.6 version. Syk complexed with 4-[[[(3S)-1-{7-[(3,4-dimethoxyphenyl)amino][1,3]thiazolo[5,4-d]pyrimidin-5-yl}pyrrolidin-3-yl]-carbamoyl]benzoic acid, OVF ligand (PDB ID: 4FYO with resolution of 1.4 Å) deposited in RCSB Protein Data Bank has been chosen. The structure (catalytic site), having open conformation has been employed as protein target. Virtual screening was conducted using a diversity set of 46.840 compounds (Cambridge library in ZINC database) [111] and all tests were performed considering a grid 80 x 60 x 60 and the default grid spacing (0.375 Å) was adopted, treating the docking active site as a rigid and the ligands as flexible, i.e., all non rings torsions were considered active (free to rotate). The results have been analysed applying precise filters for the Energy of binding, ligand efficiency and Hbond interaction aimed to select the more suitable compounds [112]. Ligand efficiency is used in drug discovery research programs to assist in narrowing focus to lead compounds with optimal combinations of physicochemical properties and pharmacological properties [113-115]. Mathematically, ligand efficiency (LE) can be defined as the ratio of Gibbs free energy (ΔG) to the number of non-hydrogen atoms of the compound:

$$LE = (\Delta G)/N$$

where $\Delta G = -RT \ln K_i$ and N is the number of non-hydrogen atoms. It can be transformed to the equation:

$$LE = 1.4(-\log IC_{50})/N$$

Further VS has been carried out in order to find a new class of spleen tyrosine kinases type-II ligands. A special conformation of Syk (DFG-out) compared to other known has been chosen. It has a deep pocket created from the displacement of three aminoacids DFG (Asp512, Phe513, Gly514) leading to a different disposition of ligands. Among the Syk x-ray crystal available on RCSB PDB database has been picked the 3TUB (resolution of 2.23 Å) complexed with 1-{5-[(6,7-dimethoxyquinolin-4-yl)oxy]pyridin-2-yl}-3-[(1R,2S)-2-phenyl-cyclopropyl]urea, FPU ligand. The same filters were employed for the ligands selection, in order to keep in both systems, the identical condition of study [116].

4. RESULTS & DISCUSSION

4.1. *In vitro* results

4.1.1. IC₅₀ evaluation of Syk inhibitors in parasitized erythrocytes

This chapter is divided into two main parts. Firstly, the IC₅₀ concentrations of different Syk inhibitors are presented in *P. falciparum* Palo Alto strain. Secondly, the effect of Syk inhibitors related to the decrease of Tyr phosphorylation with proteomic approach has been analysed.

In the first section, five different Syk inhibitors (P505-15: 1nM, R406: 41nM, Syk II: 41nM, Gleevec 5 µM) at increasing concentration have been tested in Diamide treated erythrocytes, in order to mimic the physiological condition of infected red blood cells. IC₅₀ values were determined counting the parasitemia for each Syk inhibitor tested at fixed concentration. Already from the microscopy analysis was clearly visible a lower parasitemia related to the increase of compounds' amount. At higher concentration, all the tested compounds induced a slower growth of parasites and blocked the RBCs reinfection.

Table 3 shows the IC₅₀ concentrations of all tested compounds after 24 and 48 hours of incubation.

Palo Alto strain	24 hours		48hours	
	IC ₅₀ (µM)	Range (µM)	IC ₅₀ (µM)	Range (µM)
P505-15	0.83 ± 0.06	0.78 - 0.9	0.49 ± 0.07	0.42 - 0.61
R406	2.62 ± 0.83	1.42 - 3.85	0.55 ± 0.19	0.25 - 0.92
Gleevec	3.81 ± 0.55	3.24 - 4.95	1.55 ± 0.13	1.32 - 1.74
SYK II	5.01 ± 0.44	4.65 - 5.87	0.9 ± 0.16	0.82 - 1.25
SYK IV	7.28 ± 0.40	6.87 - 7.91	1.75 ± 0.31	1.31 - 2.58

Tab. 3. *In vitro* susceptibility (IC₅₀ values) of *P. falciparum* Palo Alto strain after 24 and 48 hours of treatment with different Syk inhibitors.

The highest efficacy was observed in Palo Alto strain following P505-15 treatment, the novel, highly selective, and orally bioavailable small molecule SYK inhibitor with an IC_{50} = 1 nM, with anti-SYK activity that is at least 80-fold greater than its affinity for other kinases, *in vitro* presented the lowest IC_{50} needed to eliminate 50% of parasitemia, the IC_{50} concentration of P505-15 was 0.83 μ M (\pm 0.06) and 0.49 μ M (\pm 0.07) at 24 and 48 hours of incubation respectively. Syk Inhibitor IV, a cell-permeable, potent ATP-competitive, reversible, and highly selective inhibitor of Syk tyrosine kinase activity, presents an IC_{50} of 10 nM but *in vitro* showed a different behaviour, in fact this compound holds a lower inhibition activity compared to the other Syk inhibitors, its IC_{50} concentration was the highest.

4.1.2. Proteomic profile of Tyr phosphorylation in treated RBCs

The proteomic approach was used in order to investigate membrane proteins changes under oxidative stress due to the *P. falciparum* infection in RBCs. The erythrocytes were pre-treated with different concentrations of Syk inhibitors and then with 2mM Diamide (oxidant agent) used to mimic the physiological condition of infected red blood cells. As shown in figure 28, the inhibitors cause a substantial decrease of band 3 phosphorylation (95-250 KDa), the decrease of phosphorylation intensity is related to the increasing amount of the inhibitors. This trend is more evident at 250 KDa bands (clusters of Band3). Taken together, these results show that Syk inhibitors efficiently suppress band 3 phosphorylation. Because of their action, Syk inhibitors are expected to substantially reduce the host cell membrane weakening occurring at the end of parasite development.

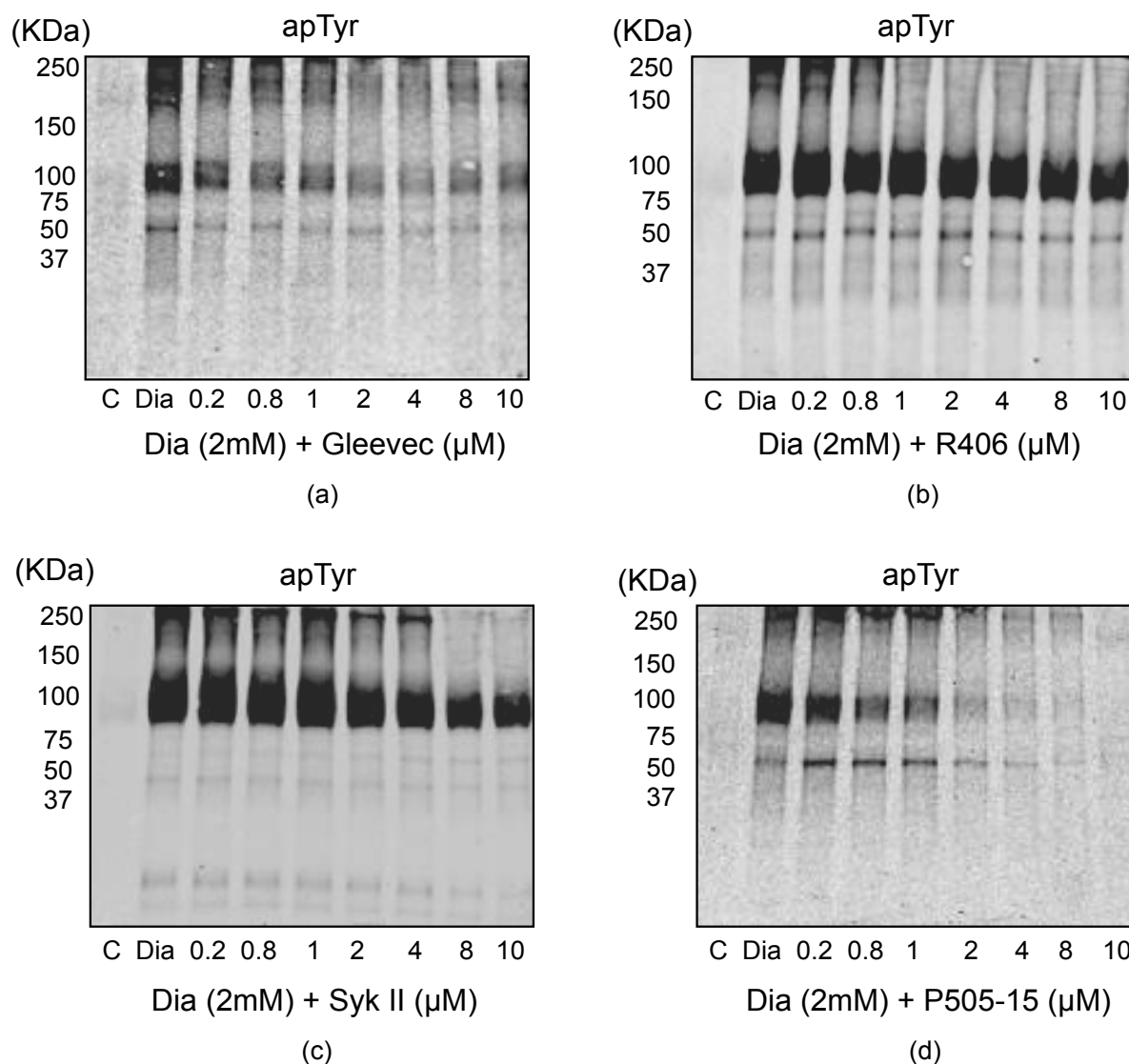


Fig. 28. Dose response course of erythrocyte membrane proteins treated with an oxidant agent and Syk inhibitors. Erythrocytes were treated with 2mM diamide (Dia) and different concentrations of Syk inhibitors (0-10 μ M), (panels **(a)** Gleevec, **(b)** R406, **(c)** Syk II, **(d)** P505-15). **C** represents the no treated control sample. Erythrocytes were separated by 8% SDS-PAGE, blotted on nitrocellulose membrane and stained with anti-phosphotyrosine (apTyr) antibodies. Images were acquired using a laser IR fluorescence detector (Odyssey, Licor, USA). The results are representative of 4 separated experiments.

Quantitative analyses carried out through Odyssey 3.0 software, confirmed the great decrease of Tyr phosphorylation levels in band 3 residues caused by Syk protein (Fig. 29). Samples treated with 2mM Diamide (see figures 28-29) showed a high level of phosphorylation due to the oxidative stress conditions.

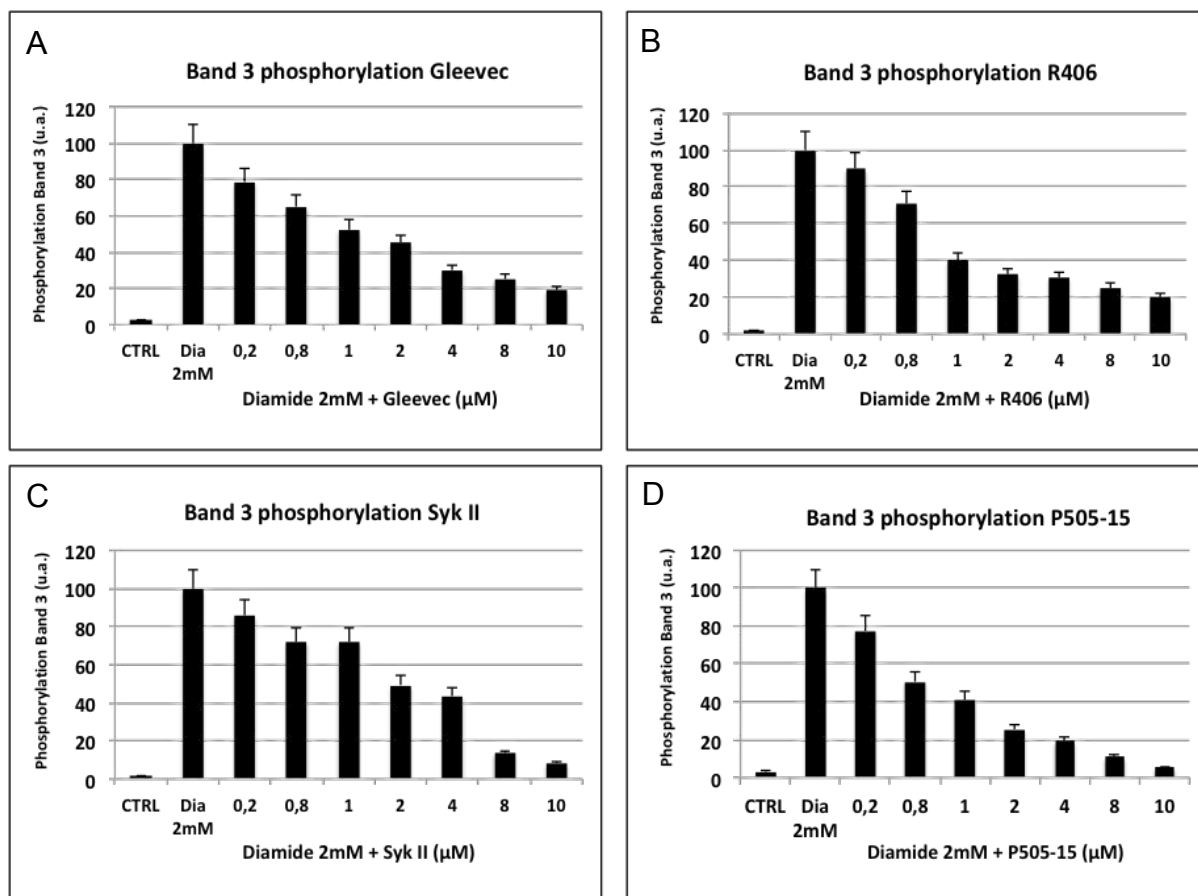


Fig. 29. Quantitative densitometry analysis was performed using Odyssey V3.0 software. Photomicrographs were acquired using Odyssey from LI-COR, setting 300dpi as definition. Results are representative of four separated experiments. Panel **A** (Gleevec), **B** (R406), **C** (Syk II) and **D** (P505-15). Results are representative of 4 separated experiments.

The IC_{50} obtained by densitometry analysis (Tab. 4) confirmed the major efficacy of P505-15 as is evident from the graph (panel D), which holds the lowest inhibition concentration.

Syk inhibitors	IC_{50} (μM)
P505-15	0.64
Gleevec	0.77
R406	0.83
SYK II	1.72

Tab. 4. IC_{50} values obtained by densitometry analysis of Syk inhibitors

4.2. Computational Results

To further investigate the action of Syk inhibitors experimental and computational studies were performed. The data concerning the validation protocol of docking analysis, molecular docking tests, molecular dynamic and the selection of new compounds through the virtual screening approach have been reported divided in different sections. A study demonstrated that the kinases, to interact with the catalytic site of protein, must have a precise pattern of binding needed to design and discover new kinase inhibitors [117]. Figure 30 clearly evidences the pattern of Syk inhibitors binding to the catalytic domain.

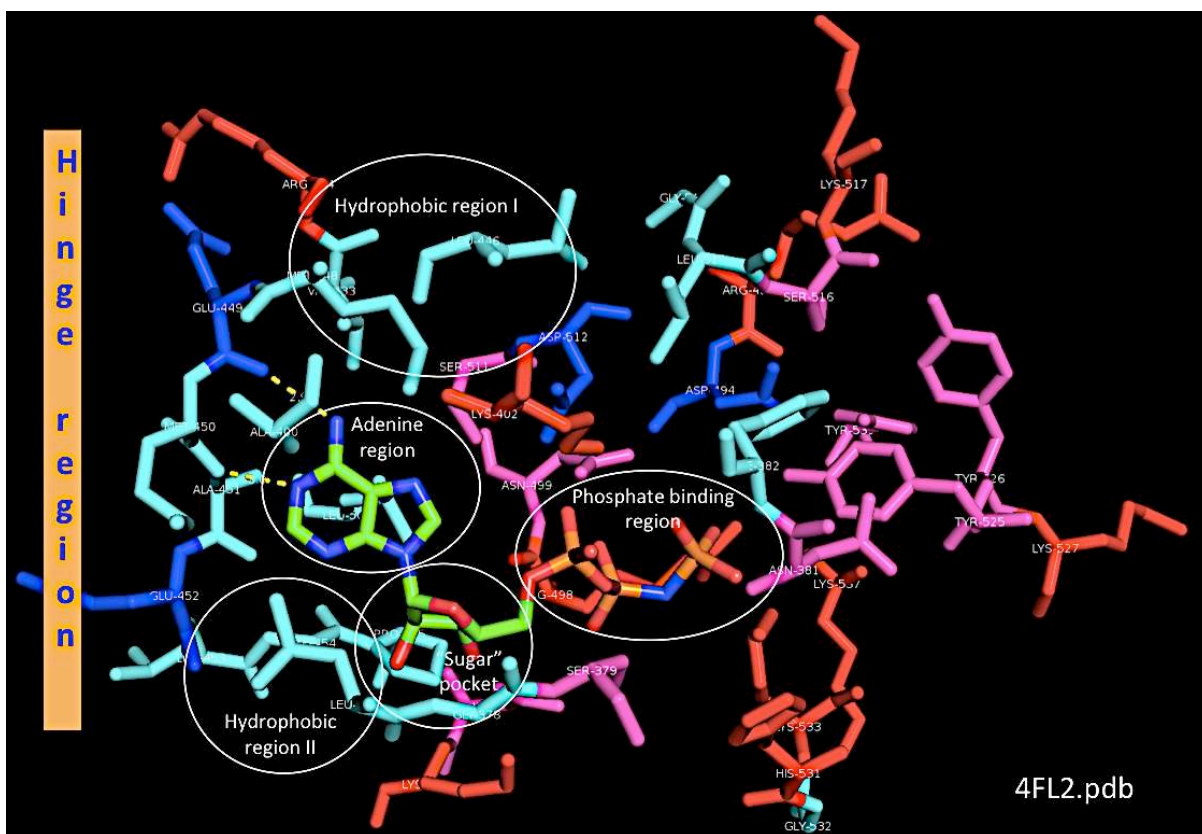


Fig. 30. Pattern of Syk inhibitors binding to the catalytic domain. A suitable compound needed to interact with the Hinge region of protein with 2 H-bond. Basic interactions must be created with hydrophobic region I and II, the sugar pocket and the phosphate binding region.

4.2.1. Results of docking validation protocol (close conformation of Syk)

Considering the two different approaches used for docking validation, the RMSD values have been computed. Both methods are helpful to verify that the ligand disposition and its interaction have been kept as the x-ray crystal structure. The re-docking among 4FL2-ANP ligand and the docking among 4FL2-OSB ligand was conducted. After repositioning both ANP and OSB into the protein, and the new location was very close to the original X-ray structure, repositioned with only minimal conformational changes, hence confirming the reliability of the system. These methods allow us to calculate the RMSD values obtained from the superposition of the ligand in crystal structure with the re-docked ligand and cross-docked ligand. Considered that a range value of RMSD among 0 and 2 is the optimum, the obtained results in both approaches, 1.54 Å and 0.99 Å respectively were satisfactory for the validation method (Fig.31).

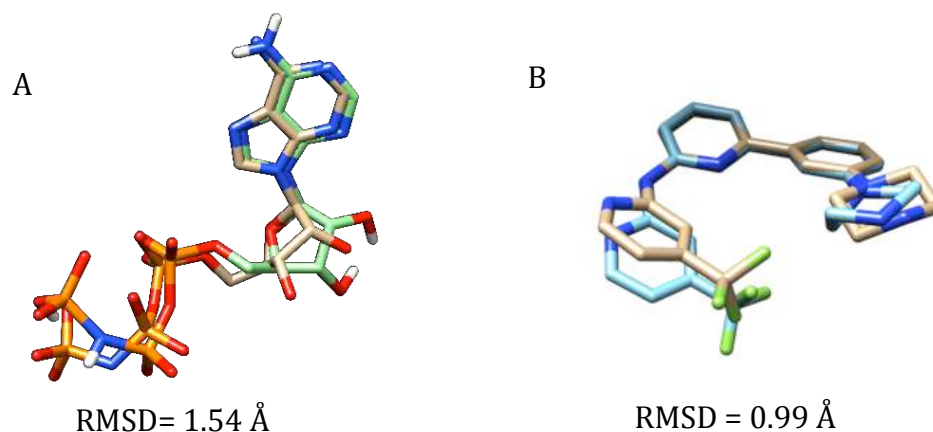


Fig. 31. Data shown represent the docking validation results. The values achieved from the superposition of the most suitable ligands poses, ANP (**A**) and OSB (**B**), are satisfactory, because in both cases we obtained RMSD < 2 Å.

4.2.2. Docking results

X-ray crystal structure (2.19 resolution, PDB accession number 4FL2) was found in RCSB-PDB database; this structure was the most complete in the database, although it has an active site closer comparing with the other structures.

Table 5 shows the docking results obtained from the crystal structure 4FL2 interacting with Syk inhibitors and clearly evidenced the conserved Hbond.

4FL2- H-bond interaction								
Tested ligands		%	H-bond	Ligands Atom	Protein Atom	Distance (Å)	LogP	Dipole Moment (D)
AD4_4FL2_Gleevec	1.c73.r59_diffusa	73	4	N33(NA)	Lys402:HZ1(HD)	2.217	3,83	5,1101
				O10(OA)	Ala451:HN(HD)	2.393		
				N38(NA)	Arg498:HE(HD)	2.147		
				H27(HD)	Asp512:OD2(OA)	1.995		
AD4_4FL2_R406	11.c16.r8_diffusa	16	3	H9(HD)	Leu377:O(OA)	1.875	3,37	3,4870
				H25(HD)	Ala451:O(OA)	2.262		
				O36(OA)	Ala451:HN(HD)	2.317		
AD4_4FL2_SykII	1.c56.r40_diffusa	56	7	H23(HD)	Glu449:O(OA)	2.075	1,22	4,4175
				H24(HD)	Glu449:O(OA)	2.233		
				O25(OA)	Ala451:HN(HD)	2.299		
				H29(HD)	Arg498:O(OA)	2.063		
				H30(HD)	Ser511:HG(HD)	2.558		
				H8(HD)	Asp512:OD2(OA)	2.191		
AD4_4FL2_P505-15	8.c37.r12_diffusa	37	4	H8(HD)	Ala451:O(OA)	2.301	1,02	2,4285
				O21(OA)	Ala451:HN(HD)	1.888		
				H23(HD)	Glu449:O(OA)	1.940		
				H24(HD)	Glu449:O(OA)	2.448		

Tab. 5. Data shown represent the Hbond binding found in docking analyses from the different inhibitors (Gleevec, R406, Syk II and P505-15) interacting with Syk protein. Hydrogen donor (**HD**), oxygen acceptor (**OA**), nitrogen acceptor (**NA**), Debie (**D**) and Angstrom (**Å**). The Cross-bridge Hbond interactions with the same aa are listed in bold"

The docking showed a different disposition of ligands in the pocket compared to the poses of crystal structures.

We observed common interactions in all Syk inhibitors of the amino acids Leu377, Val385, Ala400, Met448, Met450, Ala451, Gly454, Leu501 (Tab.6).

R406	Syk II	Gleevec	P505-15
Leu377 *	Leu377	Arg338	Leu377
Gly378	Gly378	Leu377	Val385
Ser379	Val385	Ser379	Ala400
Gly380	Ala400	Gly380	Met448
Val385	Lys402	Asn381	Glu449 **
Ala400	Met448	Phe382	<u>Met450</u>
Lys402	Glu449 **	Val385	Ala451 **
Val433	<u>Met450</u>	Ala400	Glu452
Met448	Ala451 *	Lys402 *	Gly454
Glu449	Gly454	Met448	<u>Pro455</u>
<u>Met450</u>	<u>Pro455</u>	<u>Met450</u>	Lys458
Ala451 **	Lys458	Ala451 *	Leu501
Glu452	Arg498	<u>Leu453</u>	
Gly454	Leu501	Gly454	
<u>Pro455</u>	Ser511 *	Arg498 *	
Lys458	Asp512 **	Asn499	
Leu501		Leu501	
Asp512		Ser511	
		Asp512 *	
		Tyr525	
		His531	

Tab. 6. Hydrophobic interactions and Hbonds between Syk inhibitors and protein. The bonds are shown highlighted with * (1 Hbond) and with ** (2 Hbond); we found an interesting interaction between Gleevec - Tyr525 (highlighted in yellow) that is an autophosphorylation site of Syk protein. Underlined are shown the amino acids that represent a high levels of Syk specificity.

An interesting hydrophobic interaction between Tyr525 and Gleevec was found. it represents the Syk autophosphorylation site [118] and it has hbond with Lys402, Ala451, Arg498 and Asp512. R406 forms an h-bond with Leu377, Syk II binds with Ala451 and Ser511 with an hbond whereas Glu449 and Asp512 with two hbond, while P505-15 [119] binds to Glu449 and Ala451 through two hbond as is evident from 2D diagram representation (Fig.32).

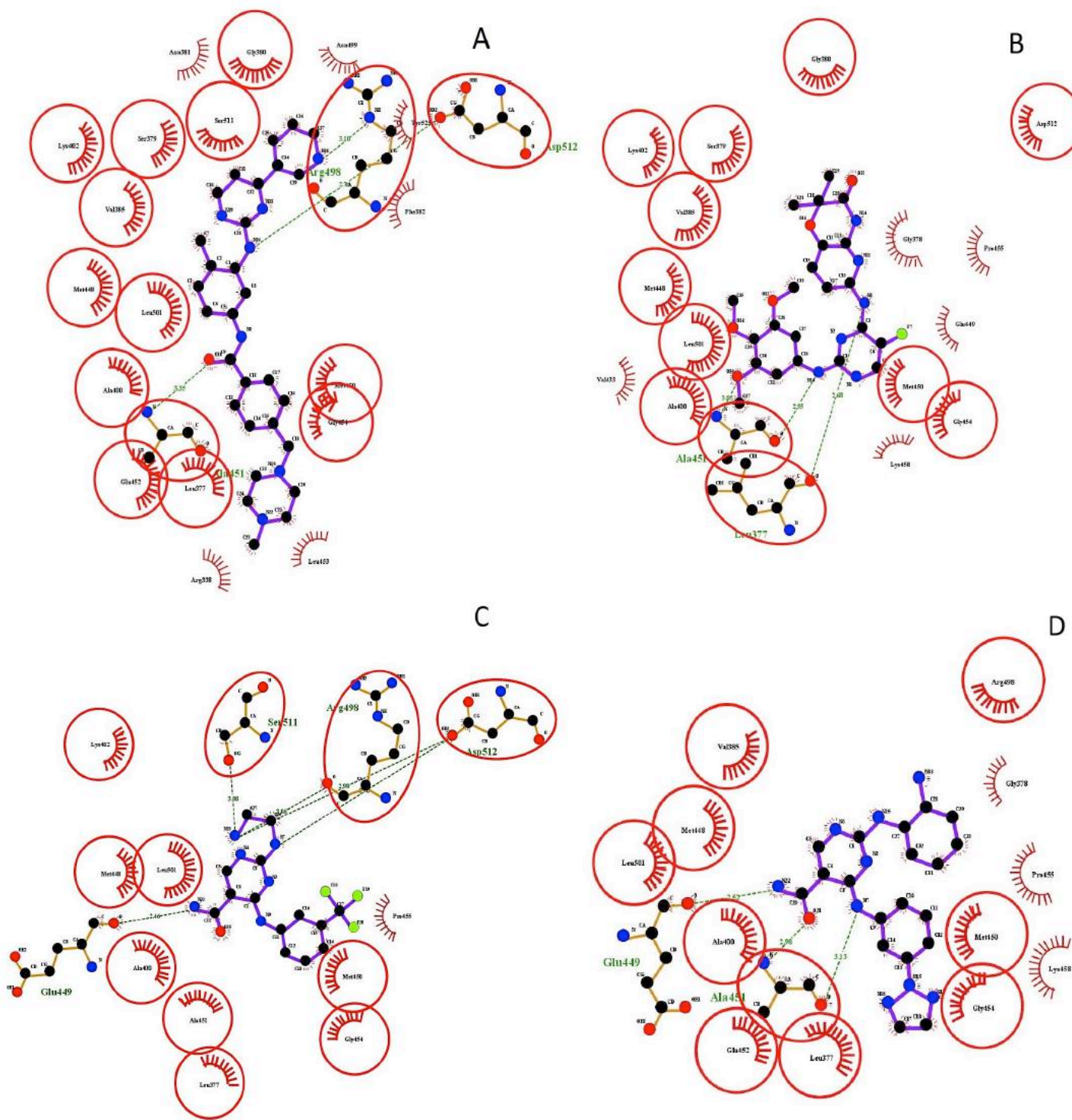


Fig. 32. 2D diagram of target structures Gleevec **(A)** R406 **(B)** Syk II **(C)** and P505-15 **(D)** docking. The ligands are represented in a ball and stick model. Hydrogen bond between the ligand and the active site residues are indicated by green dotted lines, and a crescent shape indicates the hydrophobic environment.

The docking results obtained from the structure of Syk (4FL2) in complex with ligands showed quite differences in dispositions of the same compounds compared to their crystal structures of reference. Although they hold the common pattern of interaction with Syk known for all tyrosine kinases, however, they present rotations and torsions in their conformation into the site of binding (Fig. 33).

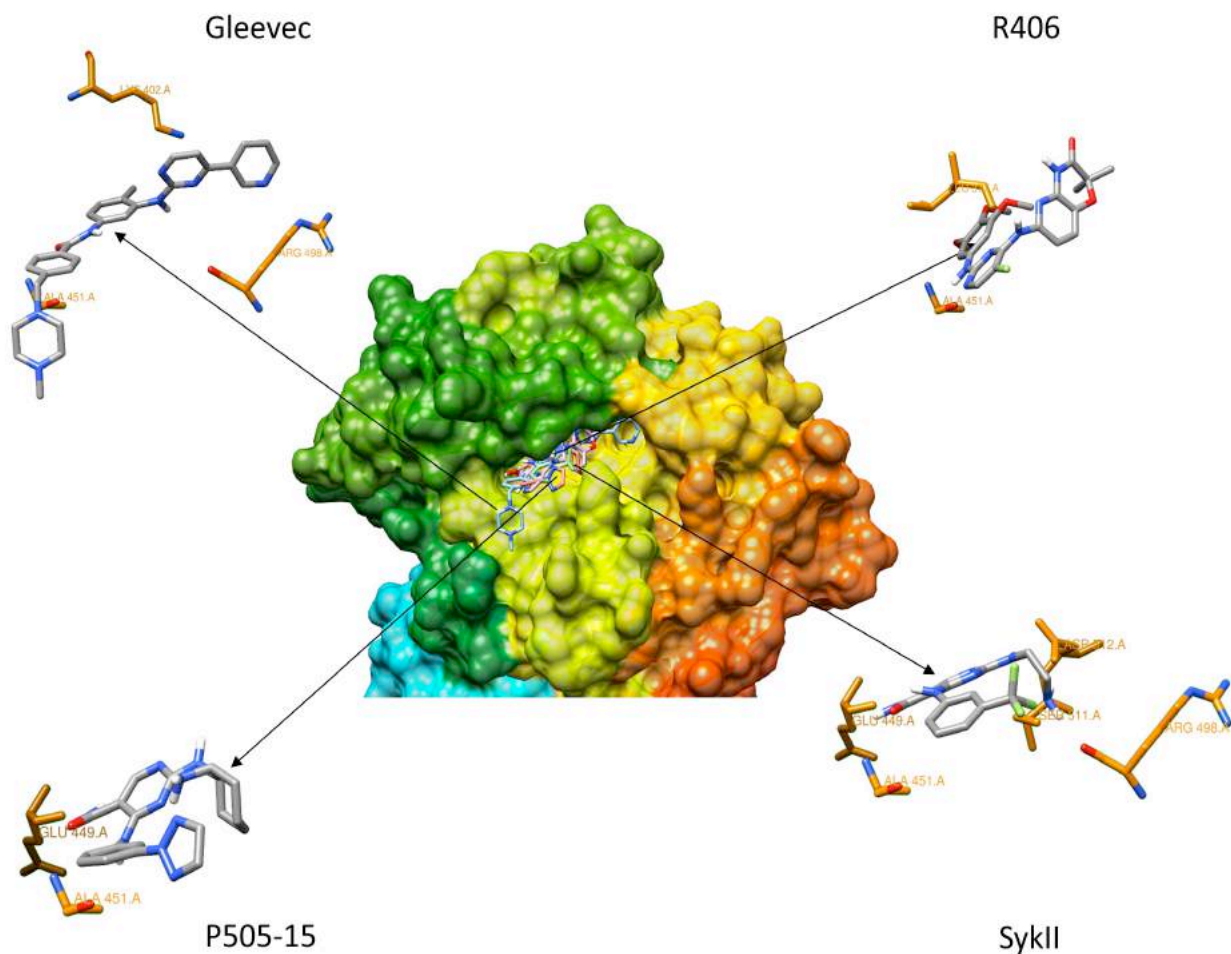


Fig. 33. 3D surface structure of Syk protein with Syk inhibitors interacting into the catalytic site. The compounds, with the principal hbond interactions were reported alone outside the pocket of binding.

These diversities might be due to the fact that we considered the crystal structure 4FL2, which is in the active conformation having a closer receptor-binding pocket if compared to the catalytic site of protein inactive conformation. The active conformation is characterised for having the Syk

activation loop that closes the ATP-binding pocket once a ligand interact with the aminoacids into the site.

The computational analyses performed with the closer conformation don't allow having the same disposition and conformation of the ligands, due to the fact that they are available in the database co-crystallized with the open conformation of Syk.

The main difference among these structures consists in the activation loop (a.a 520 – 534), [120] which translates in the active conformation of Syk, closing the ligands into the pocket.

Data relative to K_i obtained in docking showed the lowest value with Gleevec (13.65 nM). This results was unexpected; probably it could depends from the major number of interaction established with Syk which means major stability inside the pocket, although this ligand is not specific for the protein (Fig. 34).

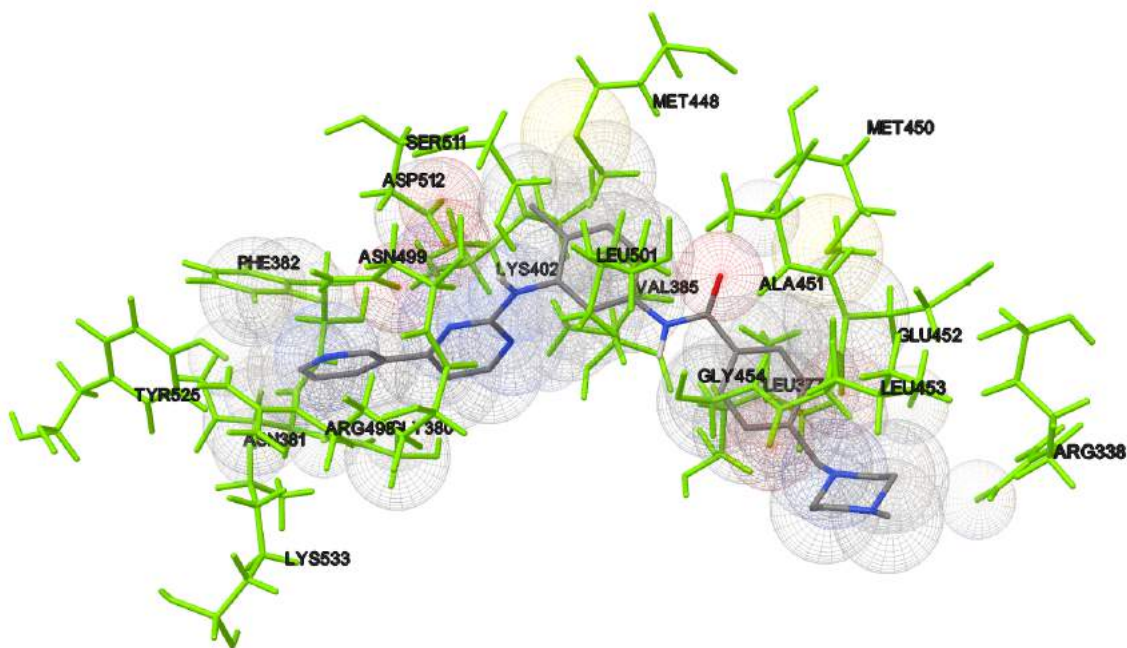


Fig. 34. 3D structure of Gleevec interaction with residues within the Syk catalytic site

4.2.3. Assessment of Syk inhibitors efficacy

Table 7 shows the values of energy of binding and the K_i obtained by computational analysis useful to deepen the role of Syk inhibitors and to better understand their efficacy in order to enable the implementation of in vitro testing by combining the results of both tests.

Conformational research on Syk inhibitors R406 [121], Gleevec, Syk inhibitor II and P505-15 [122] was performed by Sybyl software and the conformation with the lowest energies and best stability was selected.

Docking Syk inhibitors	Ligand	M.B.E	E.F.E.B	E.I.C, K_i
4FL2_Gleevec	Gleevec	-10,57	-10,73	13,65 nM
4FL2_P505-15	P505-15	-7,69	-8,81	346,88 nM
4FL2_R406	R406	-7,28	-7,94	1,5 μ M
4FL2_SykII	SykII	-6,8	-6,95	8,03 μ M

Tab. 7. Data reported show the values of Energy of binding and K_i obtained from cross-docking analysis of Syk inhibitors with 4FL2. **M.B.E** (Mean Binding Energy), **E.F.E.B** (Estimated Free Energy of Binding), **E.I.C** (Estimated Inhibition Constant).

4.2.4. Identification of residues as new sites for Syk specificity

The results achieved from the sequence alignment of Syk catalytic site compared to 65 kinases structure, lead us to the discovery of two more important residues (Ser511 and His531), which might have a role in Syk specificity. Four residues were already known in literature to be site of specificity of Syk (Met450, Leu453, Pro455 and Asn457). The main purpose was based on the identification of unique structural features of Syk binding pocket to prioritize the compounds binding to this region. To prove this, the principal residues having a role in the ligand-protein interaction have been aligned. Thereafter was used a software to generate the sequence logo. This has been analysed considering the size, the variability and the position of single aminoacid. From this analysis, we highlighted the known residues and two more residues important for the Syk specificity as showed in figure 35.

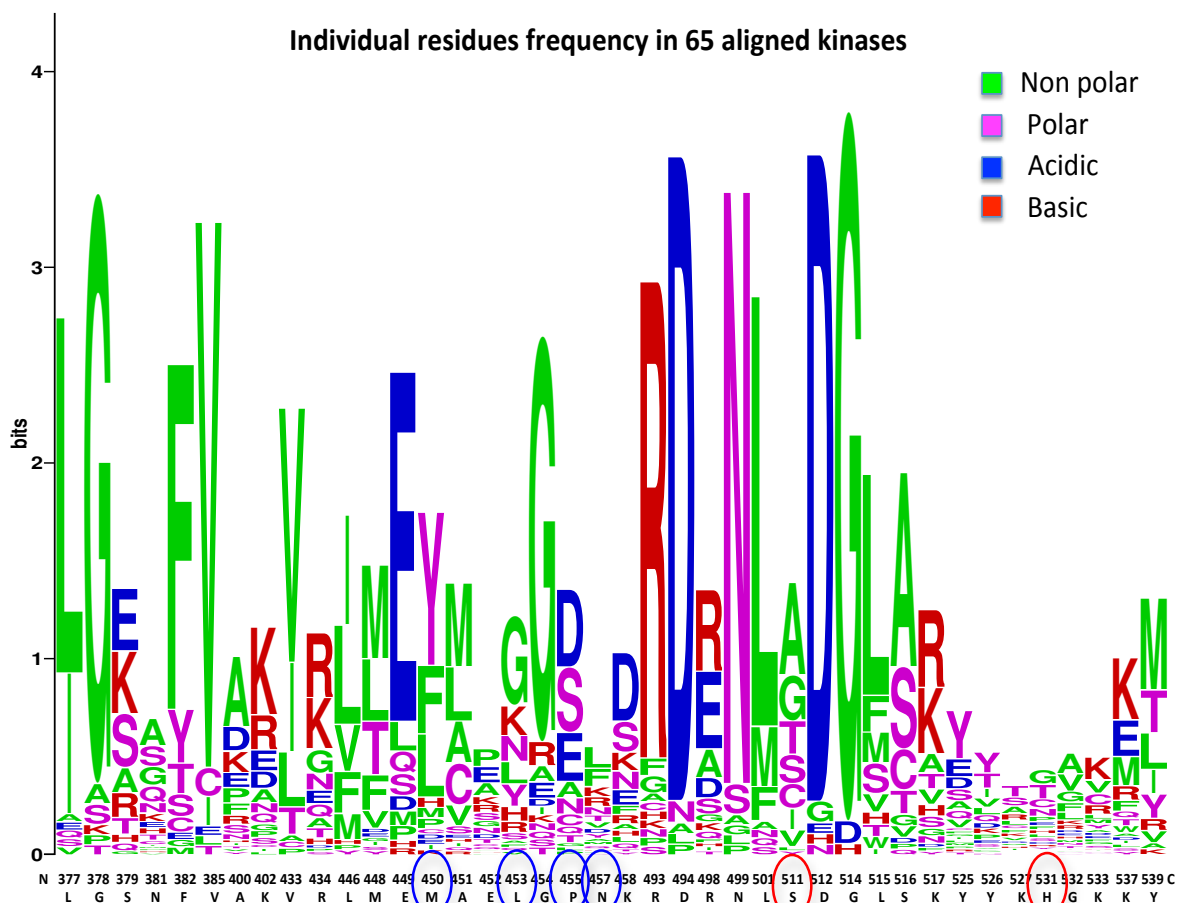
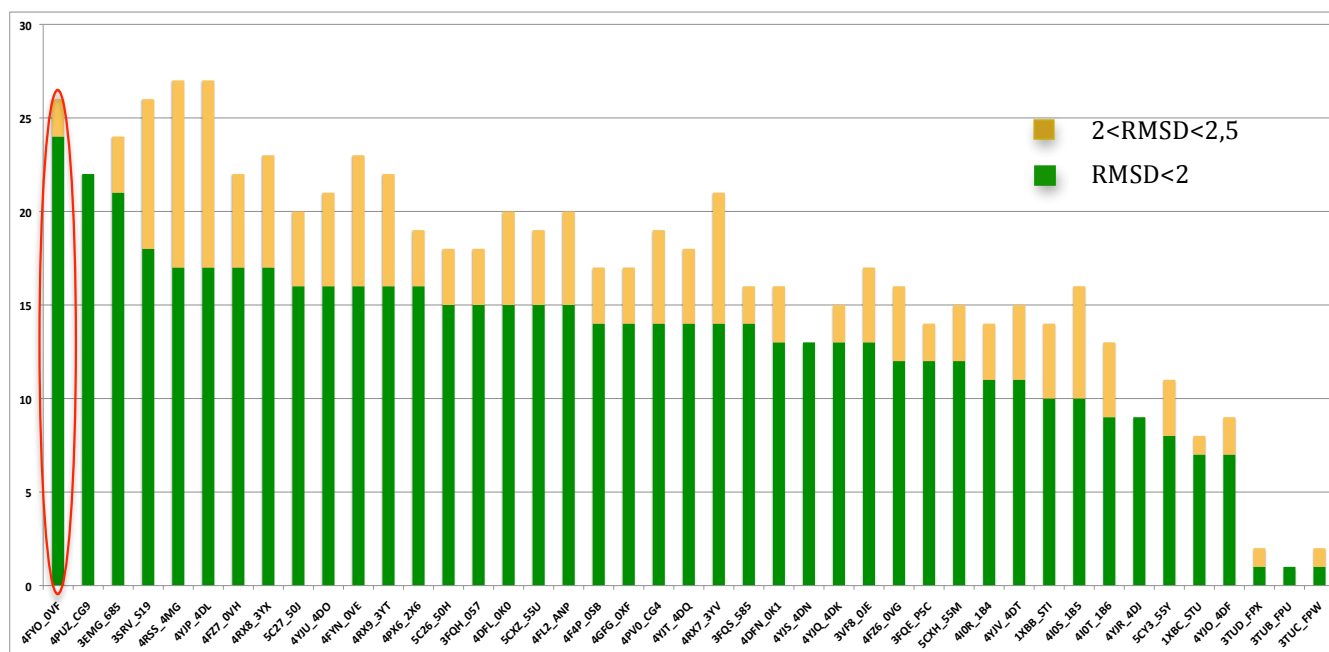


Fig. 35. The graph represents the Sequence Logo of kinase residues frequency over the sequence of Syk. Circled in blue are the aminoacid already known as site of Syk specificity; in red are the new specific residues found in Syk protein through the alignment analysis of 65 kinases.

4.2.5 Docking validation to select VS target (open conformation of Syk)

The method used for docking validation protocol has been helpful to select the suitable Syk structure performing for a virtual screening of new molecules. The first criterion of selection regard the median calculation of RMSD values obtained for each crystal structure interacting with the ligands. The second criterion is related to the number of ligands having $RMSD < 2$ and $2 < RMSD < 2.5$ for each crystal structure tested (Plot.1). These RMSD ranges were considered acceptable for a valid choice of the most suitable protein to use for VS. Forty-three catalytic domain structures have been picked from the RCSB PDB (Protein Data Bank) co-crystallized with their respective ligands and cross-docked with them (Tab.8). The best target structure has been chosen

evaluating the RMSD obtained from docking tests. Crystal structure of Syk protein (PDB ID 4FYO, resolution of 1.4 Å) has been selected (Fig. 36)



Plot. 1. The graph represents the data of crystal structures docked with the ligands. Green shows the RMSD < 2 and the yellow the 2 < RMSD < 2,5. The best Syk structure as target for the virtual screening is red circled (4FYO-0VF).

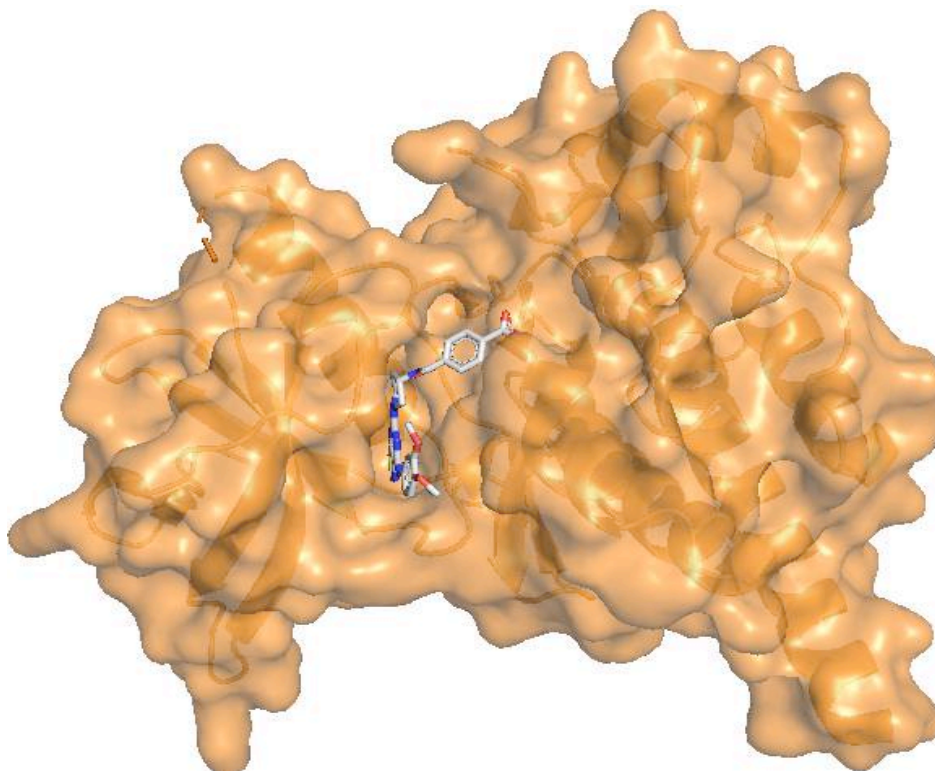


Fig. 36. 3D structure surface of 4FYO.pdb co-crystallized with its ligand OVF. Image generated with PyMOL software

The molecular orbitals HOMO-LUMO distribution, energies and energy gaps for the hit molecules were computed (Fig.37).

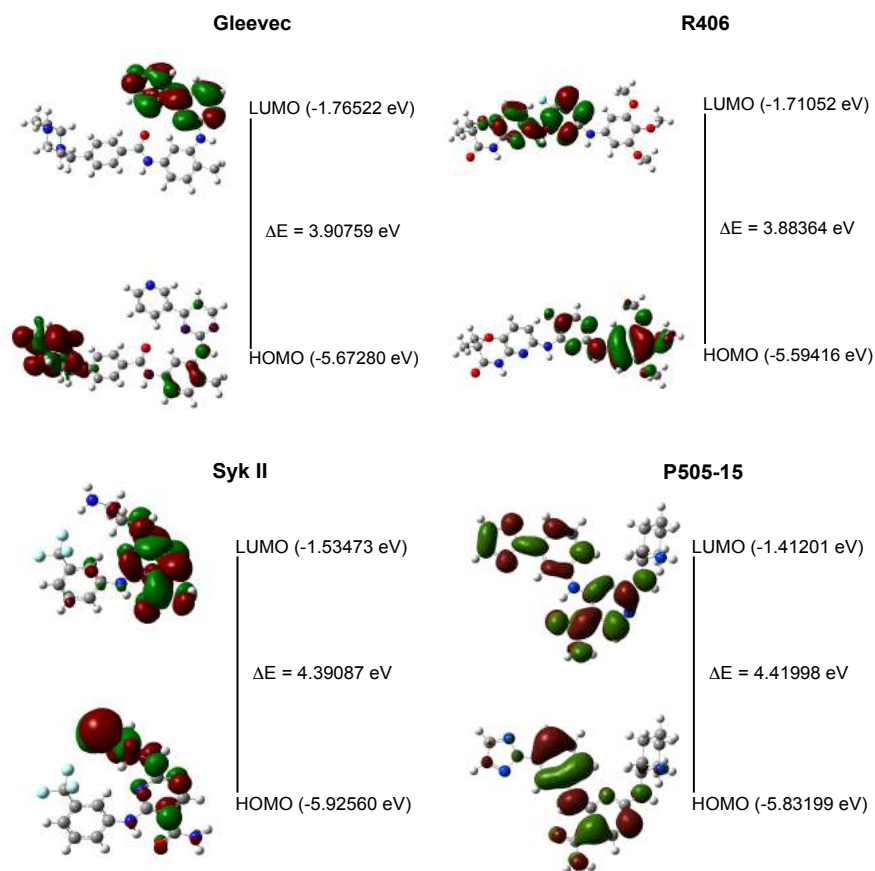


Fig. 37. The more probable statistically positions in molecular Homo-Lumo orbital descriptor. **Homo** is the highest occupied molecular orbital and **Lumo** represent the lowest occupied molecular orbital.

Energy gap between the HOMO and LUMO was used to determine the chemical stability and molecular features and contribute to explain the biological activity of the compounds [123].

The electrostatic potential maps computed shows the sites with abundant electrons by analysing charge distribution within a molecule in three dimensions; it is related with dipole moment, electronegativity and partial charges and shows the reactivity of a molecule. Positive potential values reflect nucleus predominance, while negative values represent rearrangements of electronic charges and lone pairs of electrons.

The MEP analysed is expressed in different colours depending on the density of organic molecules electrophilic electrons, where red colour represents negative charge and blue colour represents positive charge (Fig.38).

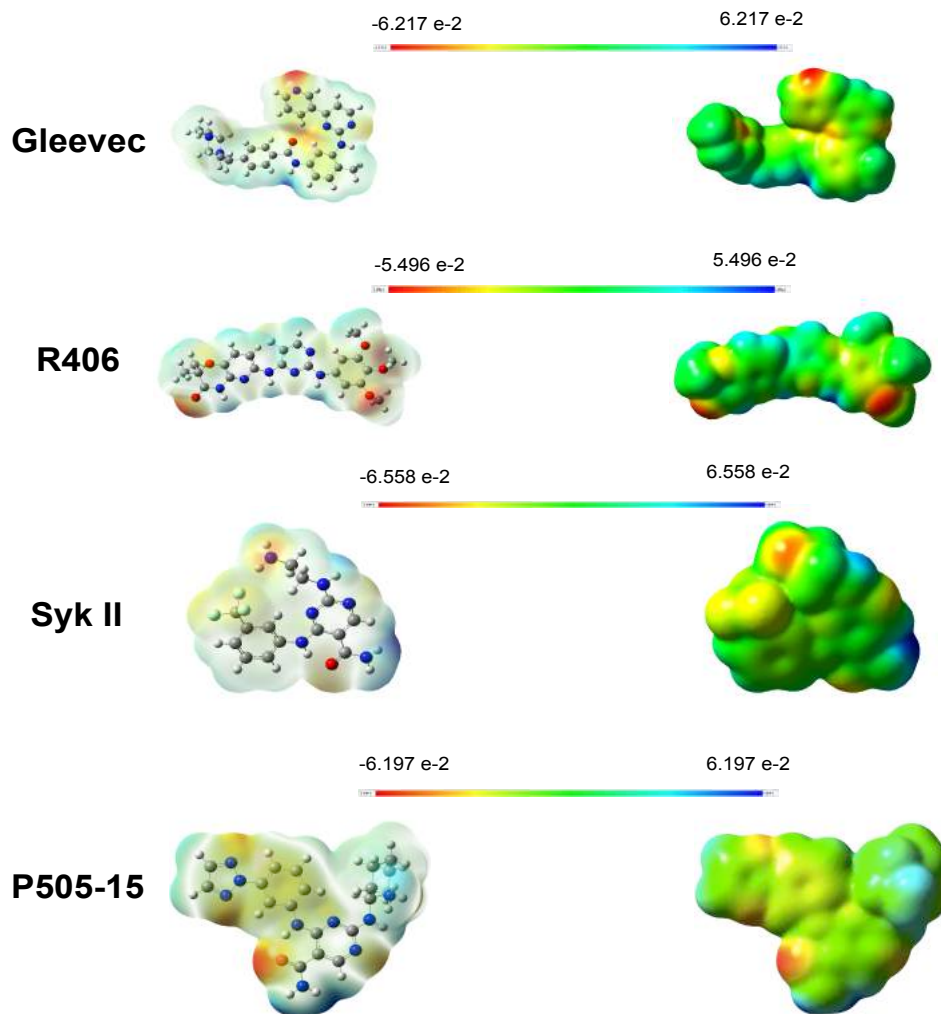
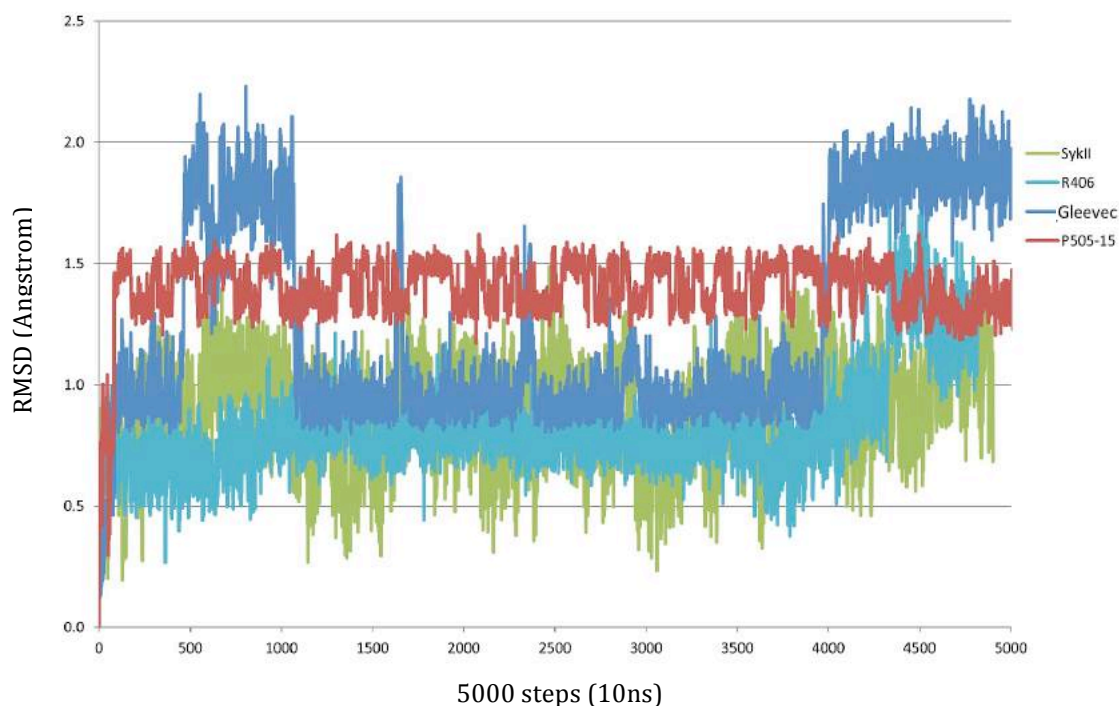


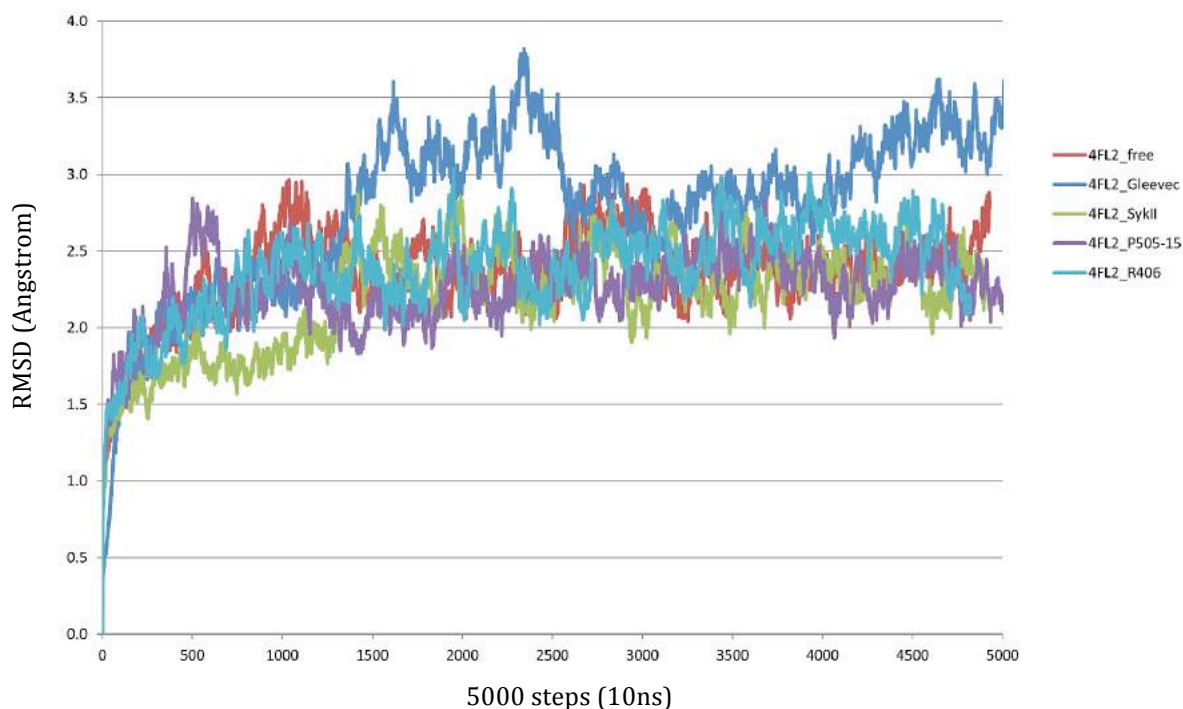
Fig. 38. MEP surface Syk inhibitors. The color scheme ranges from red (negative potential) via green (zero potential) to blue (positive potential). The unit of isosurface potential is electrostatic potential (eV).

4.2.6. Molecular Dynamic results

Molecular Dynamic results highlighted a major chemical stability and minor conformation changing of ligands P505-15 and R406 alone and in complex with crystal 4FL2 compared to Gleevec and Syk II (Plot 2,3).



Plot. 2. Molecular dynamic analysis of Syk inhibitors alone evaluated with Root Mean Square Deviation (RMSD)



Plot. 3. Molecular dynamic analysis of Syk inhibitors with protein target evaluated with Root Mean Square Deviation (RMSD)

As evidenced in plot 3, from 2-10 ns, the first complexes with P505-15 and R406 had lower changing of conformation into the pocket, deductible from the

range values, 1.8 to 2.8 Å. Instead, we observed especially that Gleevec has a significant variation of structure conformation with a range values, 2 – 3.8 Å. Thereafter a detailed analysis of compounds interaction has been performed in order to establish the differences among the ligands disposition into the Syk catalytic site in MD and the conformations obtained in docking analysis. It is evident as the ligands disposition in all molecular dynamic tests confirmed a similar pose and interaction with Syk protein (Fig.39). Furthermore, as can be seen from the plot above both ligands P505-15 and R406 present less fluctuations, namely more stability due to a better and strong interaction with residues into the pocket

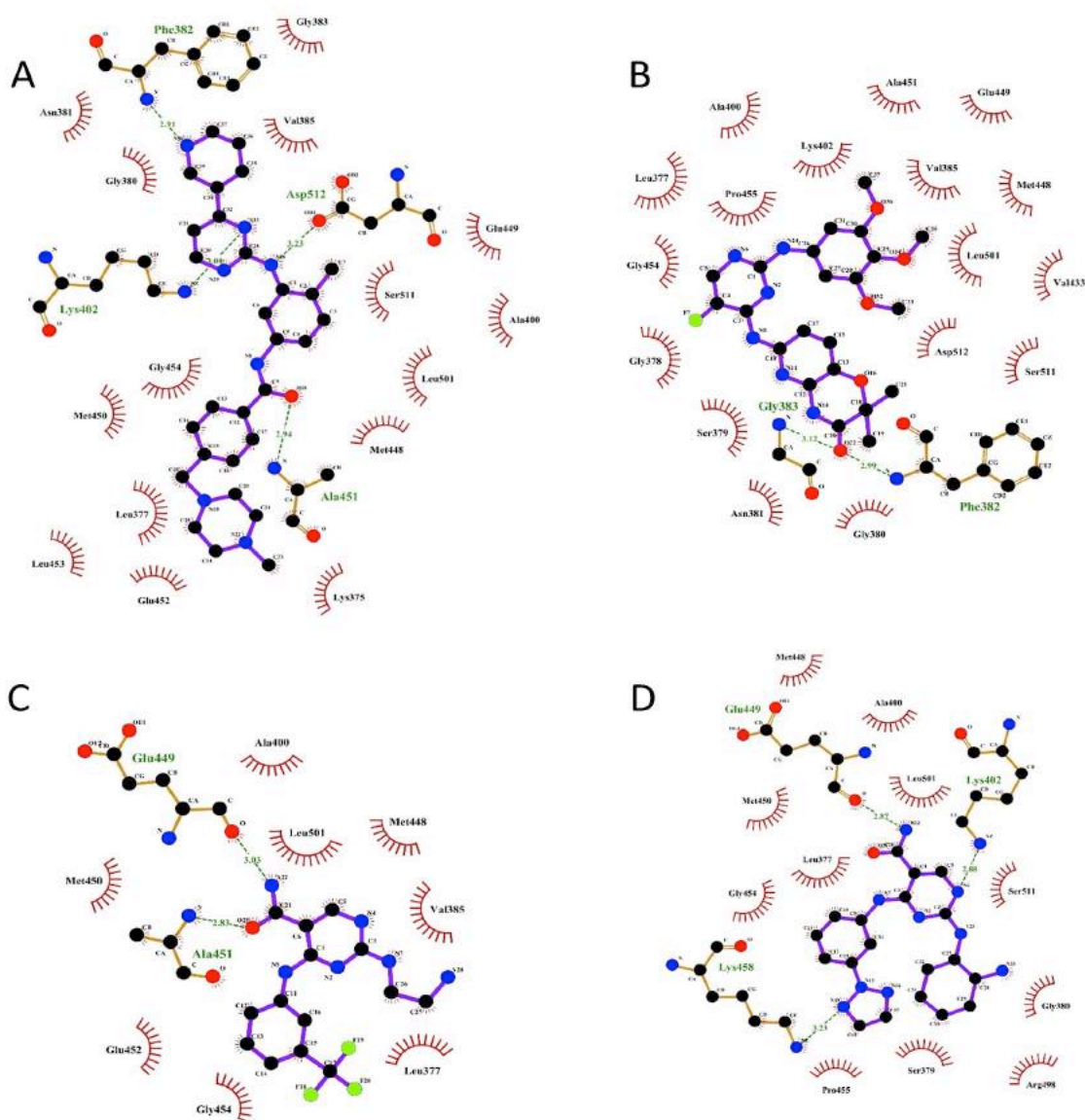


Fig. 39. Ligand plots of target structures Gleevec (A) R406 (B), SykII (C) and P505-15 (D) after 10ns molecular dynamics. As shown from the 2D diagrams don't indicate a significant changing in ligands pose compared to docking analysis.

4.2.7. RMSD maps in Molecular Dynamics

The RMSD maps after 10 ns of molecular dynamic were computed. Data achieved from the three different maps (protein alone, protein-ligands and ligands alone) provide much information about the chemical structure of the ligands and protein target as well as their interaction. The obtained maps regarding the structure of Syk (PDB ID: 4FL2) show a low variability and movement of protein domains, visible from small white squares. From the analyses of protein-ligands and ligands alone, as it is shown in the maps appear that the Gleevec has more lighter areas with stable conformation while R406 and P505-15, considered the high number of white squares, present many small conformational variations. Although they have less conformational changing and atoms movements during the interaction with Syk protein, Gleevec appear as the most stable inhibitor (Fig. 40).

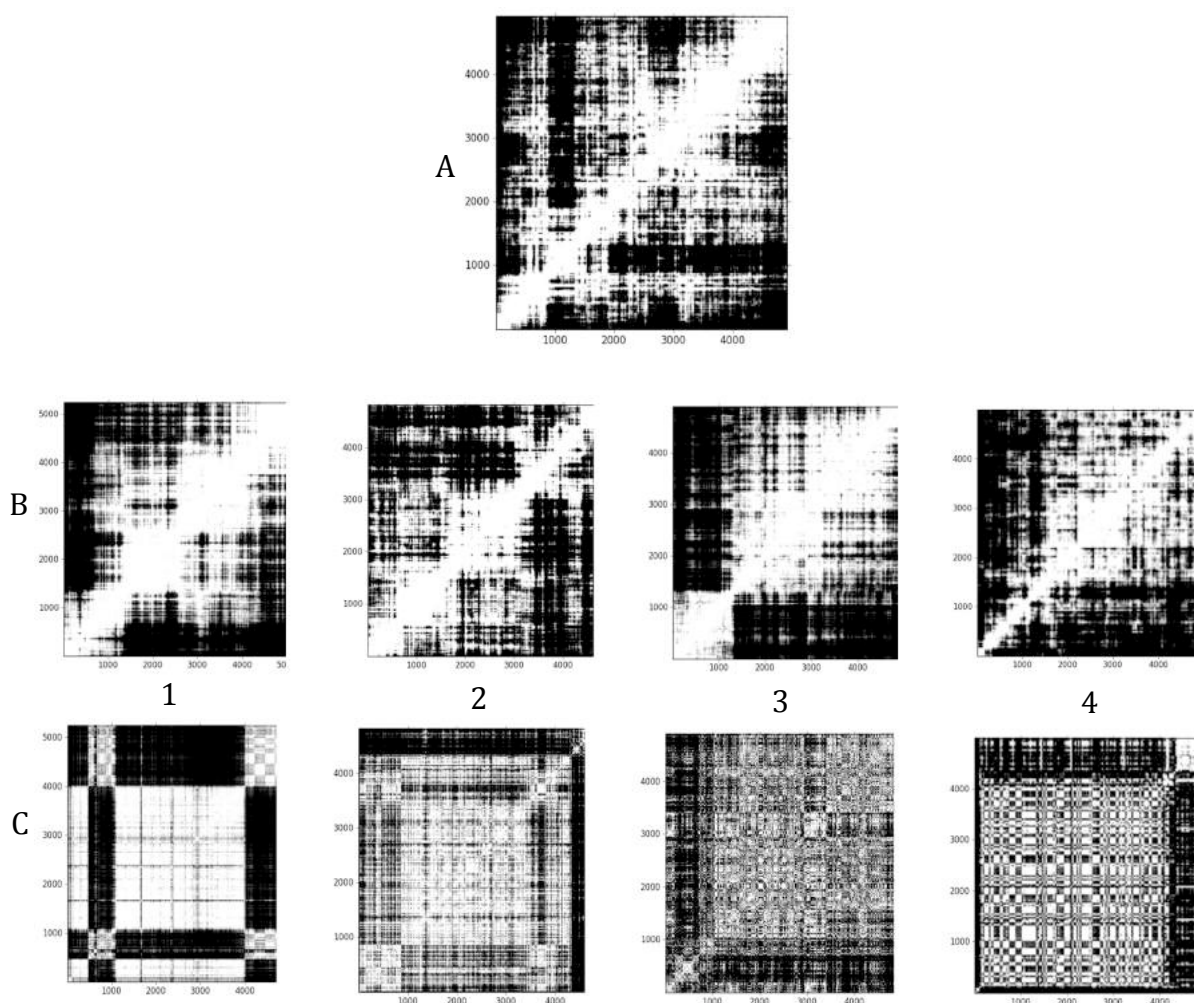


Fig.40. RMSD maps from 10ns of molecular dynamic. The greyscale representation shows the maps of the protein Syk (crystal PDB ID: 4FL2) alone (A), protein-ligands (B), Gleevec (1), R406 (2), Syk II (3), P505-15 (4) and the maps of inhibitors alone (C) Gleevec (1), R406 (2), Syk II (3), P505-15 (4).

4.2.8. Virtual Screening results

The first VS has been performed with a diversity set of 46.840 compounds (Cambridge database) using as protein target the crystal structure with open conformation of Syk (PDB ID: 4FYO with resolution of 1.4 Å) (Fig.41).

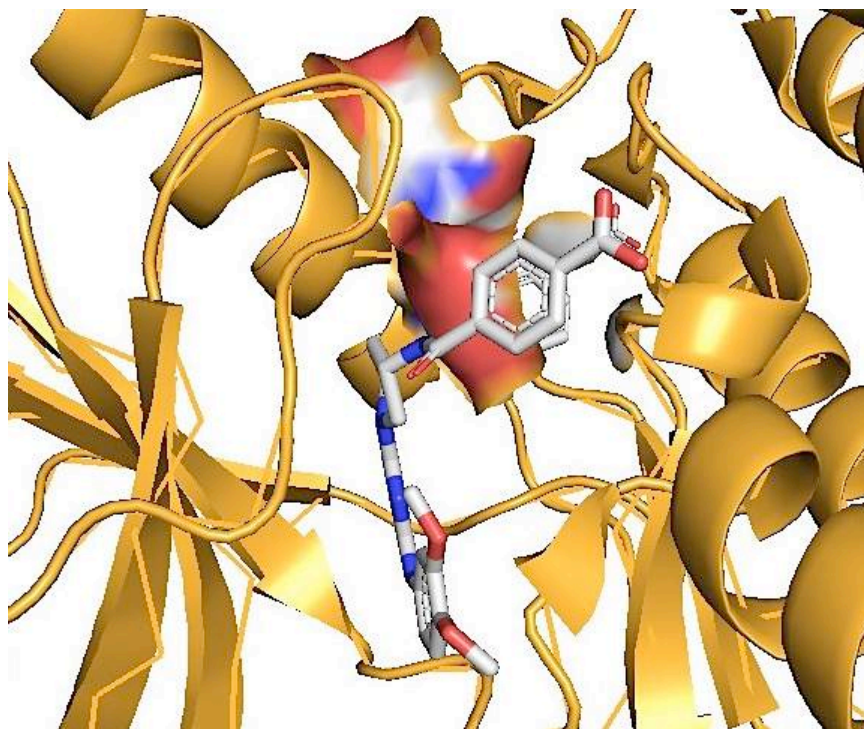


Fig. 41. 3D model of 4FYO structure co-crystallized with its ligand 0VF. The ligand is represented with sticks inside the pocket while the three residues DFG (Asp512, Phe51 and Gly514) are shown with surface and are disposed to close the deep pocket.

The second VS was conducted using a special conformation of Syk protein known as DFG-out (PDB ID: 3TUB with resolution of 2.23 Å). In this crystal structure is evident a displacement of 3 a.a. residues (Asp512, Phe513, Gly514) into the catalytic site of Syk, allowing the interaction of ligands with a deep pocket previously hidden (Fig.42).

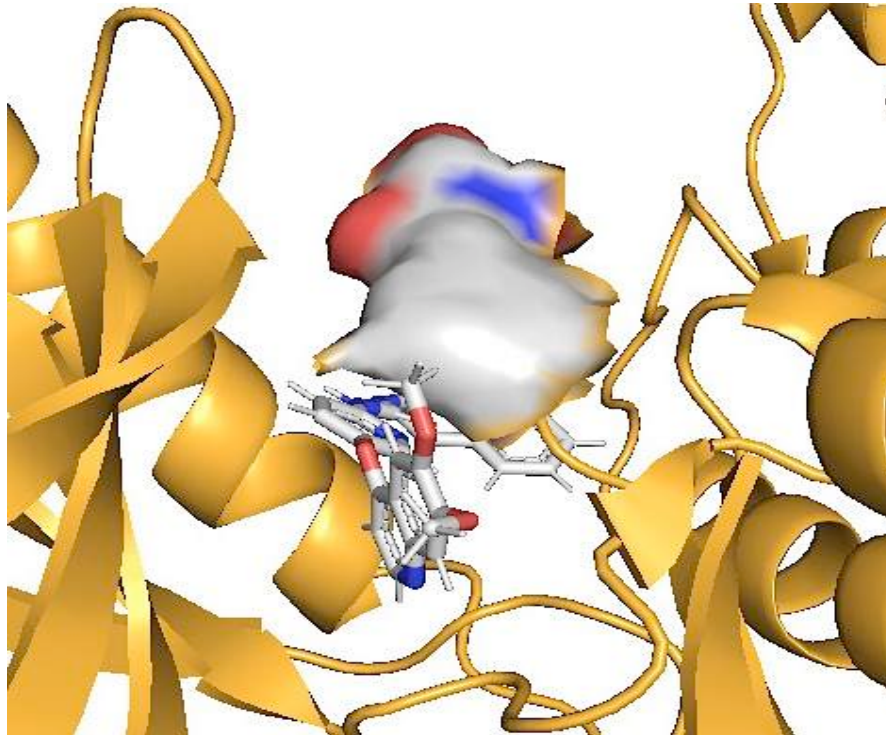


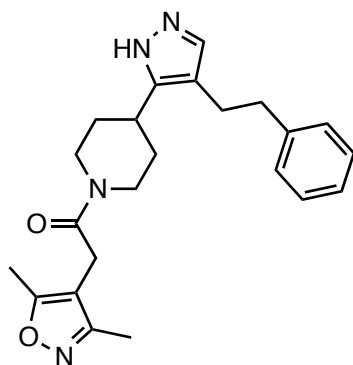
Fig. 42. 3D model of 3TUB structure co-crystallized with its ligand FPU. The ligand is represented with sticks while the three residues DFG are shown with surface and are disposed to close the deep pocket.

Both virtual screening results have been analysed applying three kind of filter considering the energy of binding, the ligand efficiency and the hydrogen bond interaction:

- **Energy** (-7 Kcal/mol to better values)
- **Ligand Efficiency** (range - 0.2 and - 0.6)
- **Hbond interaction filter:** (MET450 – ALA451 – SER511 – ASP512)

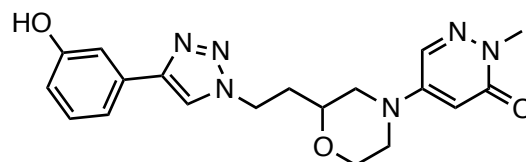
4.2.9. Compounds to test in vitro selected from Virtual screening

(Highlighted in orange are the structures found in the second VS with 3TUB crystal structure)



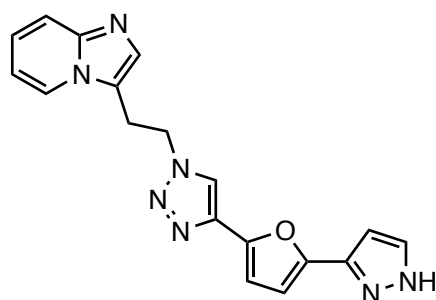
M.W. = 392.5

2-(3,5-dimethylisoxazol-4-yl)-1-(4-(4-phenethyl-1H-pyrazol-5-yl)piperidin-1-yl)ethanone



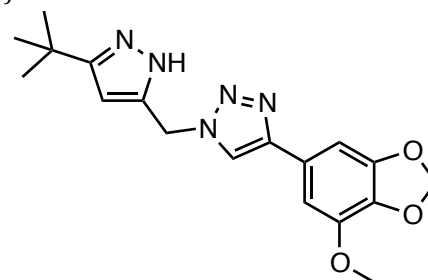
M.W. = 382.4

5-(2-(2-[4-(3-hydroxyphenyl)-1H-1,2,3-triazol-1-yl]ethyl)morpholin-4-yl)-2-methylpyridazin-3(2H)-one



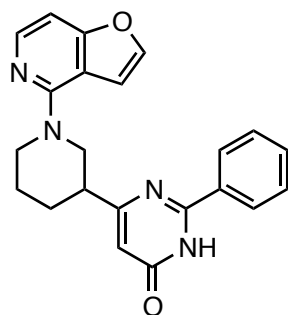
M.W. = 345.3

3-(2-(4-[5-(1H-pyrazol-3-yl)-2-furyl]-1H-1,2,3-triazol-1-yl)ethyl)imidazo[1,2-a]pyridine



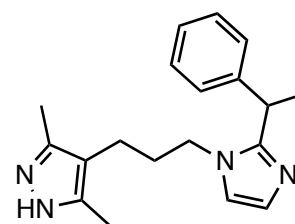
M.W. = 355.4

1-[(3-tert-butyl-1H-pyrazol-5-yl)methyl]-4-(7-methoxy-1,3-benzodioxol-5-yl)-1H-1,2,3-triazole



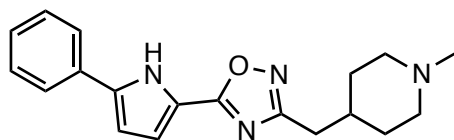
M.W. = 372.4

6-(1-furo[3,2-c]pyridin-4-yl)piperidin-3-yl)-2-phenylpyrimidin-4(3H)-one



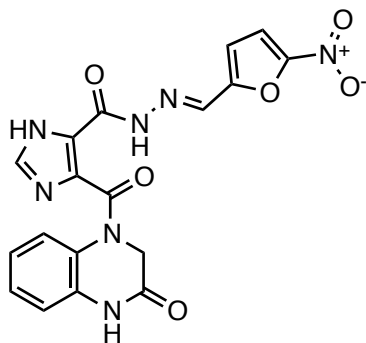
M.W. = 308.4

3,5-dimethyl-4-{3-[2-(1-phenylethyl)-1H-imidazol-1-yl]propyl}-1H-pyrazole



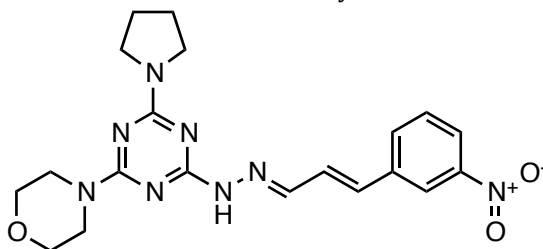
M.W. = 322.4

1-methyl-4-[[5-(5-phenyl-1H-pyrrol-2-yl)-1,2,4-oxadiazol-3-yl]methyl]piperidine

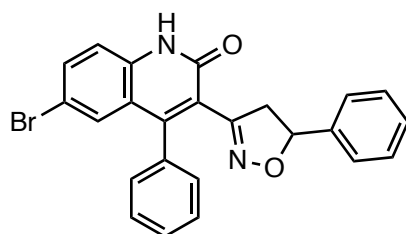


M.W. = 423,3

N'-[[5-nitro-2-furyl]methylene]-4-[[3-oxo-3,4-dihydro-1(2H)-quinoxaliny]carbonyl]-1H-imidazole-5-carbohydrazide

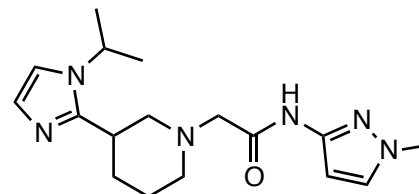


M.W. = 424,4

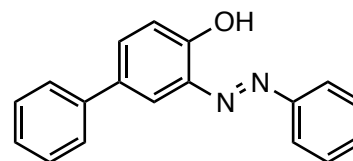
3-(3-nitrophenyl)acrylaldehyde [4-(4-morpholinyl)-6-(1-pyrrolidinyl)-1,3,5-triazin-2-yl]hydrazone

M.W. = 445.3

6-bromo-4-phenyl-3-(5-phenyl-4,5-dihydro-3-isoxazolyl)-2(1H)-quinolinone

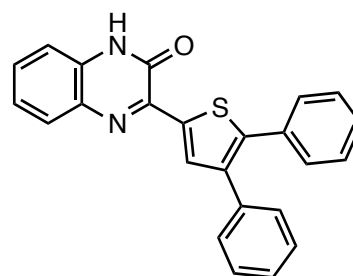


M.W. = 330.4

2-[3-(1-isopropyl-1H-imidazol-2-yl)-1-piperidinyl]-N-(1-methyl-1H-pyrazol-3-yl)acetamide

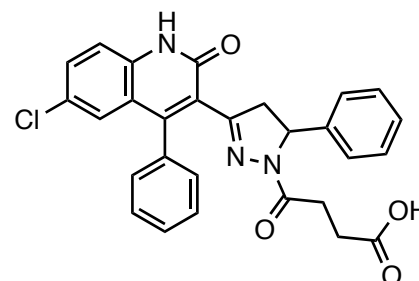
M.W. = 274,3

3-(phenyldiazenyl)-4-biphenylol



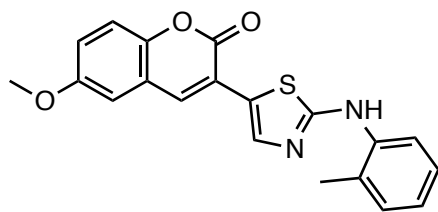
M.W. = 380.5

3-(4,5-diphenyl-2-thienyl)-2(1H)-quinoxalinone



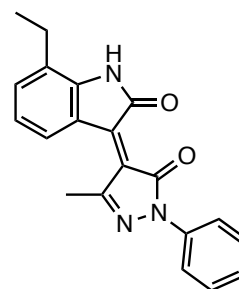
M.W. = 500.0

4-[3-(6-chloro-2-oxo-4-phenyl-1,2-dihydro-3-quinolinyl)-5-phenyl-4,5-dihydro-1H-pyrazol-1-yl]-4-oxobutanoic acid



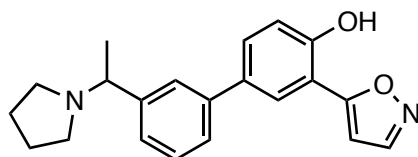
M.W. = 364.4

6-methoxy-3-{2-[(2-methylphenyl)amino]-1,3-thiazol-5-yl}-2H-chromen-2-one



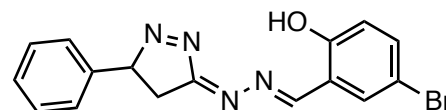
M.W. = 331.4

7-ethyl-3-(3-methyl-5-oxo-1-phenyl-1,5-dihydro-4H-pyrazol-4-ylidene)-1,3-dihydro-2H-indol-2-one



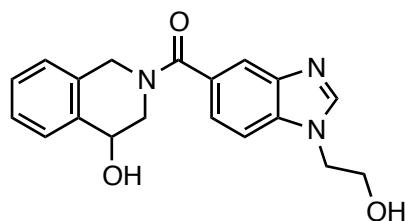
M.W. = 334.1

3-isoxazol-5-yl-3'-(1-pyrrolidin-1-ylethyl)biphenyl-4-ol



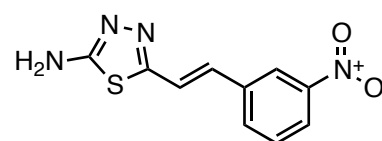
M.W. = 357.2

5-bromo-2-hydroxybenzaldehyde (5-phenyl-4,5-dihydro-3H-pyrazol-3-ylidene)hydrazone



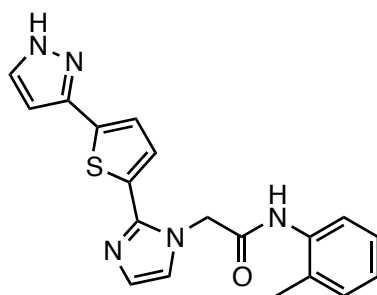
M.W. = 337.4

2-[[1-(2-hydroxyethyl)-1H-benzimidazol-5-yl]carbonyl]-1,2,3,4-tetrahydroisoquinolin-4-ol



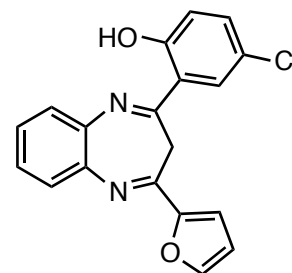
M.W. = 248.3

5-[2-(3-nitrophenyl)vinyl]-1,3,4-thiadiazol-2-amine



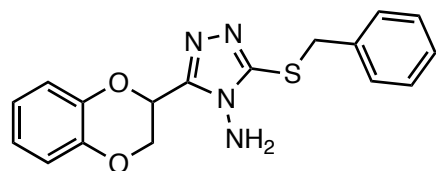
M.W. = 363.4

N-(2-methylphenyl)-2-{2-[5-(1H-pyrazol-3-yl)-2-thienyl]-1H-imidazol-1-yl}acetamide



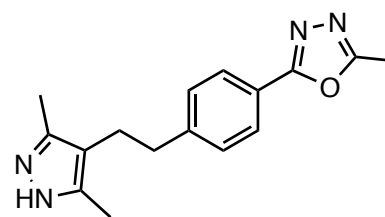
M.W. = 336.7

4-chloro-2-[4-(2-furyl)-3H-1,5-benzodiazepin-2-yl]phenol



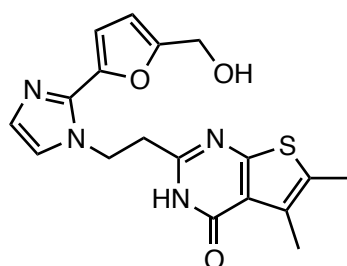
M.W. = 340.4

3-(benzylthio)-5-(2,3-dihydro-1,4-benzodioxin-2-yl)-4H-1,2,4-triazol-4-amine



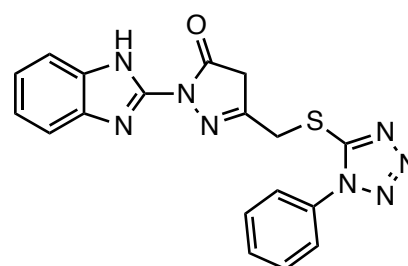
M.W. = 282.3

2-{4-[2-(3,5-dimethyl-1H-pyrazol-4-yl)ethyl]phenyl}-5-methyl-1,3,4-oxadiazole



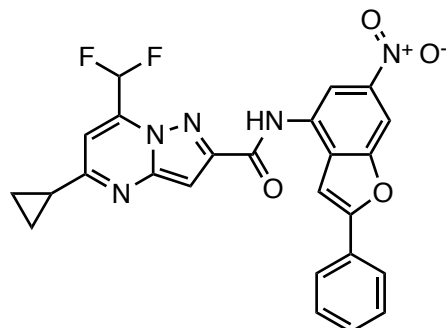
M.W. = 370.4

2-(2-{2-[5-(hydroxymethyl)-2-furyl]-1H-imidazol-1-yl}ethyl)-5,6-dimethylthieno[2,3-d]pyrimidin-4(3H)-one



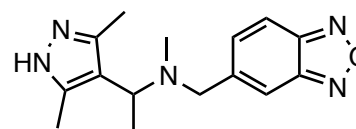
M.W. = 370.4

2-(1H-benzimidazol-2-yl)-5-[[[1-phenyl-1H-tetrazol-5-yl]thio]methyl]-2,4-dihydro-3H-pyrazol-3-one



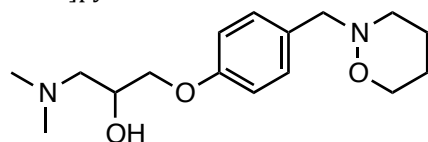
M.W. = 489.4

5-cyclopropyl-7-(difluoromethyl)-N-(6-nitro-2-phenyl-1-benzofuran-4-yl)pyrazolo[1,5-a]pyrimidine-2-carboxamide



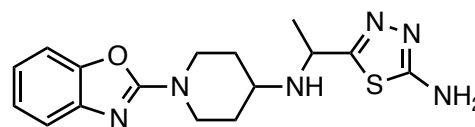
M.W. = 285.3

(2,1,3-benzoxadiazol-5-ylmethyl)[1-(3,5-dimethyl-1H-pyrazol-4-yl)ethyl]methylamine



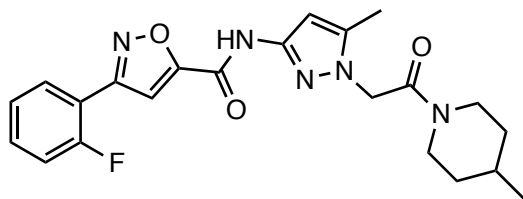
M.W. = 294.4

1-(dimethylamino)-3-[4-(1,2-oxazinan-2-ylmethyl)phenoxy]-2-propanol



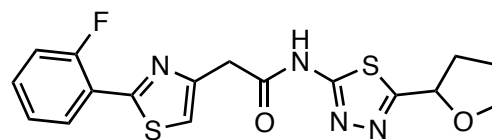
M.W. = 344.4

N-[1-(5-amino-1,3,4-thiadiazol-2-yl)ethyl]-1-(1,3-benzoxazol-2-yl)piperidin-4-amine



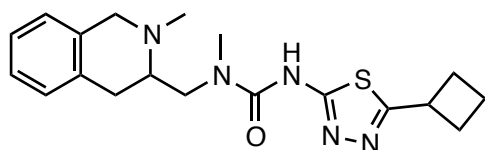
M.W. = 425.5

3-(2-fluorophenyl)-N-[5-methyl-1-[2-(4-methyl-1-piperidinyl)-2-oxoethyl]-1H-pyrazol-3-yl]-5-isoxazolecarboxamide



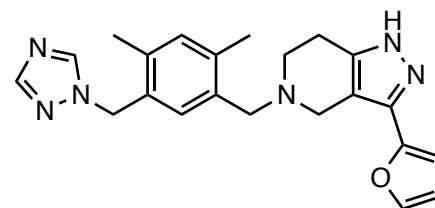
M.W. = 390.5

2-[2-(2-fluorophenyl)-1,3-thiazol-4-yl]-N-[5-(tetrahydro-2-furanyl)-1,3,4-thiadiazol-2-yl]acetamide



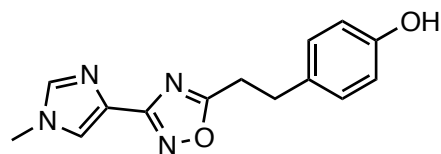
M.W. = 371.5

3-(5-Cyclobutyl-1,3,4-thiadiazol-2-yl)-1-methyl-1-[[2-methyl-1,2,3,4-tetrahydro-3-isoquinolinyl)methyl]urea



M.W. = 388.5

5-[2,4-Dimethyl-5-(1H-1,2,4-triazol-1-ylmethyl)benzyl]-3-(2-furyl)-4,5,6,7-tetrahydro-1H-pyrazolo[4,3-c]pyridine



M.W. = 270.3

4-{2-[3-(1-Methyl-1H-imidazol-4-yl)-1,2,4-oxadiazol-5-yl]ethyl}phenol

5. CONCLUSION & PERSPECTIVES

Conclusion & Perspectives

In this study, we evaluated the behaviour of promising compounds as new antimalarial drugs to block the Syk phosphorylation events, in infected RBCs by parasites, an essential prerequisite for parasite egression from the host cell. Different methodologies about *in vitro* and *in silico* studies were applied to generate the data of this thesis.

In vitro and especially through proteomic studies we noticed a great decrease of phosphorylation levels when RBCs were treated by Syk Inhibitors and diamide. The biological data were also confirmed by the computational studies. Syk inhibitors establish many interactions into the Syk protein pocket. Important hydrogen bonds and hydrophobic interaction with aminoacid within the binding pocket, involved in the inhibition process, were found. Regarding the studies on Gleevec and its interactions with Syk, the Tyr 525 could be the key to understanding the best efficacy of this inhibitor *in silico*, although this it is not specific for Syk. Furthermore, the experimental data achieved in docking and molecular dynamics analyses demonstrated that most of the amino acid interactions established by Syk inhibitors could be relevant to provide a better chemical stability and a lower binding energy. All the studied ligands respected the pattern of interaction of kinases and especially interacted with 3 amino acids Met450, Leu453 and Pro455, which are of great importance to point out high levels of Syk specificity [30-32]. We did not find a high correspondence between the data obtained *in vitro* and *in silico* especially for Gleevec. Gleevec has the largest interactions and the lowest K_i in docking results but did not evidence the same in *in vitro* studies. We are currently investigating the motivations. Probably it could be due from a lot of biological variables in the infected RBCs cultures compared with the modelling approach (i.e. RBC membrane transport, presence of parasite, drugs concentration), which could make more or less active this compounds. The inhibitors R406 and P505-15 and their IC_{50} , followed the same trend both *in vitro* and *in silico* and they have more effectiveness.

The values of free energies binding confirmed the high affinity of Syk inhibitors to the catalytic site. The Virtual Screening approach has laid the foundation to develop novel and promising compounds having antimalarial

activity. The computational studies carried out on the crystal structures of Tyr kinases, available in RCSB PDB database compared with Syk, allow us to find two new a.a. residues specific for Syk (Ser511 and His531). Compounds selected from the VS study appear good inhibitors of Syk considering the hbond and the strong pattern of interactions with the catalytic site. The virtual screening studies, performed with a particular conformation of Syk structure, having a deep binding pocket (DFG-out) enhance the research of new compounds interacting with the allosteric site of Syk.

Further studies carried out to find the site of specificity for Syk protein compared to other kinases has been the key to screen and select new suitable compounds, which interact with ATP competitive pocket. These compounds will be tested *in vitro* in order to improve the inhibition efficacy and to discover new promising therapy able to block the parasite growth.

6. REFERENCES

References

1. Report WHO (World Health Organization) 2017
2. Report WHO (World Health Organization) 2016
3. Manirakiza, A., Serdouma, E., Ngalé, R. N., Moussa, S., Gondjé, S., Degana, R. M., Sepou, A. (2017). A brief review on features of falciparum malaria during pregnancy. *Journal of Public Health in Africa* 2017, 8, 27–29.
4. Borgella S, Fievet N, Huynh BT, Ibitokou S, Hounguevou G, et al. (2013) Impact of Pregnancy-Associated Malaria on Infant Malaria Infection in Southern Benin. *PLOS ONE* 8(11): e80624.
5. Moya-Alvarez, V., Abellana, R., & Cot, M. (2014). Pregnancy-associated malaria and malaria in infants: an old problem with present consequences. *Malaria Journal*, 13, 271.
6. Sharifi-mood, B. (2015). Malaria in Pregnant Women. *International Journal of Infection*, 2(3), 2–3.
7. <https://www.cdc.gov/malaria/about/biology/index.html>
8. Chugh, M., Sundararaman, V., Kumar, S., Reddy, V. S., & Siddiqui, W. A. (2013). Protein complex directs hemoglobin-to-hemozoin formation in Plasmodium falciparum. *PNAS*, 1–6.
9. Rosenthal PJ (2011) Falcipains and other cysteine proteases of malaria parasites. *Adv Exp Med Biol* 712:30–48.
10. Klemba M, Gluzman I, Goldberg DE (2004) A Plasmodium falciparum dipeptidyl aminopeptidase I participates in vacuolar hemoglobin degradation. *J Biol Chem* 279(41):43000–43007.
11. Oliveira MF, et al. (2005) Structural and morphological characterization of hemozoin produced by Schistosoma mansoni and Rhodnius prolixus. *FEBS Lett* 579(27): 6010–6016.
12. Egan TJ (2008) Recent advances in understanding the mechanism of hemozoin (malaria pigment) formation. *J Inorg Biochem* 102(5-6): 1288–1299.
13. https://www.cdc.gov/malaria/about/biology/human_factors.html
14. <https://www.cdc.gov/malaria/about/disease.html>
15. Bartoloni, A., & Zammarchi, L. (2012). Clinical Aspects of Uncomplicated and Severe Malaria. *Mediterranean Journal of Hematology and Infectious Diseases*, 4(1), e2012026.
16. Trampuz, A., Jereb, M., Muzlovic, I., & Prabhu, R. M. (2003). Clinical review: Severe malaria. *Critical Care*, 7(4), 315–323.
17. Shikani, H. J., Freeman, B. D., Lisanti, M. P., Weiss, L. M., Tanowitz, H. B., & Desruisseaux, M. S. (2012). Cerebral Malaria: We Have Come a Long Way. *The American Journal of Pathology*, 181(5), 1484–1492.
18. Reithmeier, R. A. F., Casey, J. R., Kalli, A. C., Sansom, M. S. P., Alguel, Y., & Iwata, S. (2016). Biochimica et Biophysica Acta Band 3 , the human red cell chloride / bicarbonate anion

- exchanger (AE1 , SLC4A1), in a structural context .*BBA - Biomembranes*, 1858(7), 1507–1532.
19. Arakawa, T., Kobayashi-Yurugi, T., Alguel, Y., Iwanari, H., Hatae, H., Iwata, M., Iwata, S. (2015). Crystal structure of the anion exchanger domain of human erythrocyte band 3. *Science*, 350(6261), 680 LP-684.
 20. Iv, S. E. L., Bennett, G. V., Branton, D., Bruce, L., Delaunay, J., Discher, D., Palek, J. (2018). Review Article Anatomy of the red cell membrane skeleton : unanswered questions. *Blood*, 127(2), 187–200.
 21. Saito, M., Watanabe-nakayama, T., Machida, S., & Osada, T. (2015). Biophysical Chemistry Spectrin – ankyrin interaction mechanics : A key force balance factor in the red blood cell membrane skeleton. *Biophysical Chemistry*, 200–201, 1–8.
 22. Rui, Z., Chenyu, Z., Qi, Z., & Donghai, L. I. (2013). Spectrin : Structure, function and disease. *Science China Life Sciences*, 56(12), 1076–1085.
 23. Berton, G., Mocsai, A. & Lowell, C. A. (2005). Src and Syk kinases: key regulators of phagocytic cell activation. *Trends Immunol*, 26, 208–214.
 24. Sada, K., Takano, T., Yanagi, S. & Yamamura, H. (2001). Structure and function of Syk protein tyrosine-kinases. *J. Biochem*, 130, 177–186.
 25. Siraganian, R. P., Zhang, J., Suzuki, K. & Sada, K. (2002). Protein tyrosine kinase Syk in mast cell signaling. *Mol. Immunol*, 38, 1229–1233.
 26. Singh, R., Masuda, E. S. & Payan, D. G. (2012). Discovery and development of spleen tyrosine kinase (SYK) inhibitors. *J. Med. Chem*, 55, 3614–3643.
 27. Van Oers, N. S. & Weiss, A. (1995). The Syk/ZAP-70 protein tyrosine kinase connection to antigen receptor signalling processes. *Semin. Immunol*, 7, 227–236.
 28. Kulathu, Yogesh, G. G., & Reth, M. (2009). Autoinhibition and adapter function of Syk. *Immunological Reviews*, 232, 286–299.
 29. Arias-Palomo et al (2010). *NIH Public Access*, 1794(8), 1211–1217.
 30. Pantaleo, A., Ferru, E., Carta, F., Mannu, F., Simula, L. F., Khadjavi, A., Turrini, F. (2011). Irreversible AE1 Tyrosine Phosphorylation Leads to Membrane Vesiculation in G6PD Deficient Red Cells. *PLoS One*, 6(1).
 31. Pantaleo A, Ferru E, Carta F, Mannu F, Giribaldi G, Vono R, Lepedda AJ, Pippia P, Turrini F (2010). Analysis of changes in tyrosine and serine phosphorylation of red cell membrane proteins induced by *P. falciparum* growth. *Proteomics*, 10(19), 3469-79.
 32. Pantaleo, A., Ferru, E., Vono, R., Giribaldi, G., Lobina, O., Nepveu, F., Turrini, F. (2012). New antimalarial indolone- N - oxides, generating radical species, destabilize the host cell membrane at early stages of *Plasmodium falciparum* growth : role of band 3 tyrosine phosphorylation. *Free Radical Biology and Medicine*, 52(2), 527–536
 33. Ayi, K., Turrini, F., Piga, A., & Arese, P. (2004). Enhanced phagocytosis of ring-parasitized mutant erythrocytes : a common mechanism that may explain protection against *falciparum* malaria in sickle trait and beta-thalassemia trait. *Blood*, 104(10), 3364–3372.

34. Ferru, E., Pantaleo, A., Carta, F., Mannu, F., Khadjavi, A., Gallo, V., Turrini, F. (2014). Thalassemic erythrocytes release microparticles loaded with hemichromes by redox activation of p72Syk kinase. *Haematologica*, 99(3):570-8.
35. Pantaleo, A., Ferru, E., Carta, F., Valente, E., Pippia, P., & Turrini, F. (2012). Effect of heterozygous beta thalassemia on the phosphorylative response to Plasmodium falciparum infection. *Journal of Proteomics*, 76, 251–258.
36. Pantaleo, A., Ferru, E., Carta, F., Mannu, F., Simula, L. F., Khadjavi, A., Turrini, F. (2011). Irreversible AE1 Tyrosine Phosphorylation Leads to Membrane Vesiculation in G6PD Deficient Red Cells. *PLoS One*, 6(1).
37. White NJ (1997). Assessment of the pharmacodynamic properties of antimalarial drugs in vivo. *Antimicrob. Agents Chemother*, 41 (7): 1413–22.
38. Brown, Geoff (2006). Artemisinin and a new generation of antimalarial drug. Education in Chemistry. Vol. 43 no. 4. *Royal Society of Chemistry*, pp. 97–99.
39. Fairhurst, R. M., Dondorp, A. M., Medicine, M. T., & Kingdom, U. (2016). Artemisinin-resistant Plasmodium falciparum malaria. *Microbiology spectrum*, 4(3), 1–25.
40. Winzeler EA, Manary MJ (2014). Drug resistance genomics of the antimalarial drug artemisinin. *Genome Biology*, 15 (11): 544
41. Cravo P, Napolitano H, Culleton R (2015). How genomics is contributing to the fight against artemisinin-resistant malaria parasite. *Acta Tropica*, 148: 1–7.
42. Wang J, Zhang CJ, Chia WN, Loh CC, Li Z, Lee YM, He Y, Yuan LX, Lim TK, Liu M, Liew CX, Lee YQ, Zhang J, Lu N, Lim CT, Hua ZC, Liu B, Shen HM, Tan KS, Lin Q (2015). Haem-activated promiscuous targeting of artemisinin in Plasmodium falciparum. *Nature Communications*, 6: 10111.
43. Woo, Soon Hyung; Parker, Michael H.; Ploypradith, Poonsakdi; Northrop, John; Posner, Gary H. (1998). Direct conversion of pyranose anomeric OH→F→R in the artemisinin family of antimalarial trioxanes. *Tetrahedron Letters*. 39 (12): 1533–6.
44. Arinaitwe, Emmanuel; Sandison, Taylor G.; Wanzira, Humphrey; Kakuru, Abel; Homsy, Jaco; Kalamya, Julius; Kanya, Moses R.; Vora, Neil; et al. (2009). Artemether-Lumefantrine versus Dihydroartemisinin-Piperaquine for Falciparum Malaria: A Longitudinal, Randomized Trial in Young Ugandan Children. *Clinical Infectious Diseases*, 49 (11): 1629–37.
45. Cumming JN; Ploypradith P; Posner GH (1997). Antimalarial activity of artemisinin (qinghaosu) and related trioxanes: mechanism(s) of action. *Adv. Pharmacol. Advances in Pharmacology*, 37: 253–97.
46. Gary H. Posner & Paul M. O'Neil (2004). Knowledge of the Proposed Chemical Mechanism of Action and Cytochrome P450 Metabolism of Antimalarial Trioxanes Like Artemisinin Allows Rational Design of New Antimalarial Peroxides. *Acc. Chem. Res*, 37 (6): 397–404.
47. Zhou Y, Li W, Xiao Y (2016). Profiling of Multiple Targets of Artemisinin Activated by Hemin in Cancer Cell Proteome. *ACS Chemical Biology*, 11 (4): 882–8.

48. Arieu, F., Witkowski, B., Amaratunga, C., Beghain, J., Ma, L., Lim, P., Sreng, S. (2016). *Nature*, 505(7481), 50–55.
49. http://www.who.int/malaria/areas/treatment/drug_efficacy/en/
50. Kesely, K. R., Pantaleo, A., Turrini, F. M., Olupot-olupot, P., & Low, P. S. (2016). Inhibition of an Erythrocyte Tyrosine Kinase with Imatinib Prevents Plasmodium falciparum Egress and Terminates Parasitemia. *PLoS One*, (1979), 1–19.
51. Tramontano, A. (2006). The role of molecular modelling in biomedical research. *FEBS Letters*, 580, 2928–2934.
52. Forster, M. J. (2002). Molecular modelling in structural biology. *Micron*, 33.
53. Lu, D., Aksimentiev, A., Shih, A. Y., Cruz-chu, E., Freddolino, P. L., & Schulten, K. (2008). *NIH Public Access*, 3(1), 1–27.
54. Vanommeslaeghe et al. (2015). Molecular Mechanics. *NIH Public Access*, 20(20), 3281–3292.
55. Huang, M., Li, X., Zou, J., & Timson, D. J. (2013). Role of Arg228 in the Phosphorylation of Galactokinase: The Mechanism of GHMP Kinases by Quantum Mechanics/Molecular Mechanics Studies. *Biochemistry*, 52, 4858–4868
56. Rester U (2008). "From virtuality to reality - Virtual screening in lead discovery and lead optimization: a medicinal chemistry perspective". *Current Opinion in Drug Discovery & Development*, 11 (4): 559–68
57. Rollinger JM, Stuppner H, Langer T (2008). "Virtual screening for the discovery of bioactive natural products". *Progress in Drug Research*, 65 (211): 211, 213–49
58. Huang, Y., Zhang, Y., Fan, K., Dong, G., Li, B., Zhang, W., & Li, J. (2017). Letters Discovery of new Syk inhibitors through structure-based virtual screening. *Bioorganic & Medicinal Chemistry Letters*, 27(8), 1776–1779.
59. Pugazhendhi, D. (2013). *In silico* Methods in Drug Discovery - A Review. *International Journal of Advanced Research in Computer Science and Software Engineering*, 3(5), 680–683.
60. McGregor MJ, Luo Z, Jiang X (2007). "Chapter 3: Virtual screening in drug discovery". In Huang Z. Drug Discovery Research. New Frontiers in the Post-Genomic Era. Wiley-VCH: Weinheim, Germany. pp. 63–88
61. Sun H (2008). "Pharmacophore-based virtual screening". *Current Medicinal Chemistry*. 15 (10): 1018–24
62. Kroemer RT (August 2007). "Structure-based drug design: docking and scoring". *Current Protein & Peptide Science*. 8 (4): 312–28.
63. Cavasotto CN, Orry AJ (2007). "Ligand docking and structure-based virtual screening in drug discovery". *Current Topics in Medicinal Chemistry*. 7 (10): 1006–14.
64. Orry AJ (2007). "Ligand docking and structure-based virtual screening in drug discovery". *Current Topics in Medicinal Chemistry*. 7 (10): 1006–14.

65. Irwin JJ, Shoichet BK, Mysinger MM, Huang N, Colizzi F, Wassam P, Cao Y (2009). "Automated docking screens: a feasibility study". *Journal of Medicinal Chemistry*. **52** (18): 5712–20.
66. Li H, Leung KS, Ballester PJ, Wong MH (2014-01-24). "istar: a web platform for large-scale protein-ligand docking". *PLoS One*. **9** (1): e85678.
67. Kaur, M., Kumari, A., Bahia, M. S., & Silakari, O. (2013). Designing of new multi-targeted inhibitors of spleen tyrosine kinase (Syk) and zeta-associated protein of 70 kDa (ZAP-70) using hierarchical virtual screening protocol. *Journal of Molecular Graphics and Modelling*, **39**, 165–175.
68. Yang, L., Zou, J., Xie, H., Li, L., Wei, Y., & Yang, S. (2009). Steered Molecular Dynamics Simulations Reveal the Likelier Dissociation Pathway of Imatinib from Its Targeting Kinases c-Kit and Abl. *PLoS One*, **4**(12).
69. Pimentel, A. S., Guimarães, C. R. W., & Miller, Y. (2013). Molecular Modeling : Advancements and Applications. *Journal of Chemistry*, **2013**(001), 2–4.
70. Hasan, A. M., Mazumder, H. M. H., Chowdhury, S. A., Datta, A., & Khan, A. M. (2015). Molecular-docking study of malaria drug target enzyme transketolase in Plasmodium falciparum 3D7 portends the novel approach to its treatment. *Source Code for Biology and Medicine*, **10**(1), 1–14.
71. Bhat, H. R., Ghosh, S. K., Prakash, A., Gogoi, K., & Singh, U. P. (2012). In vitro antimalarial activity and molecular docking analysis of 4-aminoquinoline-clubbed 1 , 3 , 5-triazine derivatives,. *Letters in Applied Microbiology*, 483–486.
72. Rout, S., Warhurst, D. C., Suar, M., & Mahapatra, R. K. (2015). In silico comparative genomics analysis of Plasmodium falciparum for the identification of putative essential genes and therapeutic candidates. *Journal of Microbiological Methods*, **109**, 1–8.
73. Nag, S., Prasad, K. M. N., Bhowmick, A., Deshmukh, R., & Trivedi, V. (2012). PfR10-2 Kinase is a Potential Therapeutic Target of Antimalarial Protein Kinase Inhibitors. *Current Drug Discovery Technologies*, **2013**, **10**, 85-91
74. Prudêncio, M., & Mota, M. M. (2013). Targeting Host Factors to Circumvent Anti-Malarial Drug Resistance. *Current Pharmaceutical Design*, 1–10.
75. Ruzza, P., Biondi, B., & Calderan, A. (2009). Expert Opinion on Therapeutic Patents Therapeutic prospect of Syk inhibitors, **19**(10)
76. Kesely, K. R., Pantaleo, A., Turrini, F. M., Olupot-olupot, P., & Low, P. S. (2016). Inhibition of an Erythrocyte Tyrosine Kinase with Imatinib Prevents Plasmodium falciparum Egress and Terminates Parasitemia. *PLoS One*, (1979), 1–19.
77. Sylvia Braselmann, Vanessa Taylor, Haoran Zhao, Su Wang, Catherine Sylvain, Muhammad Baluom, Kunbin Qu, Ellen Herlaar, Angela Lau, Chi Young, Brian R. Wong, Scott Lovell, Thomas Sun, Gary Park, Ankush Argade, Stipo Jurcevic, Polly Pine, Rajinder Singh, Elliott B. Grossbard, Donald G. Payan, and Esteban S. Masuda (2006). R406, an Orally Available Spleen Tyrosine Kinase Inhibitor Blocks Fc Receptor Signaling and Reduces Immune

- Complex-Mediated Inflammation. *Journal of Pharmacology and Experimental Therapeutics*, 319 (3) 998-1008;
78. Michael E. Weinblatt, Mark C. Genovese, Meilien Ho, Sally Hollis Krystyna Rosiak-Jedrychowicz, Arthur Kavanaugh, David S. Millson, Gustavo Leon, Désirée van der Heijde (2014). Effects of Fostamatinib, an Oral Spleen Tyrosine Kinase Inhibitor, in Rheumatoid Arthritis Patients With an Inadequate Response to Methotrexate: Results From a Phase III, Multicenter, Randomized, Double-Blind, Placebo-Controlled, Parallel-Group Study. *Arthritis Rheumatol*, 66(12):3255-64.
 79. Anna Podolanczuk, Alan H. Lazarus, Andrew R. Crow, Elliot Grossbard, and James B. Bussel (2009). Of mice and men: an open-label pilot study for treatment of immune thrombocytopenic purpura by an inhibitor of Syk. *Blood*, 113(14):3154-60.
 80. Safety and Efficacy Study of Fostamatinib to Treat Immunoglobulin A (IgA) Nephropathy – Full Text View – *ClinicalTrials.gov*. Retrieved 2016-11-19.
 81. Jonathan W. Friedberg, Jeff Sharman, John Sweetenham, Patrick B. Johnston, Julie M. Vose, Ann LaCasce, Julia Schaefer-Cuttillo, Sven De Vos, Rajni Sinha, John P. Leonard, Larry D. Cripe, Stephanie A. Gregory, Michael P. Sterba, Ann M. Lowe, Ronald Levy, and Margaret A. Shipp (2010). Inhibition of Syk with fostamatinib disodium has significant clinical activity in non-Hodgkin Lymphoma and chronic lymphocytic leukemia. *Blood*, 115(13):2578-85.
 82. Greg Coffey, Francis DeGuzman, Mayuko Inagaki, Yvonne Pak, Suzanne M. Delaney, Dan Ives, Andreas Betz, Zhaozhong J. Jia, Anjali Pandey, Dale Baker, Stanley J. Hollenbach, David R. Phillips, and Uma Sinha (2011). Specific Inhibition of Spleen Tyrosine Kinase Suppresses Leukocyte Immune Function and Inflammation in Animal Models of Rheumatoid Arthritis. *The Journal of pharmacology and experimental therapeutics*, Vol. 340, No. 2,
 83. Spurgeon, S. E., Coffey, G., Fletcher, L. B., Burke, R., Tyner, J. W., Druker, B. J., Loriaux, M. M. (2013). The Selective Syk Inhibitor P505-15 (PRT062607) Inhibits B Cell Signaling and Function In Vitro and In Vivo and Augments the Activity of Fludarabine in Chronic Lymphocytic Leukemia. *Journal of Pharmacology and Experimental Therapeutics*, 344(2), 378–387.
 84. Hisamichi, H., Naito, R., Toyoshima, A., Kawano, N., Ichikawa, A., Orita, A., Tsukamoto, S. (2005). Synthetic studies on novel Syk inhibitors. Part 1 : Synthesis and structure-activity relationships of pyrimidine-5-carboxamide derivatives. *Bioorganic & Medicinal Chemistry*, 13, 4936–4951.
 85. Yi, Y., Son, Y., Ryou, C., Sung, G., Kim, J., & Cho, J. Y. (2014). Functional Roles of Syk in Macrophage-Mediated Inflammatory Responses. *Mediators of Inflammation*, 2014.
 86. Wang, X., Mychajlowycz, M., Lau, C., Gutierrez, C., & Scott, J. A. (2012). Spleen Tyrosine Kinase Mediates BEAS-2B Cell Migration and Proliferation and Human Rhinovirus-Induced Expression of Vascular Endothelial Growth Factor and Interleukin-8. *The Journal of Pharmacology and Experimental Therapeutics*, 340(2)

87. Yamamoto, N., Takeshita, K., Shichijo, M., Kokubo, T., Sato, M., & Yakuhin, B. (2003). The Orally Available Spleen Tyrosine Kinase Inhibitor nicotinamide Dihydrochloride (BAY 61-3606) Blocks Antigen- Induced Airway Inflammation in Rodents. *The Journal of Pharmacology and Experimental Therapeutics*, 306(3), 1174–1181.
88. Le Nagard H, Vincent C, Mentré F, Le Bras J. 2010. Online analysis of in vitro resistance to antimalarial drugs through nonlinear regression. *Comput Methods Programs Biomed*
89. U.K. Laemmli (1970). Cleavage of structural proteins during the assembly of the head of bacteriophage T4. *Nature*, vol.227, no. 5259, pp. 680-685.
90. F. Mohamadi et al. (1990). Macromodel-an integrated software system for modeling organic and bioorganic molecules using molecular mechanics. *J. Comput. Chem.*, vol. 11, n. 4, pagg. 440–467.
91. G. Chang, W. C. Guida, e W. C. Still. (1989). An internal-coordinate Monte Carlo method for searching conformational space. *J. Am. Chem. Soc.*, vol. 111, n. 12, pagg. 4379–4386.
92. J. Gasteiger e M. Marsili. (1980). Iterative partial equalization of orbital electronegativity— a rapid access to atomic charges. *Tetrahedron*, vol. 36, n. 22, pagg. 3219–3228.
93. M. J. Frisch et al. (2009). Gaussian 09, Revision D.01. Gaussian Inc. Wallingford.
94. R. Dennington, T. Keith, e J. Millam. (2009) Gauss View, Version 5. Semichem Inc., Shawnee Mission KS.
95. M. F. Sanner. (1999). Python: a programming language for software integration and development. *J. Mol. Graph. Model*, vol. 17, n. 1, pagg. 57–61.
96. G. M. Morris et al. (1998). Automated docking using a Lamarckian genetic algorithm and an empirical binding free energy function. *J. Comput. Chem.*, vol. 19, n. 14, pagg. 1639–1662.
97. R. Huey, G. M. Morris, A. J. Olson, e D. S. Goodsell. (2007). A semiempirical free energy force field with charge-based desolvation, *J. Comput. Chem.*, vol. 28, n. 6, pagg. 1145–1152.
98. H. M. Berman et al. (2000). The Protein Data Bank. *Nucleic Acids Res.*, vol. 28, n. 1, pagg. 235–242.
99. R. A. Laskowski e M. B. Swindells. (2011). LigPlot+: Multiple Ligand–Protein Interaction Diagrams for Drug Discovery, *J. Chem. Inf. Model.*, vol. 51, n. 10, pagg. 2778–2786.
100. Islam, N., & Kaya, S. (2017). The Application of Some Computing Techniques in the Drug Design, 2(5). *Organic & Medicinal Chem, IJ* 2(5)
101. Banavath, H. N., Sharma, O. P., Kumar, M. S., & Baskaran, R. (2014). Identification of novel tyrosine kinase inhibitors for drug resistant T315I mutant BCR-ABL: a virtual screening and and molecular dynamics simulations study. *Scientific Reports*, 1–11.
102. D. A. Case et al. (2014) AMBER 14. University of California, San Francisco.
103. I. S. Joung e T. E. Cheatham. (2008). Determination of Alkali and Halide Monovalent Ion Parameters for Use in Explicitly Solvated Biomolecular Simulations, *J. Phys. Chem. B*, vol. 112, n. 30, pagg. 9020–9041.
104. E. F. Pettersen et al. (2004). UCSF Chimera--a visualization system for exploratory research and analysis, *J. Comput. Chem.*, vol. 25, n. 13, pagg. 1605–1612.

105. W. Humphrey, A. Dalke, e K. Schulten. (1996). VMD: visual molecular dynamics, *J. Mol. Graph*, vol. 14, n. 1, pagg. 33–38, 27–28.
106. J. W. Kaus, L. T. Pierce, R. C. Walker, e J. A. McCammon. (2013). Improving the Efficiency of Free Energy Calculations in the Amber Molecular Dynamics Package. *J. Chem. Theory Comput*, vol. 9, n. 9, pagg. 4131–4139.
107. Pettersen, EF; Goddard, TD; Huang, CC; Couch, GS; Greenblatt, DM; Meng, EC; Ferrin, TE (2004). "UCSF Chimera--a visualization system for exploratory research and analysis". *J Comput Chem*, **25** (13): 1605–12
108. Seeliger, D., Groot, B. L. De, & Pymol, V. (2010). Ligand docking and binding site analysis with PyMOL and Autodock / Vina. *Journal of Computer Aided-Molecular Design*, 417–422.
109. Chaudhari, R., & Li, Z. (2015). PyMine : a PyMOL plugin to integrate and visualize data for drug discovery. *BMC Research Notes*, 1–5.
110. <https://www-bimas.cit.nih.gov/clustalw/clustalw.html>
111. John J. Irwin, Teague Sterling, Michael M. Mysinger, Erin S. Bolstad, and Ryan G. Coleman (2012). ZINC: A Free Tool to Discover Chemistry for Biology. *Journal of Chemical Information and Modeling*, 52 (7), 1757-1768
112. Forli, S. (2015). Charting a Path to Success in Virtual Screening. *Molecules*, 20(10), 18732–18758.
113. Hopkins, A. L., Keserü, G. M., Leeson, P. D., Rees, D. C., & Reynolds, C. H. (2014). The role of ligand efficiency metrics in drug discovery. *Nature Reviews Drug Discovery*, 13, 105.
114. Murray, C. W., Erlanson, D. A., Hopkins, A. L., Keseru, G. M., Leeson, P. D., Rees, D. C., ... Richmond, N. J. (2014). Validity of Ligand Efficiency Metrics. *American Chemical Society*, 616–618.
115. Zapatero, A. C., & Metz, J. T. (2005). Ligand efficiency indices for drug discovery. *Drug Discovery Today*, 10(7), 464–469.
116. Kufareva, I., & Abagyan, R. (2008). Type-II Kinase Inhibitor Docking, Screening, and Profiling Using Modified Structures of Active Kinase States. *Journal of Medicinal Chemistry*, 51(24), 7921–7932.
117. Traxler, P., & Furet, P. (1999). Strategies toward the Design of Novel and Selective Protein Tyrosine Kinase Inhibitors. *Pharmacology & Therapeutics*, 82(2–3), 195–206.
118. Miah, S. M. S., Sada, K., Tuazon, P. T., Ling, J., Maeno, K., Kyo, S., Yamamura, H. (2004). Activation of Syk Protein Tyrosine Kinase in Response to Osmotic Stress Requires Interaction with p21-Activated Protein Kinase Pak2 / -PAK, 24(1), 71–83.
119. Thoma, G., Smith, A. B., Eis, M. J. Van, Vangrevelinghe, E., Blanz, J., Aichholz, R., Zerwes, H. (2015). Discovery and Profiling of a Selective and Efficacious Syk Inhibitor. *Journal of Medicinal Chemistry*, 58, 1950–1963.
120. Grädler, U., Schwarz, D., Dresing, V., Musil, D., Bomke, J., Frech, M., ... Wegener, A. (2013). Structural and biophysical characterization of the Syk activation switch. *Journal of Molecular Biology*, 425(2), 309–333

121. A. G. Villaseñor et al. (2009). Structural Insights for Design of Potent Spleen Tyrosine Kinase Inhibitors from Crystallographic Analysis of Three Inhibitor Complexes. *Chem. Biol. Drug Des*, vol. 73, n. 4, pagg. 466–470.
122. M. Castillo et al. (2012). Highly potent aminopyridines as Syk kinase inhibitors. *Bioorg. Med. Chem. Lett*, vol. 22, n. 17, pagg. 5419–5423.
123. Ahmed M. Al-Sabagh, Notaila M. Nasser, Ahmed A. Farag, Mohamed A. Migahed, Abdelmonem M.F. Eissa, Tahany Mahmoud. (2013). Structure effect of some amine derivatives on corrosion inhibition efficiency for carbon steel in acidic media using electrochemical and Quantum Theory Methods. *Egyptian Journal of Petroleum*, 22, 101–116.

Publications

- 1) **G. Marchetti**, A. Dessì, R. Dallochio, I. Tsamesidis, M. C. Pau, F. Turrini, A. Pantaleo. “*In vitro* and computational studies of Syk Inhibitors with antimalarial activity in RBCs ”, Manuscript in preparation.
- 2) **Pau M.C.**, Pantaleo A., Tsamesidis I., Hoang H., Tran A., Nguyen H., Phan G., Ton A., Ngo C., Marchetti G., Schawarzer G., Fiori P.L., Low P.S., Turrini F.M. “Evaluation of the impact of artemisinin resistance on the clinical efficacy of the antimalarial dihydroartemisinin-piperaquine therapy in Vietnam”. Manuscript under revision
- 3) **Tsamesidis I.**, Reybier K., Marchetti G., Pau M.C., De Lucia S., Viridis P., Fozza C., Nepveu F., Low P.S., Pantaleo A., Turrini F.M. “ Syk Inhibitors cause hemichrome accumulation in the *P. falciparum* parasitized erythrocytes determining a synergistic activation of artemisinins”. Manuscript in preparation

Communications

- 1) **I. Tsamesidis**, A. Pantaleo, M. C. Pau, G. Marchetti, F. Turrini, “New antimalarial drugs tyrosine kinase inhibitors”, PhD day (Verona), 29 January 2016.
- 2) **G. Marchetti**, I. Tsamesidis, M. C. Pau, A. Dessì, R. Dallochio, A. Pantaleo, “In vitro and in silico studies of syk inhibitors as new antimalarial drugs”, The 4th International PhD Students’ Symposium, Hue Science Festival 2016 (Vietnam), 28-30 April 2016.
- 3) **A. Pantaleo**, M. C. Pau, I. Tsamesidis, G. Marchetti, F. Turrini. “Effects of SYK inhibitors on erythrocyte membrane modifications induced by *Plasmodium falciparum* growth”, 67th SIF National Congress – Italian Physiological Society, Catania 21-23 September 2016.
- 4) **G. Marchetti**, A. Dessì, R. Dallochio I. Tsamesidis, A. Pantaleo, F. Turrini. “In vitro studies and computational analysis of Syk inhibitors as new antimalarial drugs”. 2nd Stintino Seminars in Microbiology “Infections in cancer and autoimmunity”, Stintino 5 June 2017
- 5) **G. Marchetti**, A. Dessì, R. Dallochio, I. Tsamesidis, M. C. Pau, F. Turrini, A. Pantaleo. “In vitro and computational studies of Syk inhibitors as new antimalarial drugs”. 4th year of the Prague Summer School in DRUG discovery and DEVELOPMENT from basic research through preclinical to clinical phases, Prague, Czech Republic 4th – 8th, 2017
- 6) **G. Marchetti**, A. Dessì, R. Dallochio, I. Tsamesidis, M. C. Pau, F. Turrini, A. Pantaleo. “In vitro and computational studies in the fight against malaria”. 90^o SIBS Congress – Italian Society of Experimental Biology, Trapani 27-28 October 2017
- 7) **A. Manca**, S. Duras, M.M. Trias, I. Tsamesidis, G. Marchetti, M.C. Pau, F. Turrini, A. Pantaleo. “New antimalarial drugs on the Horizon?”. 90^o SIBS Congress – Italian Society of Experimental Biology, Trapani 27-28 October 2017.
- 8) **G. Marchetti**¹, A. Dessì², R. Dallochio², I. Tsamesidis¹, C. D’Avino¹, E. Avitabile¹, A. Pantaleo¹. “Computational and *in vitro* studies of Syk Inhibitors as new drugs in *P. falciparum* malaria”. 90^o SIBS Congress – Italian Society of Experimental Biology, Ancona 9-10 November 2018